EGFR AND WNT/β-CATENIN SIGNALLING

IN AIRWAY HOMEOSTASIS AND REPAIR

Liwen Lu

A thesis submitted to UCL for the degree of Doctor of Philosophy

2011

DECLARATION

I, Liwen Lu confirm that the work presented in this thesis is my own. Where information has been derived from other sources, I confirm that this has been indicated in the thesis.

ABSTRACT

Lung cancers are a leading cause of death worldwide, and although there is some evidence that both Epidermal Growth Factor Receptor (EGFR) and Wnt/β-catenin signalling are involved in initiation and progression of this disease the molecular mechanisms regulating these processes remain poorly described. Here I show that deletion of LRIG1, an endogenous EGFR inhibitor, leads to epithelial hyperplasia in the murine airway and continued proliferation post confluence in vitro. This occurs via phosphorylation of EGFR and its downstream effector molecule ERK1/2. Human lung cancer cell lines lacking LRIG1 showed a reduction of proliferation on LRIG1 replacement. Using co-localisation experiments I have defined LRIG1 inhibition of density dependent growth occurs through LRIG1 forming a complex with EGFR and E-Cadherin at the cell confluence. Examination of matched human pre-invasive lung cancer lesions with normal airway from the same individuals delineated loss of LRIG1 supporting its role in the early stages of cancer development.

I further show that β-catenin regulates epithelial cell phenotype in both normal airway stem cells and preinvasive lung cancers. β-catenin inhibition within keratin 14-expressing stem cells impairs airway repair whilst activation increases cell proliferation, directs lineage choice, and promotes an epithelial-to-mesenchymal transition that includes loss of cadherin-mediated adhesions and increased Twist and Snail transcription influencing both

intercellular and cell-matrix adhesiveness. These findings were recapitulated in vitro both by pharmacological β-catenin activation and direct E-cadherin inhibition. Thus, β-catenin modulation of cadherin-dependent intercellular adhesions determines cell phenotype and its overexpression is a key early step in pre-invasive disease development.

ACKNOWLEGEMENTS

Coming to the UK and doing PhD was a big challenge to me. And it didn't seem any smaller to my supervisor, Dr Sam Janes. As his first overseas PhD student, I have been receiving massive input from him throughout the project. He has always been supportive, inspiriting, and understanding, who is a supervisor I could never have a better one. Particularly, his calmness and optimism with reality boundary have been a good example which I will benefit in life as well as research.

Dr Adam Giangreco, who has been helping me with the β-catenin project, has been a constant source of encouragement and inspiration. His broad science knowledge and strictness in research has uplifted this project. I would also like to thank Professor Rachel Chambers, my secondary supervisor, who has strongly supported me throughout. My thanks go to Dr Vitor Hugo as well, for his contribution to the LRIG1 analysis in human CIS samples.

Everyone in CRR has made my experience here rich and colorful. I would particularly like to thank Emilie, Iona, Melissa, Michael, Nicola, and Natalia for their support and friendship.

At Cancer Research UK, I would like to thank Dr Kim Jensen for his support in the LRIG project.

In addition, I would like to thank the Overseas Research Scholarship (ORS) for funding my PhD.

Last but not least, I would like to acknowledge my parents and sisters. They have supported me throughout unconditionally.

Table of Contents

LIST OF FIGURES

CHAPTER 1. INTRODUCTION

1.1 Background

Lung cancer is the world's most common fatal cancer, with non small cell lung cancer (NSCLC) accounting for 80% of all cases (Felip, Cedres et al.). Given the fact that cigarette smoking causes 90% of lung cancers worldwide (Giangreco, Groot et al. 2007), one hypothesis is that this disease is caused by the failure of restoration of normal homeostatic cell division after injury. Therefore, understanding the mechanism involved in normal airway epithelial maintenance and repair after injury is crucial for lung cancer early detection and possibly therapy.

1.2 Airway homeostasis and repair

1.2.1 Normal airway cellular composition in mouse and human upper airway

In mice, the airway epithelium is pseudostratified in the large airways, becoming columnar in the intrapulmonary airways and cuboidal in the small airways. The trachea is

lined by a pseudostratified epithelium comprising about 30% basal cells, 55% ciliated cells, a few secretory cells and sparse neuroendocrine cells (Rock, Randell et al.). The intrapulmonary airways (bronchioles) are lined by a columnar epithelium consisting of Clara and ciliated cells with interspersed clusters of neuroendocrine (NE) cells (Rawlins, Okubo et al. 2009). The more distal airways have fewer ciliated cells compared to more proximal airways, whilst basal cells are absent in intrapulmonary airways and further distally (Rock, Randell et al. 2010). The major populations of cells within the upper airways can be immunophenotyped by the expression of Keratin 14/ Keratin 5 (K14/K5) in basal cells, Clara cells expressing high levels of secretoglobin SCGB1A1, also known as CCSP, and ciliated cells expressing acetylated tubulin (Mercer, Russell et al. 1994).

In humans, the airway epithelium remains pseudostratified from trachea to terminal bronchioles before it turns into a simple cuboidal epithelium lacking basal cells in the respiratory bronchioles. The pseudostratified epithelium has a higher number of secretory cells than in mice and consists of ~ 30% basal cells, 30% ciliated cells and 30% secretory cells (majorly goblet cells and a few Clara cells) (Mercer, Russell et al. 1994). Hence, the mouse tracheal epithelium is similar to the upper human airways and is the model system I use in large parts of my thesis.

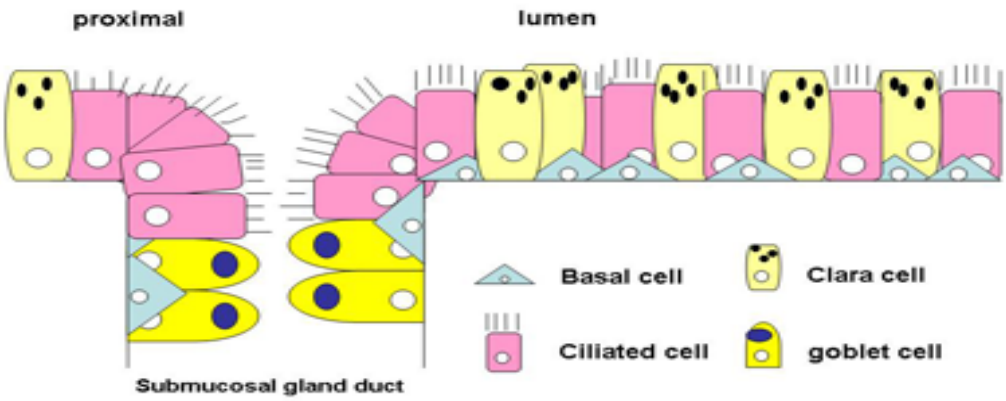

Figure 1.1 Diagram showing the cellular composition of the mouse trachea

The pseudostratified epithelium in mouse tracheal comprises basal, ciliated and Clara cells in similar proportions. The submucosal glands (SMGs) are only present in the proximal trachea. In laboratory mice, goblet cells which responsible for mucus producing are largely restricted to the SMGs. (Adapted from Rock et al. 2010)

1.2.2 Epithelial homeostasis and repair

1.2.2.1 Airway epithelial homeostasis

Maintenance of respiratory epithelium in steady state involves the balance between airway epithelial cell proliferation, differentiation and apoptosis. Disruption of this balance and failure to restore homeostasis may lead to the pathological changes such as hyperplasia, metaplasia or carcinogenesis. Hence, a greater understanding and control of the involved signalling pathways is clinical relevant.

The airway epithelium is slowly renewing compared with the tissues such as the intestine or skin. Turnover of the intestinal epithelium occurs in around 5 days (Snyder, Teisanu et al. 2009) compared to the estimated half-life of ciliated cell lifespan of 6 months in trachea and 17 months in the bronchi (Rawlins and Hogan 2008).

Many tissues such as pancreas, skin, and corneal epithelium, are maintained by the non-stem progeny, named transit amplifying cells, undergo a small number of rounds of division before withdrawing from the cell cycle and undergoing terminal differentiation (Dor, Brown et al. 2004; Dor and Melton 2004; Teta, Rankin et al. 2007; Majo, Rochat et al. 2008). Interestingly chimeric studies in the lower airways have demonstrated a stochastic self-renewal of Clara cells is responsible for intrapulmonary airway homeostasis (Giangreco, Arwert et al. 2009).

In the steady state tracheal epithelium, basal cells have been shown to, over a long period of time, self-renew and give rise to both Clara cells and ciliated cells (Rawlins, Okubo et al. 2009).

1.2.2.2 Airway epithelial repair

A variety of animal models have been developed to investigate the repair process. Methods to induce proximal airway injury are: intratracheal instillation of detergent polidocanol, which causes widespread removal of epithelium; SO_2 inhalation, which destroys the luminal cells non-selectively; and naphthalene intraperitoneal injection, which cause selective death of Clara cells due to the enrichment of cytochrome P450 where the naphthalene is metabolised into toxic derivatives (Borthwick, Shahbazian et al.

2001; Hong, Reynolds et al. 2004). These models induce variable damage but a similar early epithelial repair process. After the neighboring cells migrate and spread to cover the denuded surfaces, cells undergo proliferation. When new-formed epithelial cells reach confluence, they undergo contact inhibition and begin to differentiate and restore normal epithelium (Borthwick, Shahbazian et al. 2001; Burgel and Nadel 2004).

In the trachea, only basal cells and a few Clara cells survive after the non-selective injury. Lineage labelling of basal cells has shown that surviving basal cells throughout the trachea divided and gave rise to ciliated and Clara cells (Rock, Onaitis et al. 2009). K14-expressing basal cells were also demonstrated to self-renew after specific Clara cell ablation, and generate Clara and ciliated cells after injury (Hong, Reynolds et al. 2004).

1.3 The EGFR pathway's role in airway epithelial homeostasis and repair

1.3.1 EGFR family signalling

The epidermal growth factor receptor (EGFR) was identified in 1978 by Cohen and co-workers as a 170-kDa membrane component, which was expressed in cells of mesodermal and ectodermal origins (Yarden and Sliwkowski 2001). EGFR consists of three functional domains, one extracellular region providing the ligand-binding site and dimerisation arm, a transmembrane domain, and a highly-conserved cytoplasmic region that encodes a tyrosine kinase and multiple phosphorylation residues. The EGFR family

comprises four structurally related receptor tyrosine kinases (RTK), which are EGFR/ErbB-1/HER-1 (Human Epidermal growth factor Receptor), ErbB-2/Neu/HER-2, ErbB-3/HER-3, and ErbB-4/HER-4. These receptors can be activated by a number of growth factors (Linggi and Carpenter 2006) and regulate diverse functions in normal cells and have a crucial role in tumorigenesis. There are three functional groups of epidermal growth factor family. The first group only binds to EGFR, consisting of EGF and its analogues TGF-α (transforming growth factor alpha), amphiregulin (AR, also known as keratinocyte autocrine factor or colorectum-cell derived growth factor). The second group binds to ErbB3 and ErbB4, consisting of Neuregulins, also known as heregulins. The third group binds both EGFR and ErbB4, consisting of batacellulin, epiregulin, and HB-EGF (heparin-binding epidermal growth factor-like factor) (Riese and Stern 1998).

Ligand binding leads to the dimerisation of receptors, and the resulting conformational change has been proposed as an essential step for kinase activation, apart from certain constitutively active mutants (Linggi and Carpenter 2006). Receptor dimerisation, including both homo- and heterodimerisation, results in the autophosphorylation of multiple tyrosine residues within the cytoplasmic domain. The activated EGFR recruits a number of signal transducers to their docking site within the cytoplasmic domain, such as growth-factor-receptor bound-2 (GRB2) and Src-homology-2-containing (Shc). GRB2 and Shc can recruit Ras and subsequently activate the mitogen-activated protein kinase (MAPK or Erk2) pathway, as well as the Ras/PI3K/AKT/PKB pathway (Citri and Yarden 2006).

1.3.2 Downstream Ras/MAPK/ERK signalling

MAPK cascade comprises a MAPK kinase kinase (MAP3K), a MAPK kinase (MAP2K) and a MAPK. The terminal MAPKs are the ERK, JNK (also called SAPK), p38 and ERK5 kinases (Montagut and Settleman 2009). Upon RAS activation, RAF kinase is subsequently phosphorylated leading to stimulation of its serine-threonine kinase activity (Malumbres and Barbacid 2003), which results in sequential phosphorylation and activation of the MEK1/MEK2 protein kinases and ERK. Activated ERKs translocates to the nucleus where they induce the transcription of immediate early genes, such as Elk1, Fos, Jun and Myc, which encode transcription factor and change the expression level of other genes responsible for cell proliferation (Yoon and Seger 2006).

1.3.3 Downstream Ras/PI3K/AKT/PKB signaling

EGFR activation by multiple ligands leads to the recruitment and subsequent stimulation of class I PI3K. PI3K can also be activated by RAS. The activated kinase catalyses the phosphorylation of phosphatidylinositol bisphosphate (PIP2) to phosphatidylinositol triphosphate (PIP3), the latter one acts as a docking site for Akt. Akt is a serine-threonine kinase which performs as the key regulator of the PI3K pathway, and phosphoinositide-dependent kinase 1. Upon the phosphorylation, Akt is activated and exerts its effects in the cell by phosphorylating various downstream substrates such as BAD (BCL2 Antagonist of Cell Death), Caspase 9, FKHR (Forkhead Transcriptional

Factor) and therefore regulates apoptosis, cell growth and mobility (Baselga, 2009).

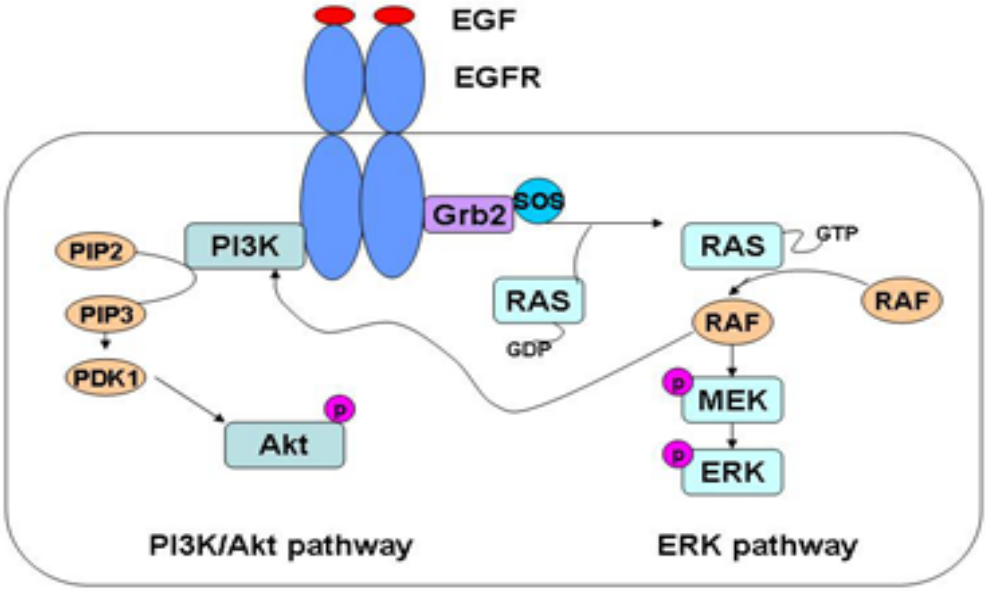

Figure 1.2 overview of EGFR signalling pathway.

Abbreviations: PIP2, phosphatidylinositol bisphosphate; PIP3, phosphatidylinositol triphosphate, PDK1, 3-phosphoinositide-dependent protein kinase 1; PI3K, hosphoinositide-3 kinase; GRB2, growth-factor-receptor bound-2; SOS, son of sevenless; MEK: mitogen-activated protein kinase; RAS, a protein subfamily of small GTPases; RAF, MAPK kinase kinase (MAP3K); ERK, extracellular signal-regulated kinase.

1.3.4 Nuclear EGFR signalling

In addition to the canonical signalling pathway occurring at the plasma membrane described above, there appears to be nuclear EGFR signalling. Intact EGFR, likely in the phosphorylated form, has been detected in the nucleus. Experiments have demonstrated this occurs in both ligand-dependent and ligand-independent manner (Lin, Makino et al. 2001; Cordero, Cozzolino et al. 2002; Dittmann, Mayer et al. 2005). The initial step of receptor trafficking likely depends on its internalisation. It has been proposed that EGFR, without a putative DNA binding site, first associates with DNA-binding transcription factor STAT3, and then targets promoters such as cyclin D1 and B-myb. By upregulating the promoter expression, EGFR therefore positively regulates G1/S cell cycle progression which is closely associated with tumorigenesis, tumor proliferation and progression (Lo, Hsu et al. 2005; Hanada, Lo et al. 2006). However, to what extent in vivo nuclear EGFR effects cell homeostasis remains largely unknown and requires further investigation.

1.3.5 EGFR regulation

1.3.5.1 Endocytosis and degradation of EGFR

On ligand-binding and subsequent dimerisation, receptors undergo internalisation into endosomes where the ligand-receptor complex either experiences disassociation followed by recycling back to the cell surface in a kinase-independent manner, or recruits c-Cbl, an

E3 ubiquitin ligase, and undergoes ubiquitylation. Notably, the other three ErbB proteins are more often recycled back to the cell surface due to the impaired endocytosis. C-Cbl preferentially binds to the EGFR homodimers either directly (Tyr 1045) or indirectly through GRB2 (Waterman, Katz et al. 2002),

1.3.5.2 Intrinsic EGFR regulators

1.3.5.2.1 MIG6

Mitogen-inducible gene-6 (MIG6), also known as receptor-associated late transducer (RALT), Errfi1 (ErbB receptor feedback inhibitor 1) or gene 33, was the first feedback inhibitor discovered in mammalian cells. It is a 50-kDa adapter Protein and able to bind to the kinase domain of EGFR family, and directly inhibit the EGFR catalytic activity (Xu, Makkinje et al. 2005; Anastasi, Baietti et al. 2007). Overexpression of MIG6 in cultured cells contributed to the suppression of EGFR activation and downstream signalling (Xu, Makkinje et al. 2005). Loss of MIG6 resulted in increased tyrosine phosphorylation of EGFR in primary keratinocytes isolated from MIG6-defective mice. These mice also experienced overproliferation and impaired differentiation of epidermal keratinocytes, eventually developed spontaneous tumors in various organs (Ferby, Reschke et al. 2006).

1.3.5.2.2 LRIG1

The LRIG1 (leucine-rich and immunoglobulin-like domain 1) protein is an integral membrane protein, comprising an extracellular part consisting of a leucine-rich repeat (LRR) domain and three immunoglobulin-like domains, a transmembrane region and a

cytoplasmic tail. The LRIG family comprises three structurally similar proteins, LRIG1-3, which also share molecular functions (Hedman and Henriksson 2007).

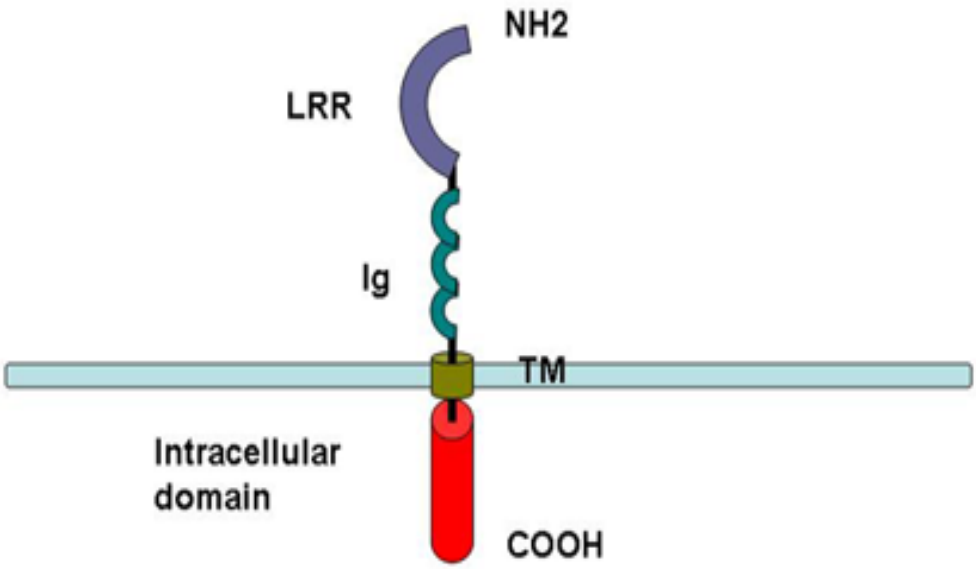

Figure 1.3 Schematic drawing of the LRIG1 construct.

LRIG1 comprises an extracellular domain including the leucine-rich repeat domain (LRR) and immunoglobulin-like domain (Ig), a transmembrane domain (TM) and a cytoplasmic domain. Either the extracellular or the Ig-like domains are sufficient to couple with EGFR

LRIG1 is considered a negative regulator of EGFR signalling. In vitro work on various human cell lines shows that LRIG1 expression is induced upon receptor activation, followed by binding to the extracellular domain of EGFR whilst its juxtamembrane domain constitutively recruits and activates c-Cbl, therefore facilitating EGFR unbiquitylation. In the mutant Y1045F-EGFR, whose cbl-docking site was mutated and underwent only minimal cbl-dependent unbiquitylation, LRIG1 supplied a surrogate

mechanism that enables cbl recruitment and subsequent receptor degradation (Gur, Rubin et al. 2004). However, another in vitro study using a different ectodomain of LRIG1 fragment, consisting of only the extracellular domain, could also suppress EGFR signalling and cell proliferation (Goldoni, Iozzo et al. 2007). Consistent with this result, Yi et al. reported that ectopic LRIG1 could be cleaved by ADAM (a metalloproteinase) and released extracellular domain which inhibited EGFR signalling without the downregulation of receptor expression. Therefore the author proposed a novel paracrine mechanism by which LRIG1 inhibits the EGFR signalling by competing with EGF for binding to EGFR (Yi, Holmlund et al. 2011).

The interaction of LRIG1 with EGFR has been further studied in a recent manuscript showing LRIG1 was also able to couple with EGFRvIII, a mutant EGFR with exons 2–7 deleted resulting in the extracellular domain deletion, and subsequent downregulation of the receptor. Results from this study indicated that LRIG1 can interact with EGFR either via the extracellular or the transmembrane domain (Stutz, Shattuck et al. 2008).

LRIG1 not only interacts with EGFR. Ectopic expression of LRIG1 suppresses the expression of each of the EGFR family proteins. Interestingly however, there was no downregulation in the expression of fibroblast growth factor receptor and nerve growth factor receptor, indicating this effect is specific to EGFR family proteins (Gur, Rubin et al. 2004).

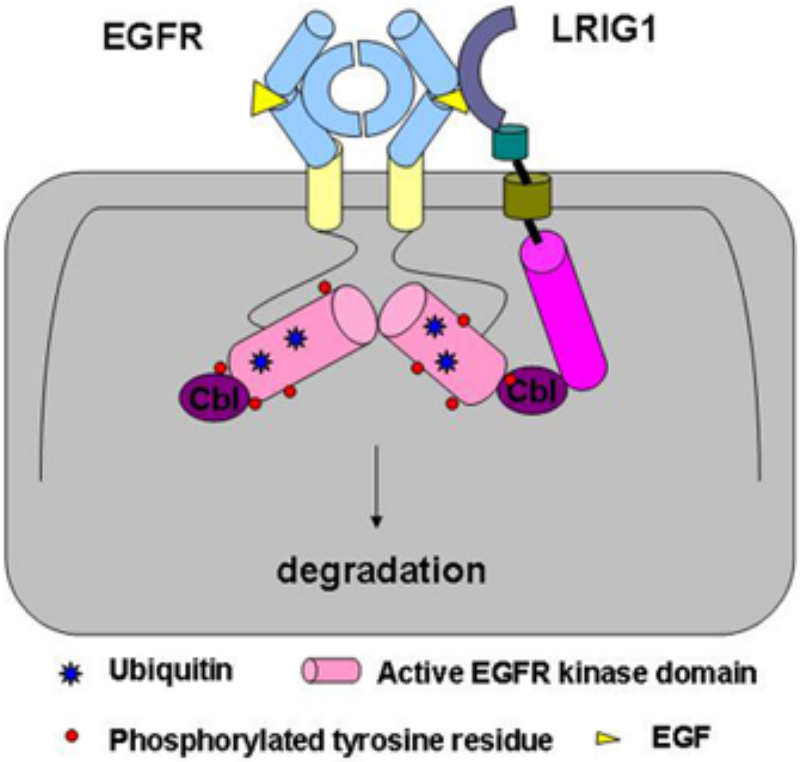

Figure 1.4 LRIG1 facilitates EGFR ubiquitylation

C-Cbl binds to EGFR in a phosphorylation-dependent manner, whilst to LRIG1 in a phosphorylation-independent manner (Rubin, Gur et al. 2005). In addition to the recruitment of c-Cbl by EGFR itself, LRIG1 introduces c-Cbl to activated EGFR. C-Cbl is phosphorylated by activated EGFR and then capable of directing EGFR ubiquitylation. (Adapted from Segatto et al. 2011)

LRIG1 and Cancer

The LRIG1 gene maps to chromosome 3p14, a region frequently deleted in human tumours, which indicates the role for LRIG1 in tumour suppression. As a consequence of the EGFR suppression, proliferative inhibition of various cells has been shown by ectopic

LRIG1 expression, including such as human embryonic kidney-293 cells (Gur, Rubin et al. 2004), NIH3T3 fibroblasts (Laederich, Funes-Duran et al. 2004), keratinocytes (Jensen and Watt 2006), bladder carcinoma cells (Yang, Yan et al. 2006), and prostate tumor cells (Laederich, Funes-Duran et al. 2004). Concordantly, LRIG1 has been reported downregulated in skin cancer (Jensen and Watt 2006), renal cell carcinoma (Thomasson, Hedman et al. 2003) and squamous cell lung carcinoma (SCC) (Boelens, van den Berg et al. 2009), which have been associated with upregulated EGFR signalling.

LRIG1 and Tissue Homestasis

LRIG1 also plays a role in epidermal homeostasis with the Lrig1-defective mouse model generating in epidermal hyperplasia and psoriasiform epidermal hyperplasia (Suzuki, Miura et al. 2002). Jensen et al. used the same murine model to demonstrate Lrig1-expressing cells in epidermis are a multipotent stem cell population. LRIG1 seems to regulate epidermal stem cell quiescence by downregulating EGFR and decreasing cMyc, resulting in the balance of proliferation and differentiation (Jensen, Collins et al. 2009). The same group knocked-down LRIG1 in cultured human keratinocytes, and found the expansion of stem cell population contributing to the increase of cell proliferation (Jensen and Watt 2006).

1.3.5.2.5 E-cadherin

E-Cadherin is a calcium dependent cell adhesion protein expressed predominantly in epithelial tissues (Andl and Rustgi 2005). The mechanism of E-cadherins interaction with EGFR is poorly understood despite its likely biological importance in epithelial

homeostasis and control of proliferation at cell-cell contact. It has been demonstrated that the EGFR family inhibit E-cadherin resulting in epithelial mesenchymal transitions (EMT) (Fujita, Krause et al. 2002; Thiery 2002). In addition to that, E-cadherin has also been reported as an inhibitor of EGFR family (Qian, Karpova et al. 2004). By using cultured MDCK (Madin Darby Canine Kidney) cells, Qian et al. tested EGFR activity at both low and high culture density. They found no EGFR activity upon EGF stimulation at high density culture, whilst low density cells with little surface E-cadherin activate the EGFR signalling. They used a forced-ErbB2 expression cell model to further demonstrate that E-cadherin inhibits EGFR signalling by lowering the ligand binding affinity rather than preventing dimerisation. An E-cadherin/EGFR complex was found in their MDCK cells, and the complex seemed unstable in low calcium conditions or in the presence of E-cadherin neutralising antibody, indicating the effects of E-cadherin on EGFR are adhesion dependent therefore underscoring the importance of contact inhibition.

1.3.6 EGFR and epithelial repair

EGFR and its ligands are detected at low levels in conducting airway epithelial cells.

In a study using naphthalene injury mouse model, EGFR was found increased in distal bronchioles immediately after injury (1 to 2 days), decreased slightly 4-7 days after injury and back to basic line 14-21 days after injury. The pattern of EGFR was reflected in the corresponding changes of BrdU staining, but not corresponded to the pattern of the EGF and TGF-α expression, suggesting the cell proliferation is modulated at receptor level (Van Winkle, Isaac et al. 1997). Indeed, EGFR hyper-expression and activation in airway epithelium has been shown increased in response to various stimuli including TNF-α

(Takeyama, Dabbagh et al. 1999), mechanical damage (Lee, Takeyama et al. 2000), cigarette smoke (Takeyama, Jung et al. 2001), and inhalation of noxious product (Madtes, Busby et al. 1994). EGFR activation is thought to be ligand-dependent. Although some early studies reported the ligand-independent EGFR occurred in response to oxidative stress caused by cigarette smoke, however, these stimuli can induce EGFR proligand shedding from the epithelial cell surface and subsequent ligand binding to the receptor.

1.4 The Wnt/β-catenin signalling pathway and its role in airway epithelial homeostasis and repair

1.4.1 The Wnt/β-catenin signalling pathway

The Wnt proteins are a family of around 19 secreted glycolproteins (Konigshoff and Eickelberg 2010). They are involved in cell-cell signalling and have been shown to effect cell fate decisions and proliferation (Dale 1998). They exert their action on cells via three main pathways: the planar cell polarity pathway, which is involved in the organization of epithelial cells; the Wnt/Ca2+ pathway and the "canonical" pathway involving β-catenin (Konigshoff and Eickelberg 2010). In the canonical pathway, when a cell is stimulated by Wnt ligands, β-catenin mediated signalling is activated.

β-catenin is a cytosolic protein containing approximately 100 amino acids (Huber, Nelson et al. 1997). It can be found in two cellular locations: plasma membrane acting as an essential component of cell-cell adhesion (shown in Figure 1.5), and cytoplasm playing an important role in signal transduction of the Wnt pathway (Case and Rubin 2010).

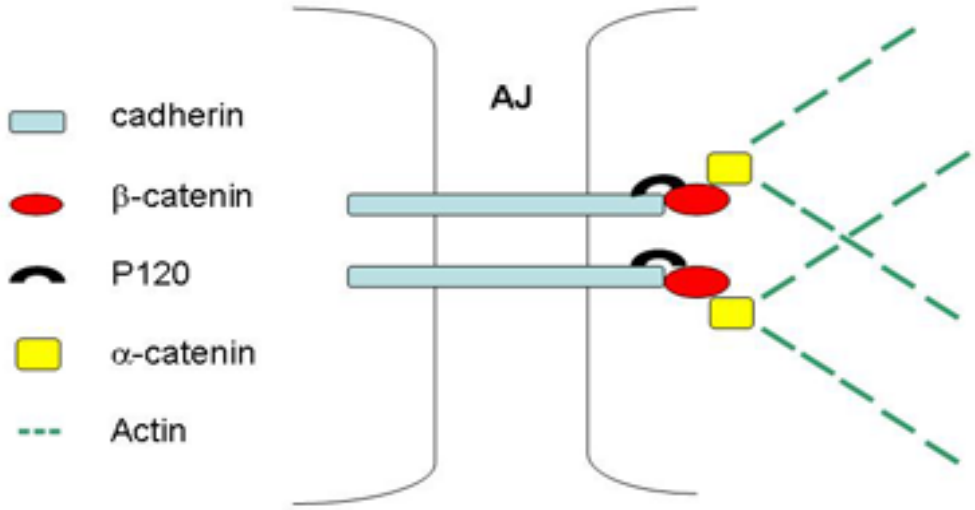

Figure 1.5 The involvement of β-catenin in cell-cell adhesion.

Cadherins including E-, P-, N- and VE-cadherin are bound with P120 which, in turn binds to β-catenin, the latter binds to actin via α-catenin. This complex effectively forms a link between cadherin and the actin cytoskeleton.

In the non Wnt stimulated cells, cytoplasmic β-catenin has a very short half-life as its breakdown is rapidly initiated by the complex shown in Figure 1.6. Once phosphorylated by the degradation machinery, β-catenin is marked out for ubiquitination and then degraded by proteasomes. It is thought that the GSK3β component of the degradation machinery is responsible for phosphorylation of β-catenin (Behrens 2000). When the concentration of cytoplasmic β-catenin is high, GSK3β can act to phosphorylate parts of APC which increases the phosphorylation and therefore degradation of β-catenin (Rubinfeld, Albert et al. 1996). Therefore, in the nucleus, prospective target genes of the pathway are kept in a repressed state.

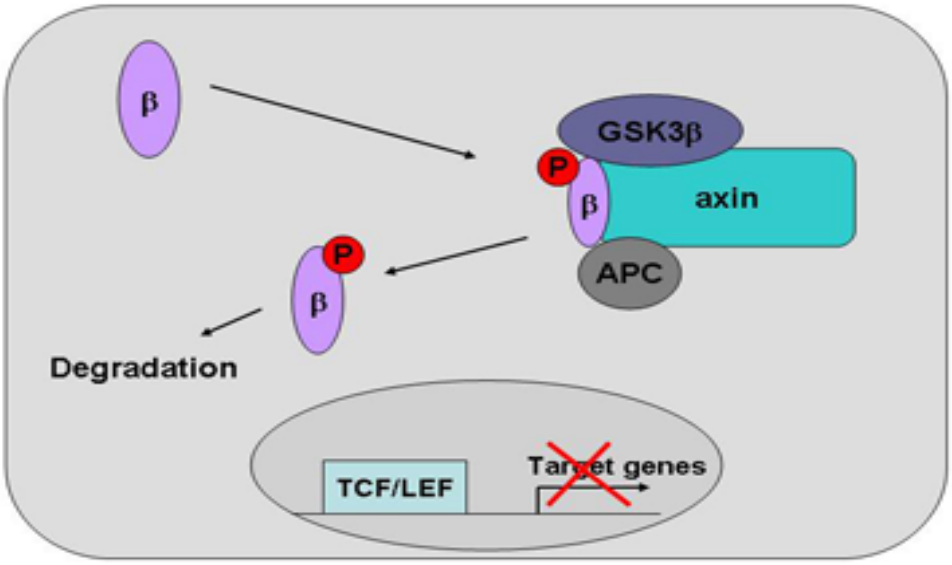

Figure 1.6 The breakdown of cytoplasmic β-catenin

In the absence of Wnt, cytoplasmic β-catenin is phosphorylated by a complex of glycogen synthase kinase 3β (GSK3β), axin (also known as conductin) and adenomatous polyposis coli (APC), follow by ubiquitylation targeted by β-transducin repeat containing protein (βTrCP) and subsequent degradation by the proteosome.

When the frizzled receptor is activated it is thought that, through interaction with low density lipoprotein receptor-related protein 6 (LRP6) and dishevelled proteins, β-catenin is prevented from being phosphorylated by the axin/GSK3β/APC complex, see Figure 1.7. The exact mechanism for this inhibition is unknown but it most likely involves axin binding to the LRP6/frizzled/dishevelled complex at the cell membrane, thereby reducing the availability of axin to form the degradation machinery (MacDonald, Tamai et al. 2009).

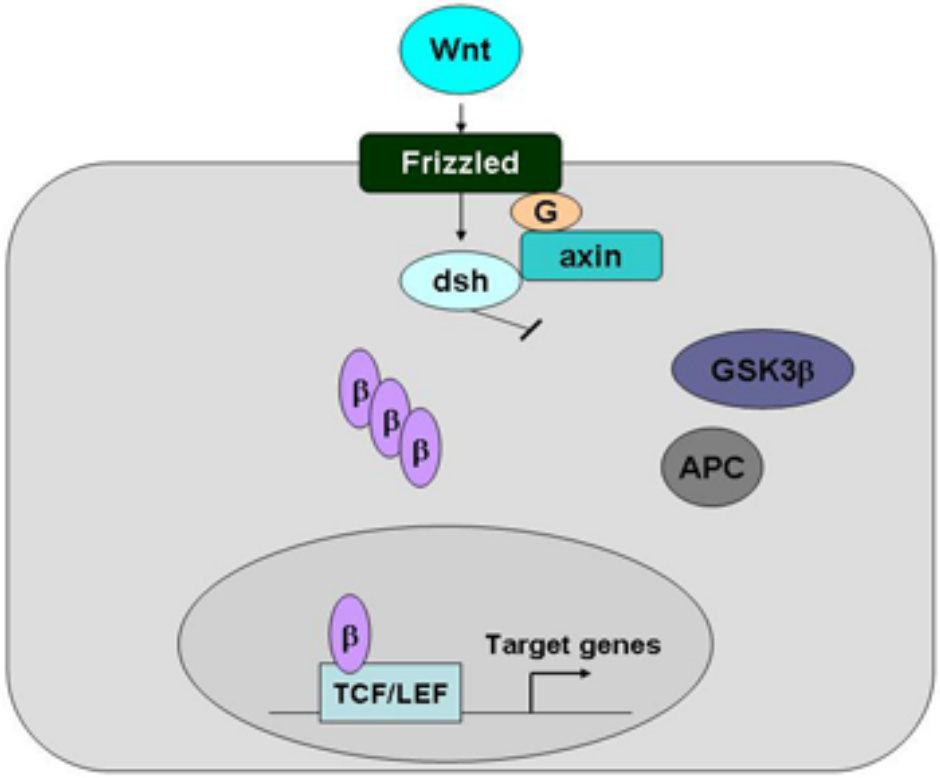

Figure 1.7 Canonical β-catenin signalling pathway.

With the presence of Wnt ligands, the "frizzled" G-protein coupled receptor is activated and induces a phosphorylation cascade involving the disheveled family proteins (dsh) which recruits axin to plasma membrane, resulting in the destruction of the degradation machinery. Therefore β-catenin escapes the phosphorylation and subsequent degradation and accumulates in cytoplasm. The active β-catenin translates to the nucleus where it interacts with transcription T-cell factor (TCF) and lymphoid enhancer factor (LEF) to cause transcription of target genes.

As a consequence, the β-catenin is increased in the cytoplasm. Which is then able to translocate into the nucleus where it can interact with the transcription factors of the TCF

family (TCF1, TCF3, TCF4 and LEF1) (Arce, Yokoyama et al. 2006). There are a large variety of transcription targets of the β-catenin/TCF or β-catenin/LEF complex including c-myc and cyclin-D1 (Behrens 2000) which are important for cell proliferation and regulation of cell cycle progression respectively (Alao, Gamble et al. 2006).

β-catenin has also been implicated in the genesis of epithelial mesenchymal transitions (EMT). This is when epithelial cells invade their basement membrane becoming invasive and mobile. The mechanism for this is thought to involve the products of some β-catenin transcription targets such as Slug and Twist, which inhibit the E-cadherin promoter; and L1, which inhibits E-cadherin. EMT is also thought important in the formation of tumor metastases (Heuberger and Birchmeier 2010).

1.4.2 The role of β-catenin in the epidermis – clues to the respiratory epithelium?

The role of β-catenin in the epidermis of mice has been well studied. This information could be useful when investigating the role of β-catenin in the trachea. In vitro, β-catenin was found to increase proliferation of epidermal stem cells by almost 90% whilst cells expressing a dominant negative mutation were found to exit the stem cell compartment entirely (Zhu and Watt 1999). These stem cells are also known to express high levels of cytoplasmic β-catenin in vivo (Lo Celso, Prowse et al. 2004).

In vivo experiments (Lo Celso, Prowse et al. 2004) using transgenic mice, which express stabilised cytoplasmic β-catenin under the control of Keratin 14 (K14) promoter, showed

that the increased cytoplasmic β-catenin induced hyperproliferation in both hair follicle and skin. Niemann et al. explored the epidermal phenotype of a transgenic mouse model which lacked the β-catenin binding site in LEF1 under the control of K14 promoter, leading to inhibition of β-catenin-dependent transcription in target cell compartment. These mice were born with normal skin, however after six weeks they began to lose hair and develop epidermal cysts. Adult mice developed spontaneous sebaceous skin tumors (Niemann, Owens et al. 2002).

These studies demonstrate that β-catenin is not a simple on/off signalling mechanism and that the level of β–catenin can regulate cell fate decision and proliferation in the epidermis.

1.4.3 The role of β-catenin in the lung

It has been demonstrated that canonical Wnt/β-catenin pathway is active in the development of the murine lung epithelium (Konigshoff and Eickelberg 2010). Mucenski et al. investigated the role of β-catenin in the developing lung by using a transgenic mouse model which expresses an activated form of β-catenin. At birth, lung morphogenesis was not seen to be affected, although in the early post-natal period the mice developed air space enlargement and epithelial cell dysplasia. In the adult transgenic mice goblet cell hyperplasia was noted and some mice developed pulmonary tumors (Mucenski, Nation et al. 2005). The same group investigated the effect of the deletion of β-catenin on the developing lung, the mice died at birth. Although the proximal airways were found to have developed normally in these mice, peripheral airway epithelium had failed to

develop correctly and resembled proximal airway epithelium (Mucenski, Wert et al. 2003).

To investigate the role of β-catenin on adult murine lower airway epithelium, Reynolds et al. used a transgenic mouse model with an activated form of β-catenin under the control of the Clara cell secretory protein (CCSP) promoter, which resulted in the increased expression of cytoplasmic β-catenin in Clara cells. In the steady state, there is no significant difference in the proliferative index of the epithelium in these mice, whilst after epithelial injury the transgenic mice were able to repair faster than the WT mice in response to the Clara cell-specific toxicant naphthalene, which may attribute to the amplification of variant Clara cells (Clara cells deficient in cytochrome P450-2F2 therefore resistant to naphthalene), thought to be bronchiolar stem cells (Reynolds, Zemke et al. 2008).

The effect of β-catenin deletion in murine bronchioles was investigated by Zemke et al. It was noted that although diffuse β-catenin signalling was present in the steady state bronchiolar epithelium of WT mice, the knockout mice showed no difference in proliferation. After airway injury, the knockout mice were able to restore their ciliated cell population to the same degree as the WT mice, so it was concluded that β-catenin was not necessary for the maintenance or repair of the murine epithelium (Zemke, Teisanu et al. 2009). However due to a relatively small sample size (n=3), this result remains inconclusive.

1.4.4 The Wnt/β-catenin pathway in cancer

Mutations in many different proteins involved in the canonical β-catenin signalling pathway have been shown to be present in a variety of human cancers. Up to 80% of colon tumors have been found to have APC mutations and in those tumors without APC mutations, almost 50% have activating β-catenin mutations (Paul and Dey 2008). Axin mutations have been shown in oesophageal squamous cell carcinoma (Nakajima, Fukuchi et al. 2003). These mutations, although occurring in different proteins of the signalling pathway, may prevent β-catenin from being phosphorylated, allowing it to enter the nucleus and act to increase the transcription of the target genes previously described – probably one step in the multi-step oncogenic process that can eventually lead to cancer formation.

In the lung, cancer cells over expressing Wnt-1 were induced to apoptose with the antibody to Wnt-1. The same antibody also suppressed tumor growth in vivo (He, You et al. 2004). It has also been shown that dishevelled overexpression is present in a number of NSCLC and this could lead to activation of β-catenin signalling and encourage tumor growth NSCLC (Uematsu, He et al. 2003). These studies serve to show the potential importance of β-catenin and Wnt signalling in the development of lung cancer.

1.5 Summary

Both EGFR and Wnt/β-catenin pathway have been demonstrated involved in human tumorigenesis; however, whether they initiate or accelerate this process remains inconclusive. Various animal experiments have investigated their role in bronchi and bronchioles epithelial repair and homeostasis (Wnt/β-catenin pathway), but the data referring to the murine upper airway, a closer model to human airway, is still rare. I therefore wished to study murine tracheal homeostasis and the role of these pathways, and examine their relevance to early lung cancer.

1.6 Hypothesis

LRIG1 plays a role in murine upper airway epithelial homeostasis by inhibiting EGFR pathway.

Wnt/β-catenin pathway regulates murine upper airway epithelial homeostasis and repair.

1.7 Aims

1. Using transgenic mice I will determine the effects of downregulated/upregulated signalling on tracheal epithelial proliferation and differentiation
2. I will manipulate the target pathways in vitro to investigate their roles in murine and

human epithelial cell proliferation and differentiation

3. Using biopsy samples of human pre-invasive lung cancer lesions I will examine the pathways relevance to cancer development

CHAPTER 2. MATERIALS AND METHODS

2.1 Cell Biology

2.1.1 General chemicals, solvents and plastic ware

All chemicals were of analytical grade or above and were obtained from Sigma Aldrich (Poole, UK) unless otherwise stated. All water used for the preparation of buffers was distilled and deionised (dH_2O), using a Millipore water purification system (Milipore R010 followed by Millipore Q plus; Millipore Ltd., MA, US). Polypropylene centrifuge tubes and pipettes were obtained from Becton Dickenson (Oxford, UK).

All sterile tissue culture media, sterile tissue culture grade trypsin/EDTA, tissue culture antibiotics and fetal bovine serum (FBS) were purchased from Invitrogen (Paisley, UK) unless otherwise stated. Sterile tissue culture flasks and plates were obtained from Nunc (Roskilde, Denmark) unless otherwise stated.

Phosphate buffered saline

8 g NaCl, 0.35 g KCl, 1.43 g Na_2HPO_4 and 0.25 g KH_2PO_4 were dissolved in 1L ddH_2O, adjusted to pH 7.2 and autoclaved.

Polybrene Stock solution

100mg polybrene powder (Sigma) was dissolved in 20 ml PBS to produce a concentration of 5 mg/ml (1000x stock). The stock solution was sterile filtered through a 0.22 mm filter, aliquoted and stored at –20^{o}C.

Tris Buffered Saline (TBS)

10x Stock solution was prepared by dissolving 24.2g Tris base and 80g NaCl in 1L dH2O. The pH was adjusted to 7.6 and the solution was sterile filtered.

Mitomycin C stock solution

Mitomycin C is an inhibitor of DNA synthesis and nuclear division. It is used to metabolically inactivate J2-3T3 cells to form a feeder layer for the culture of primary keratinocytes. A 100x stock solution was prepared by dissolving 4 mg of mitomycin C powder (Sigma) in 10 ml PBS. The final concentration used was 4 mg/ml.

Puromycin Stock solution

10 mg/ml puromycin solution (Sigma-Aldrich, p9620) was diluted in sterilised PBS, to give a concentration of 1mg/ml

2.1.2 Cultured cell types

A549 cells are Human lung adenocarcinoma epithelial cell line. H357 cells are human oral squamous cell carcinoma in nature. BEAS-2b cells are established normal human bronchial epithelial cells. iHBECs are immortalized human bronchial epithelial cells.

J2-3T3 cells were used as feeder cells for supporting epithelial cells growth. Murine tracheal epithelial cells were isolated from adult mice and grown as described below.

A549, H357 and J2 3T3 feeder cells were obtained from Cancer Research UK, London Research Institute (CRUK, London, UK). BEAS-2b cells were a kind gift from Dr. Chris Scotton in the host laboratory. iHBECs were a kind gift from Dr Gisli Jenkins (University of Nottingham) (Vaughan, Ramirez et al. 2006). AM12-empty vector (EV), AM12-LRIG1 cells were kind gifts from Dr Kim Jensen, Cancer Research UK, London Research Institute (CRUK, London, UK).

All cells were under mycoplasma screen in host laboratory on a regular basis. If any mycoplasma contamination was detected all of those cell stocks were disposed of.

2.1.3 Culture of human cells

All cells were cultured in Dulbecco's modified Eagle's medium (DMEM) with 4mM L-Glutamine, 50U/ml penicillin and 50μg/ml streptomycin and 10% (v/v) fetal bovine serum (FBS) and incubated at 37°C in a humidified, 5% CO_2 atmosphere, unless otherwise stated.

iHBECs were cultured in Keratinocyte-SFM, supplemented with L-glutamine, EGF and BPE and antibiotic. (invitrogen, #17005-075). H357 cells were cultured in a 1:3 mix of Hams F12 medium and DMEM. In addition to FBS, L-Glutamine, and antibiotics, this medium was supplemented with 10^{-10}M cholera enterotoxin (ICN Pharmaceuticals Ltd., Oxon, UK), 0.5g/ml hydrocortisone, 10ng/ml epidermal growth factor, and 5μg/ml

insulin.

Medium was changed every 3 days. Cells were grown until approximately 80% confluent and then mobilised by washing with autoclaved phosphate-buffered saline (PBS) followed by 18μl/cm^2 of 0.05% trypsin in EDTA. The H357 and iHBECs cells would not detach efficiently using this technique and hence they were washed and then incubated in Versene (invitrogen #15040-033) for 5 minutes at 37°C before trypsinisation as above. After detachment, cells were spun and passaged into tissue culture flasks at ratios of 1:3 to 1:8 every 3 – 10 days depending on rate of proliferation.

2.1.4 Freezing and thawing of cells

Cells were harvested as above then resuspended in 50% (v/v) medium, 40% (v/v) FBS and 10% (v/v) DMSO. 1ml aliquots were then frozen in each cryovial overnight at –70˚C in insulated containers. One 75 cm^2 flask was aliquoted into 3-5 cryovials. The vials were then transferred to liquid nitrogen storage. Thawing of cells was performed by transferring cryovial tubes to a 37˚C water bath. As soon as the cell suspension was thawed it was added to 10ml of medium and centrifuged at 1,000 rpm for 5 minutes. The cells were then resuspended in medium and plated onto 75 cm^2 flasks.

2.1.5 Culture of mouse tracheal epithelial cells

2.1.5.1 Media or solution

FAD 200ml

Volume	Ingredient	Final Conc.
100ml	DMEM	-
100ml	F12/kinght	
2ml	Pen/Strep	
2ml	L-glutamin	

Pronase (0.15%=1.5mg/ml); make fresh and filter: 0.0015g=1.5mg

Volume	Ingredient	Final Conc.	Source/Cat no.
15mg	Pronase I	0.15%	Boehringer no. 165921
10ml	FAD	-	-

DNase solution (0.5mg/ml) filter and store at –20^{o}C

Volume	Ingredient	Final Conc.	Source/Cat no.
10mg	Crude pancreatic DNase I	0.5mg/ml	Sigma no. DN-25
2ml	BSA stock (10mg/ml)	0.666mg.ml	-
18ml	FAD	-	-

Retinoic acid stock A $5x10^{-3}$M (dissolve in the dark);filter and store at –80^{o}C

Volume	Ingredient	Final Conc.	Source/Cat no.
50mg	Retinoic acid powder A	$5x10^{-3}$M	Sigma no. DN-25
33.3ml	95% ethanol		-

Retinoic acid stock B $5x10^{-6}$M ; filter and store at –80^{o}C, store up to 4weeks

Volume	Ingredient	Final Conc.	Source/Cat no.
50ul	Retinoic acid stock A	$5x10^{-6}$M	
500ul OR 50mg	BSA stock (10mg/ml)	1mg/ml	-
49.45ml	HBBS	-	-

MTEC/Basic (stable for 1-1.5 months)

Volume	Ingredient	Final Conc.		
200ml	FAD	-	39.24ml	19.62ml
0.8ml	0.1M $NaHCO_3$ (filter)	0.4mM	160ul	80ul
3.0ml	1M HEPES pH7.2 (filter)	0.015M	600ul	300ul

MTEC/Basic +NuSerum + RA. Use immediately once RA added.

Ingredient	Final Conc.	Source/Cat no.	Volume	
MTEC Basic	-	-	38.8ml	19.4ml
NuSerum	2%	BD no	0.8ml	0.4ml

		51000		
Retinoic Acid stock B (100x stock)	10^{-8} M	Sigma no. R2625	0.4ml	0.2ml

NuSerum must be heat inactivated for 20mins at 56C prior to use in order to get rid of complement.

MTEC/PLUS (stable 1-2 weeks)

Volume	Ingredient	Final Conc.	40ml	20ml
200ml	FAD	-	36.68ml – BPE volume	18.34ml – BPE volume
0.8ml	0.1M $NaHCO_3$ (filter)	0.4mM	160ul	80ul
3.0ml	1M HEPES pH7.2 (filter)	0.015M	600ul	300ul
0.4ml	Insulin (5mg/ml) (filter)	10ug/ml	80ul	40ul
0.4ml	TEC (filter) 500x stock	-	80ul	40ul
0.5ml	BPE current batch 11.5mg/ml	0.03mg/ml	varies	varies
10ml	FBS	5%	2ml	1ml

TEC=transferrin, EGF, Cholera toxin.

BPE= Bovine Pituitary Extract (invitrogen 13028-014)

Insulin = sigma I6634

MTEC/PLUS+RA use immediately

Ingredient	Final Conc.	20ml	40ml
MTEC/PLUS	-	19.8ml	39.6
Retinoic acid,stock B 100x stock	10^{-8} M	0.2ml	0.4ml

2.1.5.2 Isolation of primary MTECs

Mouse Tracheal Epithelial Cells (MTECs) were harvested as previously described (You, Richer et al. 2002). Mice were sacrificed by sodium pentobarbitol overdose, and then briefly immersed in 70% ethanol (avoiding airway submersion), followed by cutting open peritoneal cavity and exsanguinations. With the use of a sterile technique, tracheas were resected from the larynx to the carina. Expose trachea with vertical incision in neck, cut open ribcage and remove salivary glands. Blunt dissect (by using outside edge of scissors) under the trachea to get it loose from the underlying tissue.

Tracheas were placed in FAD medium, + Ca^{2+}, no serum and dissect away excess tissue with tweezers under microscope. Tracheas were placed in new tube with FAD containing 1.5mg/ml Pronase (Roche) for 18 hours at 4^{o}C. The tube was then put on ice, and FBS was added to a final concentration of 10%. The tracheas were inverted 10 times, transferred to another tube of FAD medium with 10% FBS, inverted again. Repeated twice for total of 4 tubes, then combined media and discard tracheas. Contents of the four tubes were pooled and collected by centrifugation at 300 g for 10mins at 4^{o}C. Cells were resuspended in 5mls DNAase solution and incubated on ice for 5mins, centrifuged at

300g for 5 mins at 4^{o}C, and then resuspended in 5ml MTEC basic media with 10% FBS. After incubation in MTECs/Basic medium (Table 2) in tissue culture plates for 2 hours in 5% CO_2 at 37^{o}C to adhere fibroblasts, nonadherent cells were collected by centrifugation, resuspended in 200ul MTEC/Plus (Table 3) per trachea, and counted. Cell viability determined by trypan blue exclusion was >90%.

2.1.5.3 Pre-coating transwell dishes

Prior to cell seeding, transwell dishes were coated collagen-coating solution (recipe as below). With lid off, dishes were allowed air dry overnight in tissue culture hood. Before cell seeding, dishes were washed with PBS and MTEC/Basic.

Collagen-coating solution; filter and store at 4^{o}C up to 4weeks

Ingredient	Final Conc.	Source/Cat no.
rat tail collagen, type 1	50 ug/ml	B/Dickinson 354236
Diluted in PBS		-

2.1.5.4 Culture of MTECs

Enzyme isolated cells were counted and seeded in 12-well Transwell dishes (Corning) at 2x10^{5} cells/well in MTEC/plus, supplemented with Retinoic Acid (RA). Media was filled in both upper and lower compartments. Cells were incubated at 37°C in a humidified, 5% CO_2 atmosphere. Media was changed on day 3 after seeding then every the other day onwards. Upon visually reaching confluence (usually day 9 post-plating), media in upper

compartment was removed and that in lower compartment was changed to MTEC/basic plus retinoic acid and Nuserum to enhance differentiation at an air-liquid interface (ALI) (You, Richer et al. 2002). Media was changed every the other day. Cells were harvested at indicated time points and subjected to immunostaining and immunoblotting. BrdU was added 3 hours before cells fixation (ZYMED 00-0103: in vitro exp concentrated reagent 1:100 in culture media). In some experiments, cells were incubated overnight with MTEC/Basic medium with no growth factors.

2.1.6 Retroviral infection of A549 and H357 cells

A549 and H357 cells were transduced with pBabePuro-Lrig1Flag and pBabe Puro-EV. Stably transduced AM12 cells were kind gift from Fiona Watt, CRUK, UK, and were cultured with 2.5 μg/ml puromycin. One day prior to transfection, target cells were plated in T75 flask to be transduced at 25-40% confluence. In the meantime, 4.5ml fresh medium was added (which the target cells grow in) to transduced AM12 cells (50-75% confluence), without puromycin, and leave it overnight. On the next day**,** virus containing supernatant was collected from AM12 flask and passed through a 0.45mm syringe filter to get rid of cell debris, followed by adding 5μg/ml polybrene to virus (from 1000 x stock). Medium in target cells was removed and replaced with virus + polybrene. Target cells with virus containing supernatant then were incubated for 24 hrs. At the due time, removed virus containing medium and rinse once with fresh medium, then added fresh growth medium without polybrene. 48 hrs after this point, cells were split 1:4 into selection medium (growth medium contained 2.0mg/ml puromycin final concentration). Selection usually took 3 days. The success of the transduction was confirmed by

immunofluorescent staining or immunoblotting with a Flag1 antibody.

Figure 2.1 Diagram below indicating LRIG-Flag subcloning into pBabePuro vector.

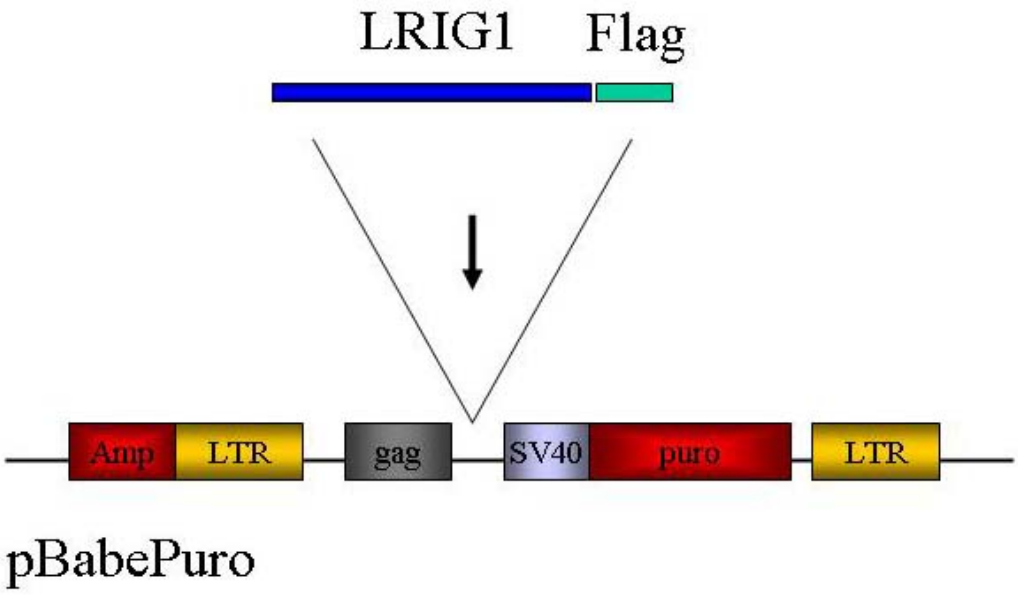

2.1.7 Manipulation of cultured cells

The inhibitors of signalling molecules used to manipulate murine epithelial cells activities are listed below.

SB415286 was administered to either MTECs on day 3 of the culture, or iHBECs at about 50% confluence, till the harvest time point. DECMA-1 was administered to MTECs right after ALI was achieved till the harvest time point.

Table of Inhibitors

Compound	**Target molecule/s**	**Working concentration**	**Source/references**
SB415286	GSK-3	10 μM. 30 μM.	Sigma (Cross, Culbert et al. 2001)
DECMA-1	Extracellular domain of E Cadherin	12 μg/ml	Abcam (ab11512) (Hordijk, ten Klooster et al. 1997)

2.1.8 Calcium-switch experiment in A549-LRIG1 cells

It has long been established that Ca^{2+} plays an important role in cell adhesion through the interaction with E-cadherin without altering protein synthesis. I used a calcium-switch technique (Tobey, Argote et al. 2004) to create an E-cadherin functional depletion model in cultured A549-LRIG1 cells. Cells were plated out in chamber slides and grown until confluence. Cells were exposed to Ca^{2+} free, EDTA containing solution for 2 hr in 5% CO2. Cells were then fixed and immunofluorescence stained (as described under relevant section).

2.2 Assays of proliferation

2.2.1 BrdU labelling cells

Human cells were cultured in chamber slides, and MTECs were cultured in transwell dishes. Cells at targeted confluence level (50%-60% confluence; or >90% confluence) were incubated with growth medium containing BrdU labelling solution (ZYMED 00-0103: 1:100 into growth medium) for either 1 hour (for human cells) or 3 hours (for MTECs). Cells were fixed with 4% PFA and ready for immonofluorescent staining.

2.2.2 Colony formation efficiency assays

300 or 500 A549, H357 and BEAS-2bs, 10,000 MTECs were plated per well in 6-well plates and cultured on a J2 3T3 feeder layer. After 14 days growth, feeder cells were washed off with PBS and versene, then fixed with 3% (w/v) paraformaldehyde (PFA) and followed by staining with 1% Rhodamine Blue for 20 minutes. The number of colonies 2mm or larger in diameter were counted and expressed as a percentage of the original 100 cells plated to give the percentage colony forming unit (Reynolds, Zemke et al. 2008)..

Preparation of J2-3T3 cells as feeder cells

The colony formation efficiency assay requires co-cultivation with mitotically inactive J2-3T3 cells which are referred to as feeder cells (Rheinwald and Green, 1975). Feeder cells were incubated with 4μg/ml mitomycin C for 2-3 hrs at 37˚C. Cells were then harvested and plated onto flasks as described earlier. Cells from a confluent 75 cm2 flask were placed onto one 12-well plate. J2-puro cells were used as feeder cells during colony forming assay.

2.2.3 Flow cytometric cell cycle analysis

One of the obvious features of the cell cycle is the synthesis and duplication of nuclear DNA before division. By measuring DNA content in cells with 4',6'-diamidino-2-phenylindole (DAPI) staining and deconvolution of the cellular DNA content frequency histograms, this approach reveals distribution of cells in three major phases of the cycle (G1 vs S vs G2/M).

This experiment was performed by Dr Adam Giangreco. The following method used for DAPI staining is modified from (Giangreco, Jensen et al. 2009).

Cell pellet was suspended in 1 mL of DAPI staining solution (0.1% (v/v) Triton X-100 and 1 μg/mL DAPI in PBS). Samples were kept in the dark, at room temperature, for 10 min. Samples were transferred to the flow cytometer and measure cell fluorescence.

Maximum excitation of DAPI bound to DNA is at 359 nm, and emission is at 461 nm.

For fluorescence excitation, use the available UV light laser line at the wavelength nearest to 359 nm. When a mercury arc lamp serves as the excitation source, use a UG1 excitation filter. A combination of appropriate dichroic mirrors and emission filters should be used to measure cell fluorescence at wavelengths between 450 and 500 nm.

All data was obtained using an LSR II flow cytometer (BD Biosciences) and analyzed with Flowjo.

2.3 Animal experiments

2.3.1 Animals

2.3.1.1 Mouse husbandry and experimentation

Adult, 2-4 month old mice (or 2-6 month old mice for β-catenin experiment) were used for experiments, housed in individually ventilated cages on a 12 hour light / dark cycle and allowed access to food and water ad libitum. All in vivo experiments involved a minimum sample size of 5 animals per group, were repeated at least twice, and were performed under the terms of a UK Home Office project license.

2.3.1.2 Lrig1 experiments

Lrig1-null mice were a kind gift from Sathoshi Itami (Suzuki, Miura et al. 2002). All transgenic mice were maintained on a mixed background of 129, C57/Bl6, and CD1 inbred strains. Homozygote deleted LRIG1 mice were compared to sex-matched littermate heterozygote LRIG1 mice as controls.

2.3.1.3 β-catenin experiments

Transgenic K14-dnLef1 and K14-Δ β-cateninER mice were provided by Prof. Fiona Watt and generated as previously described (Niemann, Owens et al. 2002); (Silva-Vargas, Lo Celso et al. 2005);(Lo Celso, Prowse et al. 2004). TOPgal β-catenin reporter mice were obtained from a commercial vendor and generated as previously described (DasGupta and Fuchs 1999) (Jackson Labs, Maine). All transgenic mice were maintained on a mixed background of 129, C57/Bl6, and CD1 inbred strains.

K14-Δ β-cateninER mice

These mice express a mutated form of β-catenin which has a truncated N-terminal, this prevents it from being phosphorylated by the degradation machinery previously discussed. This truncated form of β-catenin is under the control of the cytokeratin-14 (K14) promoter and is fused to the ligand binding domain of a mutant oestrogen receptor. The transgenic mice therefore express normal β-catenin at normal levels until the transgenic region is activated by the binding of 4-hydoxytamoxifen (4OHT) to the mutated oestrogen

receptor. As a consequence, a large amount of stabilized β-catenin is expressed. The D2 mouse has a copy number of 12Δ β-cateninER whilst the D4 mouse has a copy number of 21.

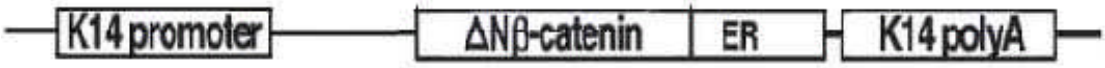

Figure 2.2 Diagram representing the K14 expression cassette and ΔNβ-cateninER transgene. (Adapted from Lo Celso et al 2004)

K14-dnLef1 mice

An N-terminally deleted mouse Lef1 cDNA (lacking amino acids 1 to 32, which contain the β-catenin-binding site) was Myc-tagged at the N terminus and inserted into the blunt ended *Bam*HI site of the keratin 14 expression cassette. The resulting construct was designated K14-dNLef1, which lacks the β-catenin binding site, under the control of the K14 promoter. These transgenic mice therefore overexpress dNLef1in K14-positive cells, leading to inhibition of β-catenin-dependent transcription in target cell compartment.

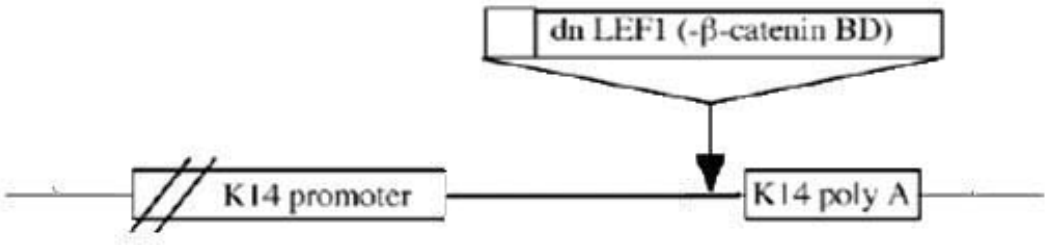

Figure 2.3 Diagram showing the K14-dnLef1 transgene construct.
(Adapted from Catherin Niemann1 et al 2002)

TOPgal reporter mice

These TOPgal transgenic mice are a reporter strain that express beta-galactosidase in the presence of the lymphoid enhancer binding factor 1/transcription factor 3 (LEF/TCF) mediated signaling pathway and activated β-catenin. They were maintained on an outbred CD1 background.

Figure 2.4 Diagram showing TOPgal construct

The promoter contains three consensus LEF-1/TCF-binding motifs (L) and a minimal c-fos promoter to drive transcription of the lacZ gene encoding β-galactosidase.

2.3.1.4 Acute Tracheal epithelial injury model

For experiments involving tracheal repair, mice were anaesthetised with isofluorane and tracheas damaged via oropharyngeal instillation of 15 µl 2% polidocanol (Sigma, UK). BrdU was injected intra-peritoneally (Zymed 00-0103; 100ml concentrated reagent per 10g body weight, intra-peritoneally, 2 hours pre sacrifice). For β-catenin experiment, tamoxifen (solution 40mg/ml in corn oil) was injected intra-peritoneally (5mg per 20g body weight) daily for 3 days before polidocanol was administered.

2.3.2 Genotyping of transgenic mice

2.3.2.1 Ear snip digestion

Mice ear snip samples were added into 50ul buffer as below and digested at 55^{o}C. After 1 hour samples were vortexed and further digested for 2 hours. Then 150µl double distilled water was added, and heated in a hot block to inactivate protein kinase at 95^{o}C for 10mins. Samples were then taken through one freeze/thaw cycle, mixed and spun for five minutes at 13000 rpm to move debris to the bottom. 1µl sample was used per PCR reaction.

Ear Snip Buffer:

1M Tris pH 8.0	1.25 ml
5M NaCl	0.1 ml
10% SDS	0.25 ml
H_2O	22.4 ml

(Protein kinase at 20mg/ml; Add 40µl to 960µl of ear buffer mix)

2.3.2.2 PCR conditions

Primers

Primer Target		Reference	Primer Sequence	Amplicon
D4	5	(Lo Celso, Prowse et al. 2004)	ATGCTGCTGGCTATGGTCAG	700bp

D4	3	(Lo Celso, Prowse et al. 2004)	GCACACAAACTCTTCACC	
dnLef1	5	(Niemann, Owens et al. 2002)	GCTTTCCTTCATCAGGGTG	400bp
dnLef1	3	(Niemann, Owens et al. 2002)	CTCTGAGTCCAAACCGGGC	
Topgal	5	(Zemke, Teisanu et al. 2009)	GTGGCAGCATCAGGGGAAAACCTT	476bp
Topgal	3	(Zemke, Teisanu et al. 2009)	GAATTCCGCCGATACTGACGGGCT	

PCR Ingredients

Ingredient	Stock conc	Quantity (µl)	Final Conc
Ear snip DNA	-	1	-
MgCl2	25mM	Varies 2-5mM	Varies 2-5mM
dNTPs	25mM	2.5µl	2.5µM
Buffer	10x	2.5	1x
5’ primer	10µM	0.5	0.2nM
3’ primer	10µM	0.5	0.2nM
Taq Bioline	5U/µl	0.2	-
H20	-	Up to 25µl total	-

D4 PCR programme

Add 2µl MgCl stock per 25µl reaction system.

1	94C	4’
2	94C	30’’
3	54C	30’’
4	72C	45’’
5	REPEAT 2-4	x32
6	72C	3’
7	15C	10'

Dnlef1 PCR programme

Add 1.5µl MgCl stock per 25µl reaction.

1	94C	2’
2	94C	45’’
3	57C	45’’
4	72C	40’’
5	REPEAT 2-4	x32
6	72C	2’
7	15C	10'

2.3.2.3 Agarose gel electrophoresis

Gel separation electrophoresis was used to confirm the products were of the expected size. The gel was prepared by dissolving 1.5% agarose (w/v) in 100 ml 1xTBE (0.045 M Tris-Borate, 0.001M EDTA, pH 8). Ethidium bromide was added to the gel at a final concentration of 0.5µg/ml). The gel, once solidified, was placed in a gel tank filled with

1xTBE running buffer. 2µl of 5 x loading buffer was mixed with 8µl of each PCR product and run on a lane of the gel. A DNA molecular marker (marker VIII, 0.25µg/ml, Boehringer Mannheim) was also used. The gel was run for 35 minutes at 80 volts. The DNA bands were visualised using a phospho-imager (Fuji, FLA-3000)

2.3.3 Assays of differentiation

2.3.3.1 Fluorescence Microscopy

Cultured primary MTECs start differentiation after ALI achievement. Differentiated MTECs were washed with PBS and fixed with 4% PFA for 10 minutes. Transwells were stored in PBS at $4^{o}C$ for immunofluorescent staining against epithelial cell markers. Details as described in immunological section.

Murine tracheal tissues were fixed, sectioned and immuno-stained against epithelial cell markers. Details as described in immunological section.

2.3.3.2 Flow cytometry

Single cell suspensions were derived from mouse tracheas after overnight 0.1% pronase digestion at 4°C and resuspened in DMEM+10%FBS to $1x10^{6}$ cells/ml and stained for epithelial and immune cell markers including CD45, EpCam, and GSI-β4 lectin. Briefly, cells were incubated with primary antibody in DMEM+10%FBS for 30 minutes on roller in cold room. Cells were then washed in PBS and incubated with secondary antibody in

DMEM+10%FBS for 30 minutes on roller in cold room. Cells were washed with PBS, filtered through 70mm cell strainer and DAPI added. as previously described (Rock, Onaitis et al. 2009; Teisanu, Lagasse et al. 2009; McQualter, Yuen et al. 2010). Dead cells were excluded on the basis of DAPI reactivity and epithelial and basal cells identified based on cell surface EpCam and GSI-β4 lectin expression. TOPgal activity was detected by fluorescein di-β-D-galactopyranoside (FDG) staining as previously described (Rakhmanova and MacDonald 1998).

All data was obtained using an LSR II flow cytometer (BD Biosciences). Electronic compensation of the recording was performed to minimise overlap of emission spectra. Samples were gated according to forward scatter and side scatter characteristics to exclude cell debris and cell doublets. A minimum of $1x10^5$ gated events was collected for each sample analysed. Sample analysis and quantitation was performed using FlowJo Software.

Single stained controls were used to set compensation parameters and unstained samples used to set negative gates.

2.4 Immunological Methods

2.4.1 General solutions

Paraformaldehyde solution

A 10 % solution was prepared by adding paraformaldehyde powder (BDH) to PBS and heating at 60^0C until mostly dissolved. A few drops of 1M NaOH were added to completely clear the solution which was then allowed to cool to room temperature before adjusting the pH to 7.6 with HCl. The stock was aliquoted and stored at -20^0C. A 4 % paraformaldehyde solution was used to fix cells and tissue.

Formol saline

50g NaCl and 150g Na_2SO_4 were dissolved in 8L of dH_2O before addition of 1L of 40 % formaldehyde. The final solution was made up to 10L and was not autoclaved.

DAPI stock solution

DAPI powder (sigma, D9542) was dissolved in ddH2O to give concentration of 1mg/ml. Solution was aliquoted and stored at -20^oC.

2.4.2 Tissue preparation

Mice were sacrificed by sodium pentobarbitol overdose and sentinel screening for common murine pathogens were used throughout the course of these studies. Murine tissue sections were fixed in 4% paraformaldehyde at 4°C. After 4 hours, samples were transferred to 15% (w/v) sucrose in PBS and stored overnight at 4°C. Samples were then washed in 30% (v/v) ethanol and transferred to 70% (v/v) ethanol. The samples were then dehydrated through graded ethanols and embedded in paraffin wax. 3μm sections were cut from paraffin embedded specimens and mounted on polylysine slides (VWR, Leicestershire, UK) for staining. Some samples were snap frozen in OCT. 5-7μm sections were cut from OCT embedded specimens and mounted on polylysine slides.

Human biopsy samples were obtained via fibre optic bronchoscopy with patient consent under institutional ethical approval by my supervisor Dr Janes or his clinical team. Tissue sections were fixed in 10% neutral buffered formalin or 4% paraformaldehyde, processed and sectioned at 4μm thickness. All human biopsy specimens were subjected to routine histopathological diagnosis by two consultant lung histopathologists.

2.4.3 Antibodies

The primary antibodies used for immunohistochemical localization studies were Lrig1 (rabbit; kind gift from F. Watt, CRUK, Cambridge), K14 (Rabbit, ABR Biosystems), K14

(LL002) (mouse IgG3; kind gift from F. Watt, CRUK, Cambridge), CCSP (goat, gift from B. Stripp, Pittsburg University, USA), acetylated-tubulin (mouse, Sigma), Ki67 (Vector Laboratories), Ki67(Abcam), BrdU (ICR1) (AbDserotec), ECCD1 (Sigma), or HECD1 (gift from F. Watt, CRUK, UK), flag1 (Sigma), phospho-EGFR1 (Zymed), EGFR1 (Abcam), ZO-1 (rabbit, Sigma), and Cyclin D1 (rabbit, Abcam), Muc5AC, β-catenin (rabbit, Abcam). Secondary antibodies conjugated to HRP, Alexa555, Alexa633 or Alexa488 (invitrogen).

Antibody	**Specificity**	**Dilution**	**Species**	**Source**
Lrig1	Lrig1 (Ms)	IF 1:600	Rabbit	CRUK
Lrig1		IF 1:		
K14	K14 (Ms)	IF 1:1000 IHC 1:5000	Rabbit	ABR Biosystems
K14 (LL002)	K14 (Ms)	IF 1:500	Mouse	CRUK
CCSP	CCSP (Ms)	IF/IHC 1:10000	Goat	B.Stripp
acetylated-tubulin	acetylated-tubulin (Ms)	IF 1:4000 IHC 1:8000	Mouse	Sigma
Ki67	Ki67 (Hu)	IHC 1:1000	Rabbit	Vector Laboratories
Ki67	Ki67 (Hu, Ms)	IF/IHC 1:200	Rabbit	Abcam
BrdU	BrdU	IF/IHC 1:150	Mouse	AbDserotec
ECCD1	E-cadherin (Ms)	IF 1:500	Rat	Sigma

HECD1	E-cadherin (Hu)	IF 1:1000	Ms	CRUK
Flag1 (M1)	Anti flag fusion proteins	IF 1:1000	Ms	Sigma
phospho-EGFR1	Anti phospho-EGFR1	IF 1:1000	Rabbit	Zymed
ZO-1	Anti-ZO-1 (Hu)	IF 1:1000	Rabbit	Sigma
Cyclin D1	Anti Cyclin D1 (Hu, Ms)	IF 1:500	Rabbit	Abcam
β-catenin	Anti- β-catenin (Hu, Ms)	IF 1:200	Rabbit	Abcam
EGFR1	Anti-EGFR (Hu, Ms)	ICC 1:500	Mouse	Abcam

2.4.4 Immunohistochemistry

Human and murine haematoxylin and eosin (H&E) staining was performed using an automated staining system (TissueTek).

2.4.4.1 Immunoperoxidase technique

For immunohistochemical staining, 3μm sections were dewaxed and rehydrated by immersion in xylene followed by decreasing concentrations of ethanol through to water. They were then washed twice in PBS. To unmask antigenic epitopes, sections were pre-treated by immersion in 0.01M sodium citrate and microwave heating at high power

for two consecutive periods of ten minutes. Pre-treated sections were then washed twice in PBS. Endogenous peroxidise was blocked by immersing sections in 3% (v/v) H_2O_2 for 30 minutes at room temperature. Sections were then washed twice in PBS and treated with a 1 in 6 solution of serum (matching that in which the secondary antibody was raised e.g. goat serum for a goat anti-rabbit secondary antibody) in PBS containing 4 drops/ml of Avidin block (Vector Laboratories) for 20 minutes at room temperature. Samples were then drained before addition of primary antibody in 1% (w/v) BSA in PBS with 4 drops/ml of Biotin block (Vector Laboratories) overnight at 4^{o}C. Appropriate isotype controls were used for each experiment. Samples were washed twice in PBS then treated with a 1:200 dilution of biotinylated secondary antibody (Dako) in PBS 1% (w/v) BSA for 1 hour at room temperature. Samples were rewashed in PBS before the addition of 1:200 Streptavadin HRP (Dako) in PBS for 30 minutes at room temperature. Sections were washed in PBS again, before 3,3-Diaminobenzidine (DAB) peroxidise substrate (Vector Laboratories) was added for 10 minutes at room temperature. Samples were drained, rinsed in dH_2O, counterstained with Gill's Haematoxylin, dehydrated in Xylene and mounted on a coveraid system (Sakura Firetek, CA, US). Microscopy was performed with an Olympus BX 40 light microscope.

The optimal pre-treatment regimen and primary antibody concentration was determined by performing a titration with each antibody with suitable positive and negative controls. This consisted of a range of antibody concentrations, including the recommended dilution, and different antibody unmasking pre-treatments including no pre-treatment, 10μg/ml Proteinase K, or microwave heating in citrate buffer. These sections were then immunohistochemically stained and the optimal conditions selected. The microwave heating in citrate buffer was used for pre-treatment for all the primary antibodies, unless

otherwise stated.

2.4.4.2 Immunofluorescence staining– sections

For immunohistochemical staining, 3μm sections were dewaxed and washed 3 times in PBS. Sections then were blocked in 10%FBS/0.2% fish gel/PBS solution for 1 hr. Samples were then drained before addition of primary antibodies in blocking solution overnight at 4^{o}C. Appropriate isotype controls were used for each experiment. Samples were washed twice in PBS then treated with secondary antibodies (1:500) for 3 hrs at room temperature. The slides were then wash in PBS and counterstained with 1μg/ml DAPI for 10 minutes. Slides were washed twice in distilled water before mounting with Immu-mount (Thermo Electron Corp., PA, US).

Images were acquired using a Leica TCS Tandem or SPE confocal or an Olympus brightfield microscope. Confocal images were imported into Volocity software (Perkin Elmer) for accurate measurement of intensity. Four representative z-stack images acquired with a 40x objective were analysed for each of three animals in Lrig-null and Het groups. All images were post-processed using Adobe Photoshop (Photomerge, rotate, crop, brightness and contrast adjustments). Epithelial height and cell density were determined using Volocity image analysis software. I quantified the abundance of specific tracheal cell phenotypes as a function of epithelial basement membrane length. Cell surface E-cadherin abundance was quantitated as previously described (El-Bahrawy, Talbot et al. 2002).

2.4.4.3 Immunofluorescence staining – cells

For staining of ex-vivo cells, the cells were cultured onto tissue culture plastic microscope slides (Nunc). They were fixed with 4% (w/v) PFA for 10 minutes at room temperature, washed 3 times in PBS, and permeabilised with 0.2% (v/v) Triton X-100 in PBS for 5 minutes if required. The cells were then blocked with PBS containing 10% (v/v) FBS and 0.2% (v/v) fish gel, before application of the primary antibodies diluted in the blocking solution overnight at 4^{o}C. After 3 washes, the fluorescent secondary antibodies were applied for another 3 hours. The cells were then rewashed and 1μg/ml DAPI applied and mounted with Immu-mount. Images were acquired and analyzed as previous describe.

2.4.4.4 BrdU cyto-immunostaining

Cells labelled with BrdU were fixed with 4% PFA for 10 minutes, and washed in PBS. Samples were permeablised with 0.2% Triton X-100 for 5 minutes, then washed in PBS. Samples were fixed again with 3.7% formaldehyde (concentrate formaldehyde 1:10 in PBS) for 10 minutes, then washed in PBS. Slides were denatured DNA by incubating sections in 2N HCL for 30 minutes at room temperature, followed by neutralising the acid with 0.1M borate buffer (pH8.5) for 2x5 minutes. Slides were washed with PBS, and blocked, stained as above described.

Solutions for BrdU cytoimmunostaining

2N HCl

10N HCl	20ml
ddH_2O	80ml

mix well

0.1M Borate Buffer, pH 8.5

Sodium borate (MW 381.4)	3.8g
ddH_2O	100ml

mix to dissolve and ajust pH to 8.5

2.5 Immunoblotting

2.5.1 Reagents

RIPA buffer	500ml
1x PBS	500ml
1% Igepal CA-630	5ml
0.5% Sodium deoxycholate	2.5ml
0.1% SDS	0.5g

10ml aliquot and freeze in -20°C.

1.5M Tris-base pH 6.8 and 8.8

181.71g TRIS made up to 1L in ddH2O.

pH with HCl.

Laemmli Buffer (x5)

312.5 mM TRIS pH 6.8	3.125ml
10% SDS	1g
20% glycerol	2ml
50mM DTT	0.5ml (add just before use)
bromophenol blue	add until dark blue

make up to 10ml with ddH20

Running Buffer (X10)

0.25M TRIS base	30.3g
1.92M Glycine	144g
1% SDS	10g

make up to 1L in ddH20

Transfer Buffer (10X) without methanol:

Glycine	2.93g
Tris	5.81g
SDS	0.375g

make up to 1L in ddH20

TBS (X10)

24.2g TRIS base

80g NaCl

make up to 1L in ddH20 and pH to 7.6 with HCl

Stripping Buffer

10% SDS	8ml
1M TRIS pH6.8	2.5ml
ß-mercaptoethanol	280ul

Make up to 40ml with ddH20.

2.5.2 Sample collection and preparation

Cells were grown in 12-well plates to reach confluence. Cell lysates were obtained by lysing the cells with 100µl RIPA buffer supplemented with complete protease inhibitor cocktail (Complete-mini; Roche Diagnostics Ltd.) and phosSTOP phosphatase inhibitor (PhosphoSafe™ Extraction Reagent Novagen). The cell layer was subsequently scraped with a pipette tip and the lysate centrifuged (13,000 rpm, 5 mins, 4°C) to remove insoluble cell debris. The supernatant was collected and the DNA sheered by passing the sample 15 times through a 25G needle. Samples were stored at -80 °C.

2.5.3 BCA protein assay

To ensure equivalent amounts of protein were loaded for the different samples, protein concentration of cell lysates or supernatants was assessed using the bicinchoninic acid (BCA) protein assay (Thermo Fisher Scientific, IL, US). 20µl of each sample or standard (bovine serum albumin (BSA)) was added to 200µl of BCA working reagent in a 96-well plate. The plate was agitated on a plate shaker for 30 seconds, and then incubated at 37°C for 30 minutes prior to reading the absorbance at 550nm on a Titertek Multiscan MCC/340 plate reader (Labsystems, Turku, Finland). The absorbance of the samples was compared to the standards (of known protein concentration) to ascertain the sample protein concentration.

2.5.4 SDS-PAGE

Equal amounts of protein from each sample (typically 10-20 mg total protein) were diluted into 5x Laemmli Buffer. 10ul 1M DTT was added to 190ul Laemmli buffer (final DTT concentration = 50mM) unless otherwise stated. The samples were then incubated on a heat block for 5 minutes at 100°C and placed on ice prior to loading on the western blot gel. The table below describes the gel compositions. Immediately after pouring the resolving gel solution, dH2O was carefully applied to level the surface. Gels were allowed to set at room temperature for approximately 30 min. The dH_2O layer was discarded from the top of the resolving gel and the stacking gel solution was then poured. An 8 or 12 well

comb was inserted to create wells and the gel was left to polymerise. After the gel had set, the comb was removed and the wells were flushed with SDS-PAGE running buffer. After being briefly spun down in a bench top centrifuge, samples were applied to the wells using capillary pipette tips. 5µl of SeeBlue® Plus 2 protein ladder (Invitrogen) was also loaded. The gel was run at 100V in Tris/Glycine/SDS running buffer until the dye front had run off the bottom of the gel and the gel was then removed and prepared for Western blot.

Table Preparation of Tris-glycine SDS-Polyacrylamide Gel (SDS-PAGE)

Resolving gel (15ml)

Concentration	6%	8%	10%	12%
30% acrylamide mix (ml)	3	4	5	6
1.5M Tris (pH8.8) (ml)	3.75	3.75	3.75	3.75
10% SDS (ml)	0.15	0.15	0.15	0.15
10% ammonium persulphate (ml)	0.15	0.15	0.15	0.15
TEMED (ml)	0.012	0.009	0.006	0.006
ddH_20 (ml)	7.95	6.95	5.95	4.95

S*tacking gel (10 ml)*

30% acrylamide mix (ml)	1M Tris (pH6.8) (ml)	10% SDS (ml)	10% ammonium sulphate (ml)	TEMED (ml)	ddH_20 (ml)
1.7	1.25	0.1	0.1	0.01	6.8

2.5.5 Western Blotting

Following separation, the gel was removed from the cassette and proteins were transferred onto a Hybond-ECL nitrocellulose membrane (GE Healthcare), using a horizontal semi-dry transfer method (NovaBlot; Pharmacia LKB, Uppsala, Sweden) with 2x transfer buffer with 20%(v/v) methanol at a current of 0.8mA per cm^2 of gel, for 1 hour. The quality of protein transfer was assessed by briefly staining the membrane with 0.1% (w/v) Ponceau solution and then the blot was placed in Tris-buffered saline (TBS) containing 0.1% (v/v) Tween20 (TBST).

Blots were incubated with blocking buffer containing 5% (w/v) non-fat dry milk in TBST for 1 hour at room temperature to block non-specific binding of antibodies.

Blots were then incubated with primary antibodies in 5% (w/v) BSA in TBST overnight at 4°C with gentle agitation. All blots were then washed 3 x 5 mins in TBST and incubated for 1 hour at room temperature with HRP-conjugated secondary antibody diluted 1:2000 in 5 % milk, TBST. Membranes were then washed 3 or 4 times with TBST. To detect bound HRP, 1ml of ECL reagent (GE Healthcare) was applied to each membrane, and incubated for 1 minute. Excess reagent was drained off and immunoreactive bands were visualized by exposing the membrane to autoradiography film (Hyperfilm, GE Healthcare), for between 30 seconds and 5 minutes. If blots were to be re-probed they were stripped in striping buffer for 30 min at 60^oC water bath with gentle agitation. Blots were then washed 3 times for 5 min each with TBST before re-blocking and subsequent

incubation with another primary antibody.

2.5.6 Antibodies

Antibody	Mol Wt	Dilution	Species	Source
GSK3b--pSer9	46 kDa	1:1000	Rabbit	Sigma
EGFR(1005)	175 kDa	1:1000	Rabbit	Santa Cruz
Phospho-EGFR (Y1086)	175 kDa	1:1000	Rabbit	Zymed
acetylated-tubulin	55 kDa	1:1000	Mouse	Sigma
HECD1	135 kDa	1:1000	Mouse	CRUK
Flag (M1)	Relevant to the fusion protein	1:1000	Mouse	Sigma
Phospho-ERK1/2	44, 42 kDa	1:4000	Rabbit	Cell signalling
ERK 1/2	44, 42 kDa	1:1000	Goat	Santa Cruz
Phosphor-Akt (Ser 473)	60 kDa	1:1000	Mouse	Cell signalling
b-actin	42 kDa	1:10000	Mouse	Sigma

2.6 Immunoprecipitation

When cultured cells reached a certain level of confluence (50% or 90%), lysates for immunoprecipitation were prepared by scrapping cells into ice-cold NP40 buffer (20 mM Tris HCl pH 8, 137 mM NaCl, 10% glycerol, 1% Nonidet P-40 (NP-40), 2 mM EDTA, supplemented by complete protease inhibitor) 0.5ml/T75, then on an agitator for 30 minutes at 4^{o}C, and followed by centrifugation at 12000rpm, 20 minutes at 4^{o}C. The supernatant was aspirated and placed in a fresh tube on ice, followed with BCA assay. Equal amount of protein samples were cultured with either EGFR (Rabbit, Santa Cruz, SC-03. 1mg/300mg total protein), or HECD1 (Mouse, CRUK, 0.6mg/ml. 1ml/200mg total protein), or relevant isotype antibodies, over night on agitation at 4^{0}C. Each sample then was baited with 30ml protein A (for rabbit IgG) or G (for mouse IgG) (made into 100ml beads slurry with PBS for each IP reaction), followed by agitation for 4h, at 4^{0}C. Lysate-beads mixture was then centrifuged to precipitate targeted protein and remove supernatant. After three times wash in lysis buffer, 20ml of 5x lamemli buffer was added to each sample, and then boiled at 100^{0}C for 5 minutes. Samples were stored at –20^{0}C, ready for western blot. For longer storage, stored at –80^{0}C.

2.7 In Situ Hybridisation assay

In situ probes were generated from Lrig1 cDNA as described previously (Suzuki, Miura et al. 2002). Hybridisation with a β-actin antisense probe served as a positive control and

was performed as described previously (Suzuki, Miura et al. 2002). This assay was performed by Richard Poulsom at the CRUK London Research Institute.

2.8 Real-time RT-PCR analysis

In order to minimise degradation of RNA, all reagents were made with molecular biology grade DEPC-treated deionised water (Ambion, TX, USA). All equipment was cleaned thoroughly using RNaseZap and nuclease free pipette tips (Continental Lab Products, CA, US) were used for all procedures involving RNA.

2.8.1 RNA extraction

2.8.1.1 Preparation of lysates from adherent culture cells

RNA was isolated from MTECs, A549, H357 and BEAS-2b cells was isolated from cultured or freshly isolated human and murine tracheal epithelial cells using a commercially available SV RNA isolation kit (Promega).

Cells were detached in trypsin-EDTA solution, then were collected in a sterile centrifuge tube by centrifugation at 500x *g* for 5 minutes, and the supernatant discarded. After adding 175 ml of RNA Lysis Buffer to up to $1x10^6$ cells (Passing through a 20 – gauge needle would be required for $1x10^6$~$5x10^6$ cells in order to shear the genomic DNA). Lysates were stored at -80^oC before use.

2.8.1.2 Preparation of lysates from tissue samples

For real time qRTPCR, tracheas were removed and immediately snap frozen in liquid nitrogen. Each sample was then pulverised into a fine powder under liquid nitrogen and then immediately transferred to the tube containing 175ml of RNA Lysis Buffer. Lysates were stored at -80°C before use.

2.8.1.3 RNA purification by centrifugation

350ml of RNA Dilution Buffer was applied to the lysates. The lysates were mixed and then placed in a heating block at 70^{o}C for 3 minutes, followed by centrifugation at 12,000-14,000 x *g* for 10 minutes at room temperature. The cleared lysates were transferred to a fresh microcentrifuge tube by pipetting, then 200ml 95% ethanol added and mixed. The mixture was transferred to the spin column assembly before centrifugation at 12,000-14,000 x *g* for one minute. The liquid in the collection tube was discarded, and 600ml of RNA Wash Solution was applied to the spin column assembly before another centrifugation at 12,000-14,000 x *g* for one minute. 50ml of freshly prepared DNase incubation mix combing 40ml yellow core buffer, 5ml 0.09M MnCl2 and 5 ml of DNase I enzyme was applied to each sample in the collection tube. After gentle pipetting, the mixture was incubated for 15 minutes at room temperature. 200ml of DNase Stop Solution was added, followed by centrifugation at 12,000-14,000 x *g* for one minute. The samples were then washed twice in RNA Wash Solution before centrifugation at high speed. 100ml nuclease-free water was added to each sample and the elution containing purified RNA was collected in the elution tube by centrifugation. RNA samples were

stored at -80^{o}C.

2.8.1.4 RNA Isolation from human biopsies and LASER capture microdissection

RNA from carcinoma in situ (CIS) lesions and a normal area of epithelium was LASER micro-dissected from formalin fixed, paraffin embedded (FFPE) tissues from 10 patients. Briefly, multiple sections of each sample were cut, with the first and last in a series stained with H&E for inspection by two lung pathologists. After confirming the diagnosis, the samples were LASER capture microdissected using the Zeiss Palm Microbeam system (Carl Zeiss). RNA was extracted from both microdissected CIS and normal lung epithelium FFPE tissues using the RNeasy FFPE kit (Qiagen). This experiment was performed by Dr Vitor Hugo Teixeira.

Total RNA was DNase-treated to remove contaminating genomic DNA using an Ambion DNA-free kit. This kit uses DNase I to nonspecifically cleave genomic DNA into 5' phosphorylated oligonucleotides. The 17µl isolated total RNA was added to 2µl DNase buffer, and 1µl DNase I reagent, vortexed, and incubated for 20 minutes at 37°C. The reaction mixtures were placed on ice, and 2µl inactivation resin, which binds DNase I, was then added. The tubes were vortexed and incubated at room temperature for 1 minute, before centrifugation at 2300g for 2.5 minutes at 4°C to pellet the inactivation resin. The supernatant containing the RNA was removed to fresh tubes without disturbing the DNase inactivation resin, which was then discarded.

The quantity of RNA was assessed using the Ultrospec 3000 spectrophotometer by measuring the A_{260}, as described previously with DNA quantification. The yield of RNA

(µg/ml) was calculated by A_{260} x 40 x dilution factor, which is based on the assumption that A_{260} = 1 for a 40µg/ml solution. The quality of the RNA was then assessed by running samples on an agarose gel. Samples were prepared as 1µl total RNA dissolved in 11µl DEPC-treated water, with 3µl loading buffer (48% (v/v) deionoised formamide (Invitrogen), 6% (v/v) formaldehyde (BDH), 5% (v/v) glycerol, 0.1% (v/v) ethidium bromide 20 mM MOPS, 5 mM sodium acetate and 1 mM EDTA pH 8.0 made up in DEPC-treated water and dyed with bromophenol blue). Each RNA sample was heated to 65°C for 5 minutes and placed on ice prior to loading. The RNA was separated through a 1.5% agarose-formaldehyde gel (6% (v/v) formaldehyde, 1.5% (w/v) agarose, 20mM MOPS, 5mM sodium acetate, 1mM EDTA, pH 8.0, made using DEPC–treated water) at 80mV for 45 minutes. RNA images were then visualised using a UV transilluminator as with the DNA previously. A ratio of approximately 2:1 of the intensities of the 28S rRNA to the 18S rRNA bands was taken as confirmation that the RNA was not significantly degraded.

2.8.2 cDNA synthesis

Complementary DNA (cDNA) was prepared by reverse transcription using qScript™ cDNA Supermix kit from Quanta Biosciences. 100ng ~1µg total RNA of each sample was added to a reaction mix of 4 ml 5x qScript Cdna supermix (containing optimized concentrations of $MgCl_2$, dNTPs, recombinant RNase inhibitor protein, qScript reverse transcriptase, random primers, oligo (dT) primer and stabilizers), RNase/DNase-free water, in a 20µl reaction volume. The mix was incubated at room temperature for 5 minutes, 42°C for 30 minutes, 85°C for 5 minutes, and then 4°C for 5 minutes, using a

pre-programmed tetrad thermocycler.

Quantitative PCR was performed under standard conditions using an Eppendorf real-time PCR machine. All samples were run as triplicates with a minimum of two samples / treatment type. Quantification was based on ΔCt calculations, and all samples were compared against β2-microglobulin and 18S as controls. Taqman pre-designed inventoried probes and 2x PCR Master mix were used for all analyses (Applied Biosystems).

2.8.3 Real-time RT-PCR

Taqman pre-designed, recommended, inventoried probes and 2x PCR Master mix were used for all analyses (Applied Biosystems). All samples were run as triplicates with a minimum of two samples / treatment type. Quantitation was based on ΔCt calculations, and all samples were compared against β2-microglobulin and 18S. cDNA (1μl) was added to 19 ml of reaction system containing10μl of a 2x mastermix, 1ml of 20x probe, and 8ml of nuclease-free water, and placed in a qPCR white plate (ABgene). Each plate was centrifuged for 2 minutes at 2000rpm at 4°C, placed in the LightCycler carousel, and run under the standard Applied Biosystems cycling conditions: one cycle of 50 °C for two minutes, and then 95 °C for 10 minutes followed by forty cycles of 95 °C for 15 seconds, 60 °C for one minute.

Probe	Gene name	Amplicon length
Hs00394267_m1	LRIG1	96
Hs01006148_m1	LRIG1	58
Hs01076090_m1	EGFR	57
Hs 01076092_m1	EGFR	103
Hs 00170423_m1	CDH1	117
Hs00187842_m1	b2M	64
Hs03928985_g1	18S	90
Mm00456116_m1	Lrig1	82
Mm01247357_m1	Cdh1	71
Mm00433023_m1	egfr	85
Mm00437762_m1	b2m	77
Mm03928990_g1	18s	61
Mm00441533_g1	snail homolog 1	79
Mm00441531_m1	snail homolog 2 (slug)	98
Mm00442036_m1	Twist homolog 1	113
Mm00432359_m1	Cyclin D1	58

2.9 Statistical analysis

Two tailed unpaired t-tests were performed to assess the significance of differences between epithelial heights and signal intensity between 2 groups and the non-parametric Mann Whitney U test was used for cell phenotype and proliferation. One way ANOVA

and Turkeys Multiple Comparison test was performed to assess signal intensity from fluorescent images between three groups. Statistical significance was accepted at $p<0.05$ for all analyses, and error bars represent standard error of the mean. All statistical analyses were performed using GraphPad Prism and Microsoft Excel.

CHAPTER 3 . RESULTS I – LRIG1

3.1 Lrig1 expression in the murine upper airways

In situ hybridisation staining shows Lrig1 present in WT murine Embryonic airways (E14.5) (Figure 3.1a) and in adult murine airways throughout the trachea and first few bronchial divisions (Figure 3.1b).

a

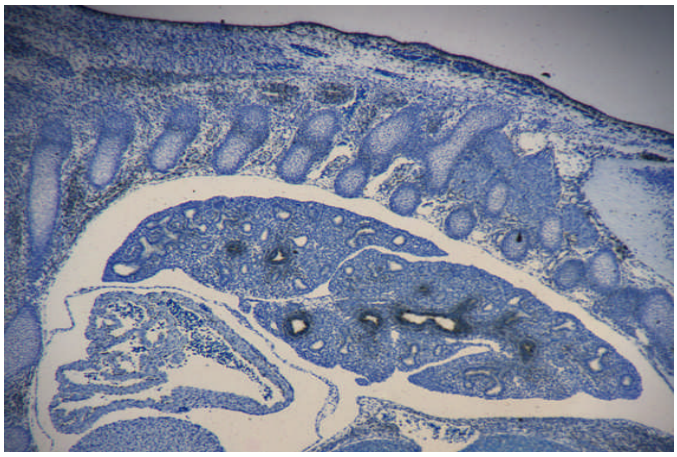

b

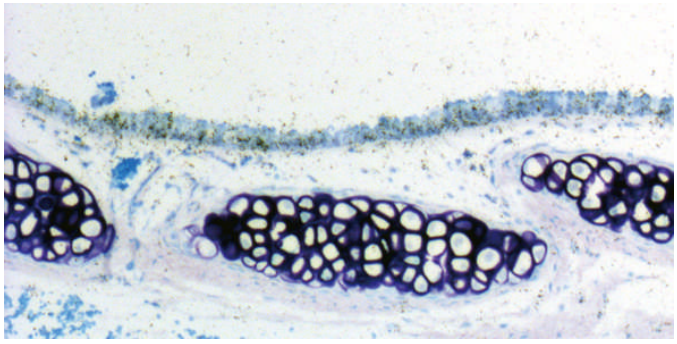

Figure 3.1 Lrig1 expression in the upper airways of mice.

In situ hybridisation staining shows Lrig1 present in WT murine Embryonic airways (E14.5) (a) and in adult murine airways throughout the trachea and first few bronchial divisions (b). Original magnification: ax5; bx20

3.2 Phenotype of Lrig1-defective mice

3.2.1 Deletion of Lrig1 causes hyperproliferation of the upper airways

To delineate the in vivo function of Lrig1 in the airways I examined Lrig1 depleted mice (*Lrig1-/-*) (Suzuki et al). The trachea and first two bronchial generations demonstrated hyperplasia (Figure 3.2a) resulting in a significant increase in airway epithelial thickness compared to litter mate controls (mean±SEM; 24.9μm ±1.2 vs 19.1μm ±1.7; unpaired T test $p<0.05$). Ki67 staining of the trachea and bronchi confirmed hyperproliferation of *Lrig1-/-* mice airway epithelium with 8.6% ± 1.1 vs 2.4% ± 0.3 of cells staining positively for Ki67 (Mann Whitney; $p<0.05$) (Figure 3.2b-c).

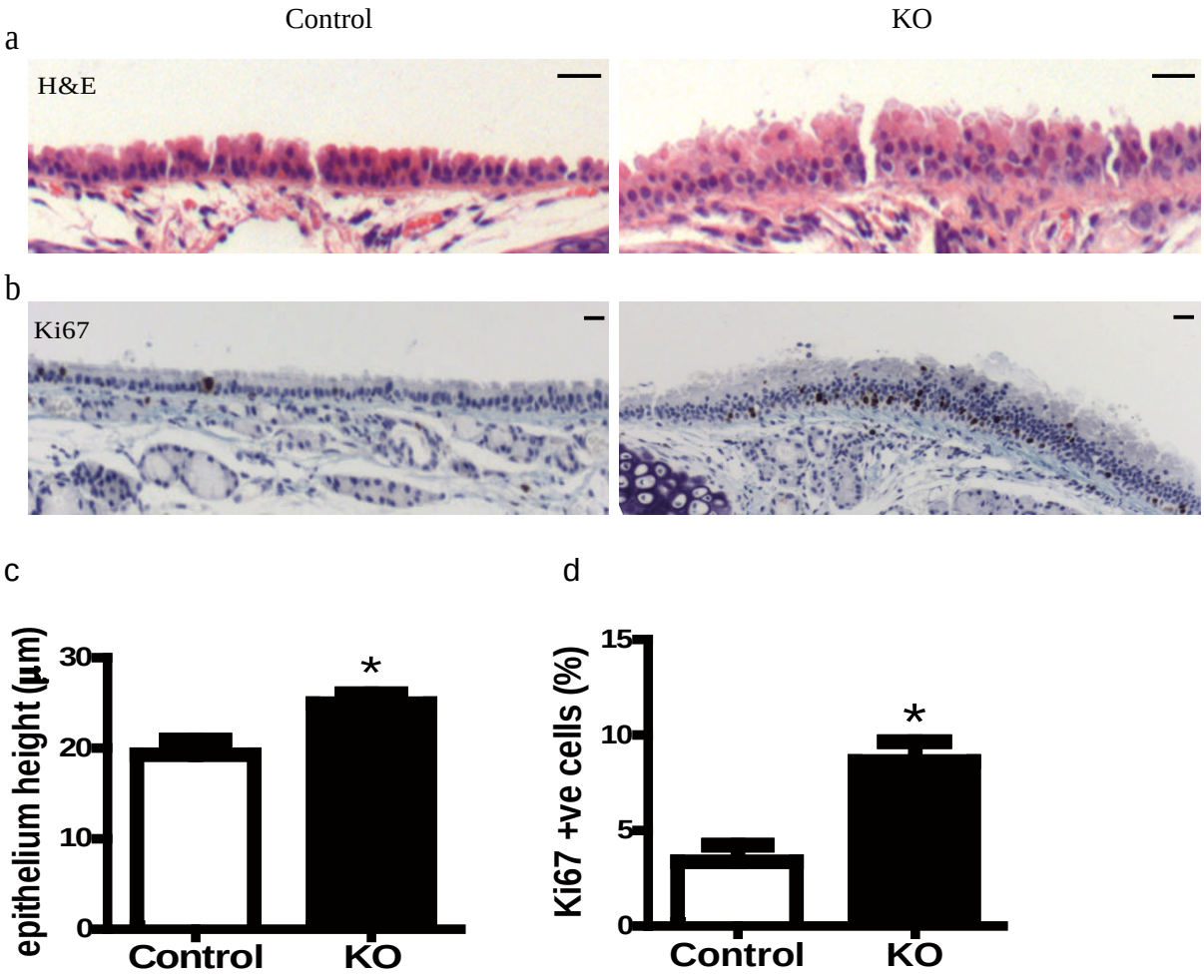

Figure 3.2 Deletion of Lrig1 causes hyperproliferation of the upper airways.

(a-d) compares *Lrig1*$^{-/-}$ mice and litter mate controls. (a,c) H&E staining with quantification of tracheal epithelial thickness (unpaired t test, mean±SEM, 24.9µm ±1.2 vs 19.1µm ±1.7; $p<0.05$). (b,d) Ki67 immunostaining and corresponding quantification (Mann Whitney test, 8.6% ±1.1 vs 2.4% ±0.3, $p<0.05$). Percentage of positive cells=antigen expressing cells over total nuclei. Scale bars: 20µm. n=4

3.2.2 Lrig1 depletion was confirmed by immunofluorescence and qPCR

Lrig1 depletion in the *Lrig1-/-* mouse upper airway was confirmed by immuofluorescence staining and qrtPCR of harvested mouse tracheal epithelial cells compared to control animals (Figure 3.3).

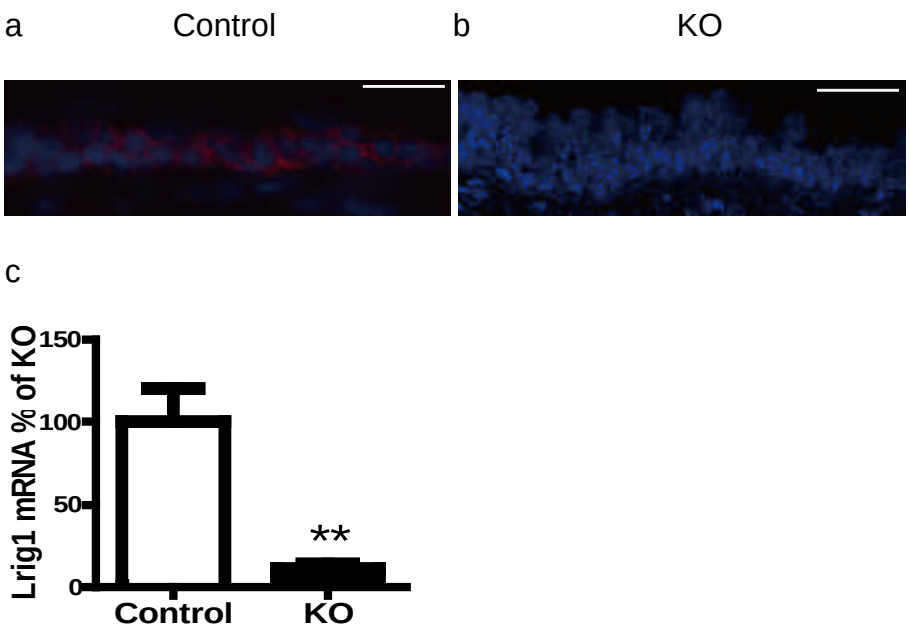

Figure 3.3 Confirmation of Lrig1 depletion in the *Lrig1*$^{-/-}$ mouse upper airway.
(a-c) compares *Lrig1*$^{-/-}$ mice and litter mate controls. Immunostaining (a,b) and qrt-PCR quantification (c) for *Lrig1*. Scale bars: 20μm

3.2.3 Lrig1 depletion does not effect airway epithelial cell differentiation

The cellular make up of the Lrig1 depleted mouse airway was normal with equivalent percentages of basal, Clara and ciliated cells (Figure 3.4).

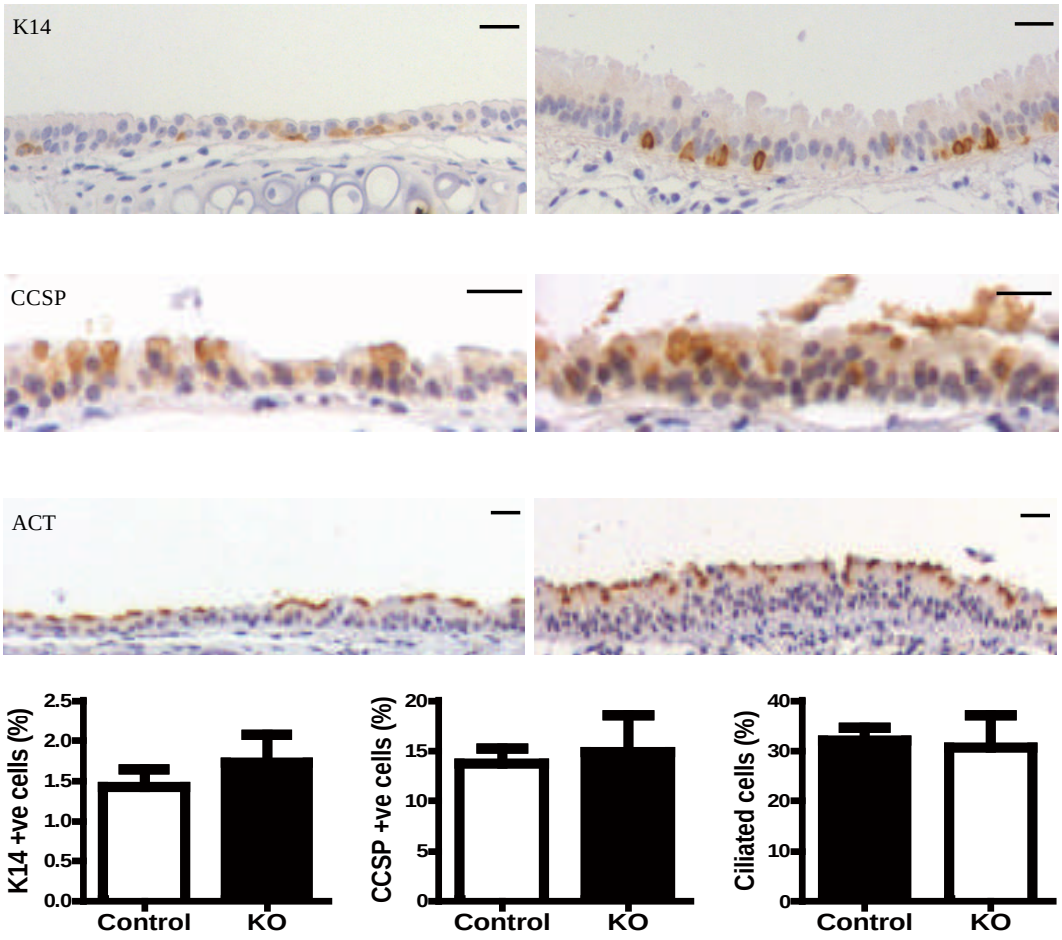

Figure 3.4 Cell type distribution of Lrig1 depleted mouse airway.

Immunostaining and percentage antigen expressing cells of total cells, of keratin 14 (K14, basal cell marker), Clara cell specific protein (CCSP, Clara cell marker) and acetylated tubulin (ACT, ciliated cell marker). Scale bars 20μm.

3.3 Lrig1 is downregulated in normal upper airway repair

On damage of the murine airways with polidocanol (a detergent agent that removes the surface airway epithelium leaving an intact basement membrane) I saw that that after 48 hours (at the time of peak proliferation in the regeneration of the airways, Figure 3.5) there was a fall in Lrig1 expression as determined by immunofluorescence, in situ hybridisation while at day 7 when the regenerated epithelium begins differentiating (Figure 3.5) I saw a return of Lrig1 expression to baseline homeostatic levels (Figure 3.6).

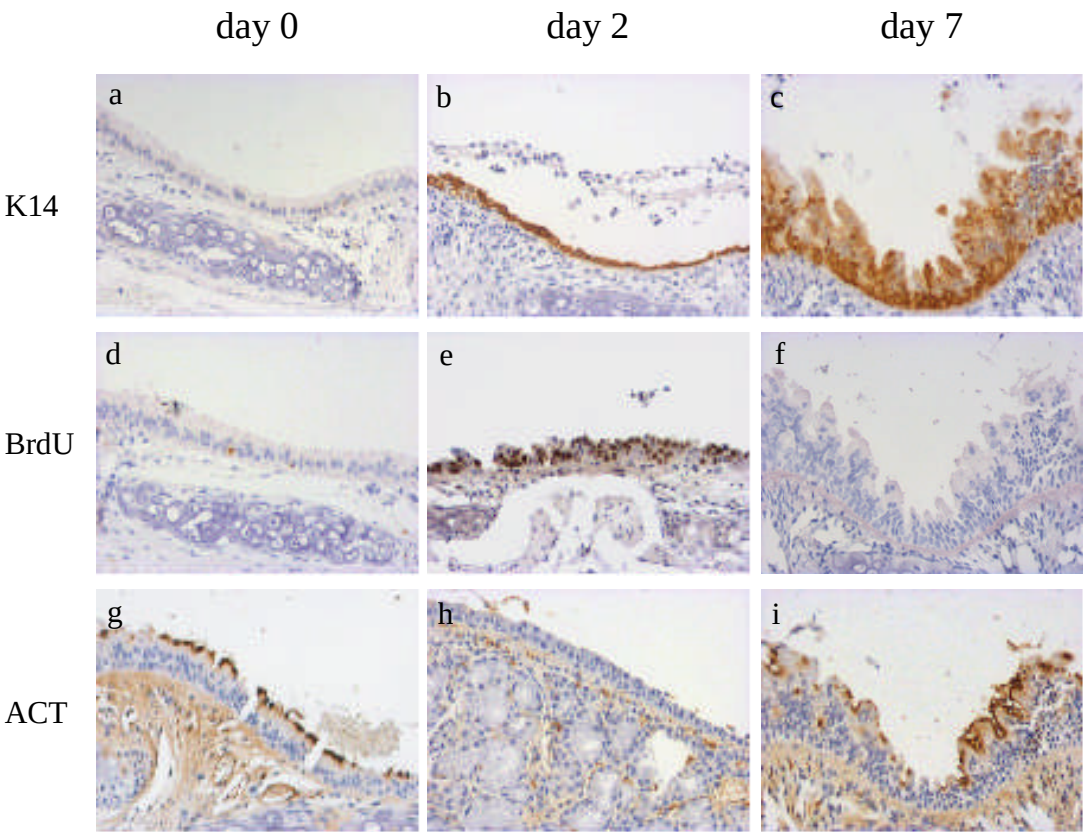

Figure 3.5 Demonstration of polidocanil damage on the upper airway.

Panels show airway epithelium at days 0 (a, d and g), day 2 (b, e and h) and day 7 (c, f and i) after damage stained with K14 (a, b and c), BrdU (d,e and f) and ACT (g, h and i). Original magnification: x20

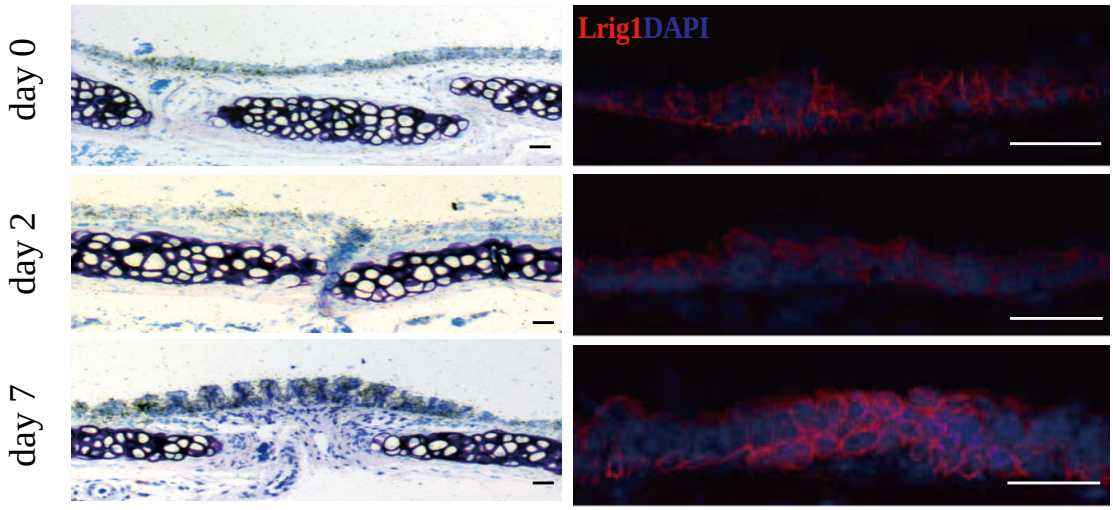

c

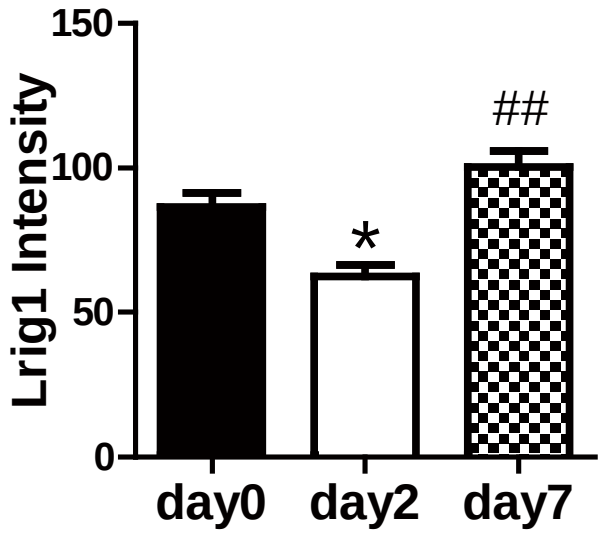

Figure 3.6 Lrig1 is downregulated in upper airway repair.

(a) in situ hybridisation and (b) immunofluorescence with histogram of signal intensity for *Lrig1* (c) in normal murine tracheal epithelium, before polidocanol-generated tracheal injury (day 0), day 2 and day 7 after injury (one way ANOVA and Turkeys multiple comparision test * day 0 vs day 2 $p<0.01$; ## day 2 vs day7 $p<0.05$). Scale bars: 20μm

3.4 Lrig1 depletion leads to increased EGFR phosphorylation

In the epidermis Lrig1 is known to regulate EGFR signalling leading to a reduction in phosphorylated EGFR (Jensen and Watt 2006). I similarly confirmed using immunofluorescent staining in normal homeostasis that *Lrig1* depleted mice had increased abundance of phospho-EGFR (Figure 3.7, day 0).

Two days post airway damage, levels increased in control animals in line with cellular proliferation and were equivalent to Lrig1 depleted animals. However, by day 7 levels had returned to baseline in control animals but remained elevated in the *Lrig1*$^{-/-}$ mice (Figure 3.7, day 2 and 7).

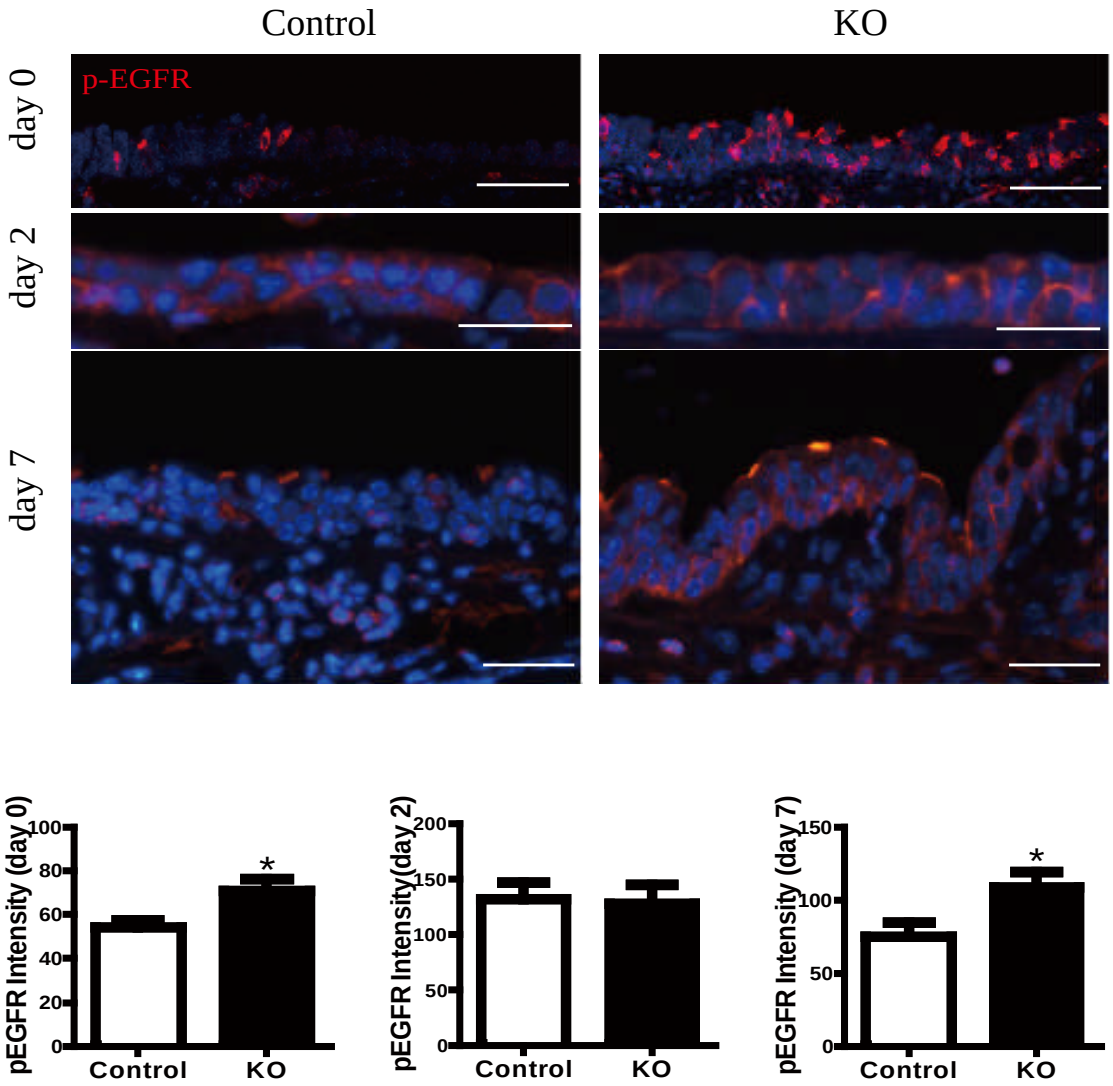

Figure 3.7 Lrig1 downregulation in murine upper airway leads to upregulated EGFR activation. Immunostaining with histogram of signal intensity of phospho-EGFR in *Lrig1*$^{-/-}$ mice (KO) and litter mate tracheal epithelium before polidocanol-generated tracheal injury day 0 (* unpaired T test $p<0.05$), and day 2 ($p=0.8$) and day 7 (* $p<0.05$) after injury. Scale bars 20µm

3.5 *Lrig1*$^{-/-}$ mice show increased cell proliferation

3.5.1 In vivo

This is associated with increased proliferation in *Lrig1*$^{-/-}$ mice compared to litter mate controls (32.7% ±5.1 vs 21.1% ±4.1, Mann Whitney p=0.03) (Figure 3.8). The dynamic expression pattern of *Lrig1* during injury suggests that it either controls airway cell differentiation or proliferation. As *Lrig1*$^{-/-}$ mice display normal epithelial differentiation, this indicates that *Lrig1* controls proliferation. We next investigated whether *Lrig1* had a role in density dependent growth inhibition.

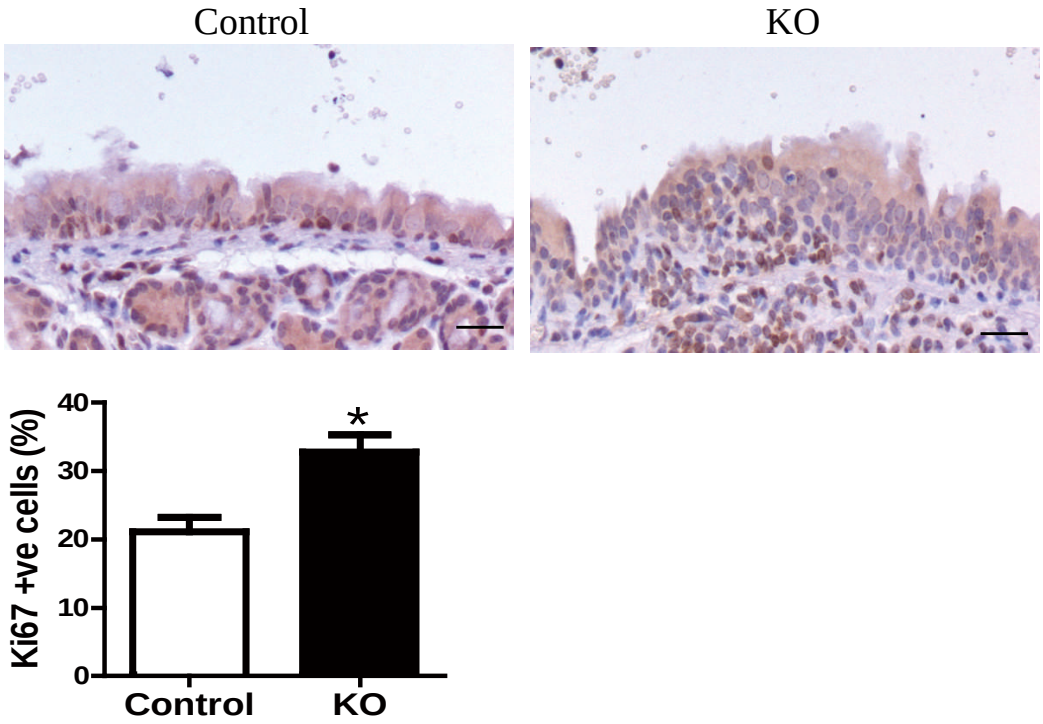

Figure 3.8 immunostaining of Ki67 in *Lrig1-/-* and litter mate control tracheal epithelium. immunostaining of Ki67 in *Lrig1*$^{-/-}$ and litter mate control tracheal epithelium , and corresponding quantification (** Mann Whitney test, $p<0.01$). Scale bars 20µm

3.5.2 Lrig1 depletion leads to a failure of cell-cell contact inhibition in vitro

To further examine the hyperproliferative phenotype of the *Lrig1*$^{-/-}$ mouse airway I used murine tracheal epithelial cell (MTEC) air liquid interface (ALI) cultures. In ALI cultures the initial proliferative phase of the culture is carried out submerged in media until day 9 followed by a differentiation phase of confluent cells at an air liquid interface (Figure 3.9a). Proliferation in sub-confluent MTEC cultures was examined at day 7 with the addition of BrdU three hours before harvest. Alternatively MTEC cultures were taken to an ALI at day 9 and then proliferation measured in confluent cultures at day 14 (Figure 3.9a).

Day 7 pre-confluent cultures showed high but equivalent cellular proliferation in *Lrig1*$^{-/-}$ and control MTECs (Figure 3.9b) however proliferation of *Lrig1*$^{-/-}$ MTECs post-confluence was significantly increased compared to litter mate controls (Figure 3.10). Cell fate decisions of confluent *Lrig1*$^{-/-}$ cultures were again normal with equivalent levels of K14 and acetylated tubulin expressing cells (Figure 3.10).

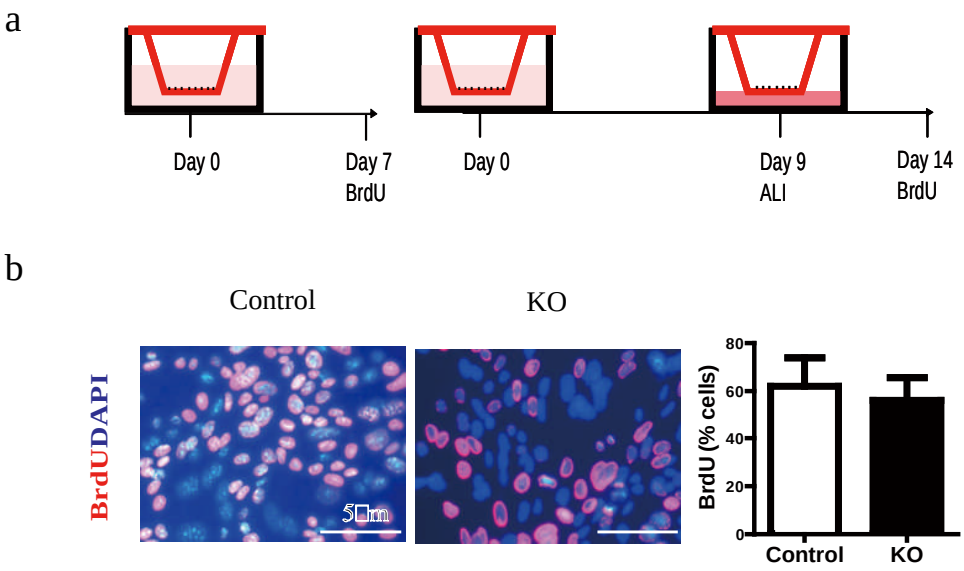

Figure 3.9 *Lrig1*$^{-/-}$ (KO) tracheal epithelial cells show similar proliferation at cell pre-confluence in ALI culture.

(a) diagram of ALI culture and experimental time points. (b) immunostaining of BrdU in MTEC culture pre-confluence and corresponding quantification (KO vs control, 55.9% ±9.5 vs 62.0% ±11.8, p>0.05, n=4). All statistical values, mean ±SEM, Mann Whitney U test.

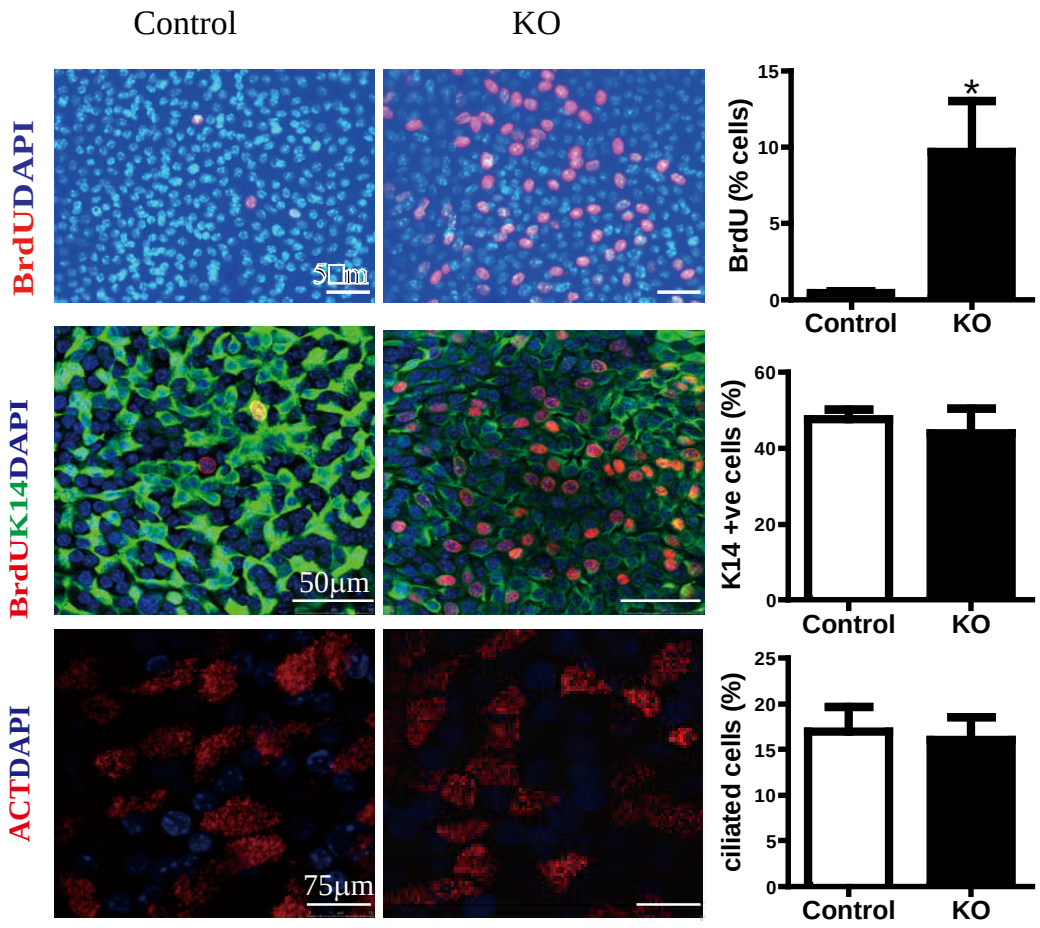

Figure 3.10 *Lrig1*$^{-/-}$ (KO) tracheal epithelial cells show continued proliferation at cell confluence in ALI culture.

Immunostaining of BrdU in MTEC cultures day 14 (5 days after cell confluence) showed increased BrdU immunostaining cells in *Lrig1*$^{-/-}$ MTECs compared to controls (9.7% ±3.4 vs 0.5% ±0.1, $p<0.05$, n=4). Co-staining of keratin14 (K14) or acetylated tubulin (ACT) with BrdU, showing no difference between KO and control MTEC differentiation at ALI culture day 14 (47.0% ±11.4, 54.2% ±9.2, respectively, $p>0.05$). All statistical values, mean ±SEM, Mann Whitney U test.

3.5.3 Lrig1-/- activated EGFR/ MAPK /ERK signalling pathway in MTEC culture

Immuno-blots of *Lrig1*$^{-/-}$ compared to control MTEC cultures demonstrated an increase in phospho-EGFR and phospho-ERK1/2 under conditions with and without the EGF ligand (Figure 3.11) confirming a downstream effect of Lrig1 expression on EGFR signalling.

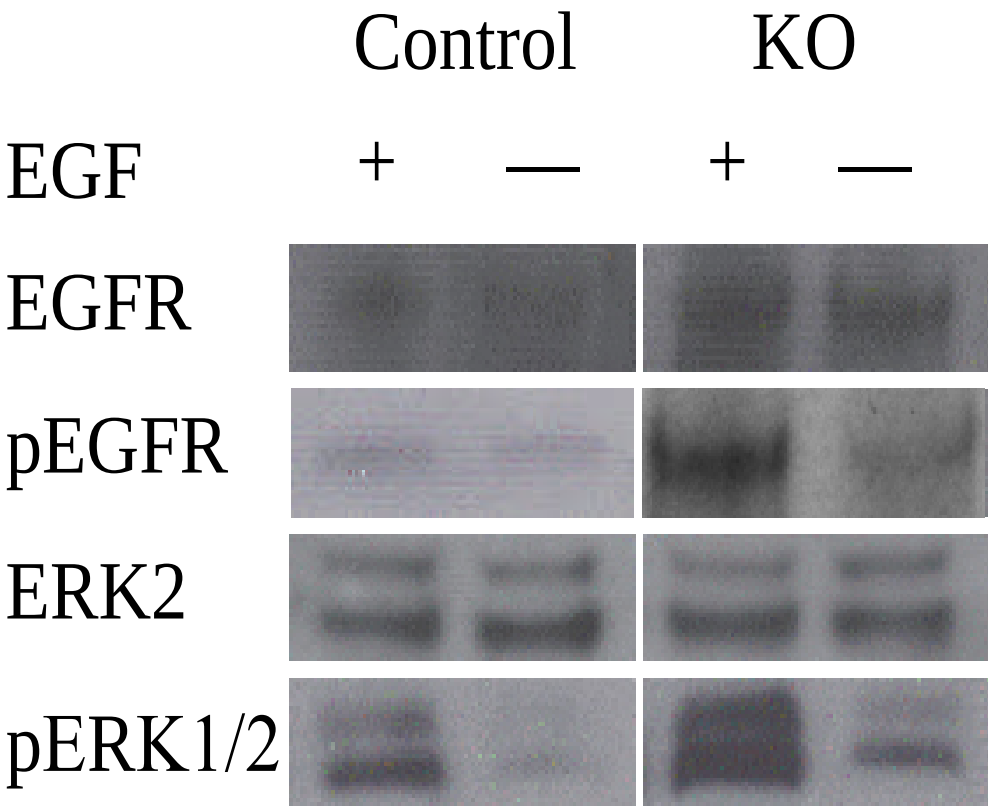

Figure 3.11 Increased ERK1/2 phosphorylation of KO MTEC compared to controls.

MTECs from control or KO mice were growth factor starved for 14h and stimulated or not for 30min with 20ng/ml EGF. Cell lysates were immunoblotted with the indicated antibodies.

3.6 Ectopic LRIG1 arrested cell proliferation in human cancer cell lines

This failure of density dependent growth inhibition in the *Lrig1*$^{-/-}$ airway epithelial cells led us to next investigate whether Lrig1 plays a role as a tumour suppressor in lung cancer cells.

Lung A549 (adenocarcinoma) and H357 (squamous) cancer cell lines show little or absent expression of LRIG1 compared to normal human bronchial epithelial cells (BEAS-2b) while having a high expression of EGFR (Figure 3.12). These cells were transduced with a retrovirus expressing a flag-tagged LRIG1 construct or empty vector control. Immunofluorescence, immuno-blotting and qPCR confirmed transduction (Figure 3.13-14). I then performed experiments examining cell proliferation in pre-confluent and confluent conditions.

3.6.1 Endogenous LRIG1 and EGFR expression in human cell lines

Lung A549 (adenocarcinoma) and H357 (squamous) cancer cell lines show little or absent expression of LRIG1 compared to normal human bronchial epithelial cells (BEAS-2b) while having a high expression of EGFR.

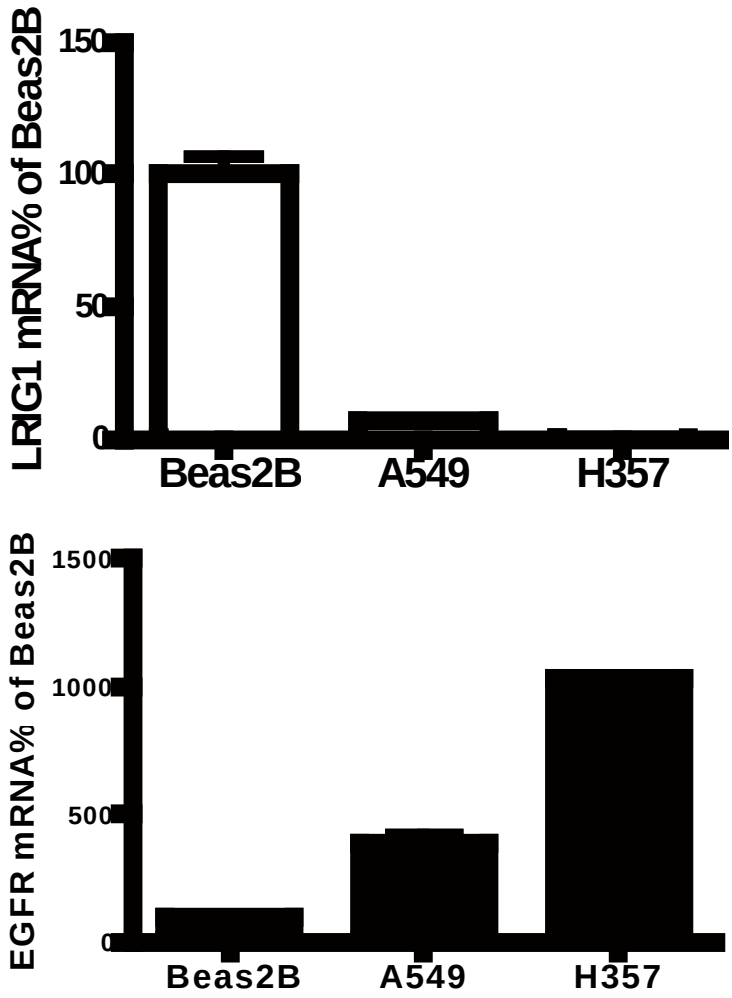

Figure 3.12 qPCR of endogenous LRIG1 and EGFR transcripts.

Shows loss of LRIG1 in cancer cells compared to control human airway cells.

3.6.2 The success of LRIG1 transduction

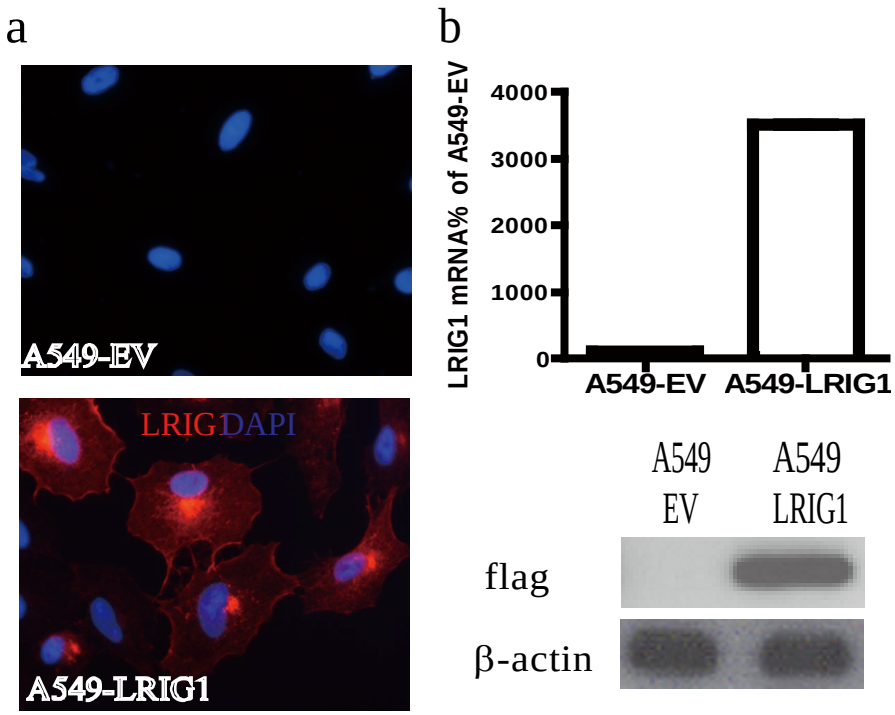

Figure 3.13 Ectopic LRIG1 expression in A549.

Immunostaining of LRIG1 in A549-empty vector (EV) and A549-LRIG1flag transduced cells (a) with LRIG1 qPCR and immunoblotting of flag-tagged LRIG1 (b) confirming expression. Original magnification x40

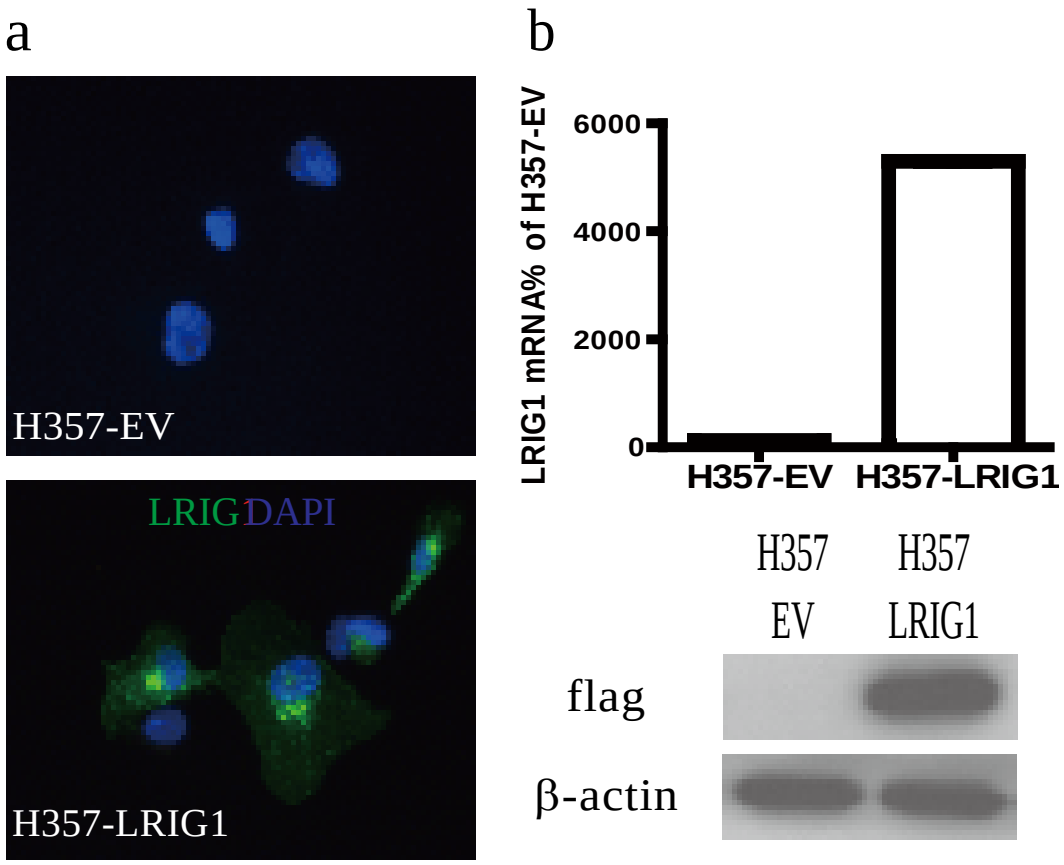

Figure 3.14 Ectopic LRIG1 expression in H357

Immunostaining of LRIG1 in H357-empty vector (EV) and H357-LRIG1flag transduced cells (a) with LRIG1 qPCR and immunoblotting of flag-tagged LRIG1 (b) confirming expression. Original magnification x40

3.6.3 LRIG1 transduction reduces post confluence cancer cell proliferation

Pre-confluent LRIG1 expressing A549 and H357 cells showed no change in proliferation rate compared to empty vector control cells (A549; 78.2% ±3.8 vs 74.9% ±4.4, $p>0.05$: H357; 58.0% ±6.6 vs 56.1% ±3.9%, $p>0.05$) (Figure 3.15a and 16a). However at confluence, LRIG1 transduced A549 and H357 cells demonstrated a significantly reduced proliferative rate (A549s: 13.3% ±0.7, 6.1% ±1.7, $p<0.05$: H357; 56.3% ±7.7 vs 40.1% ±6.9, $p<0.05$) (Figure 3.15b and 16b).

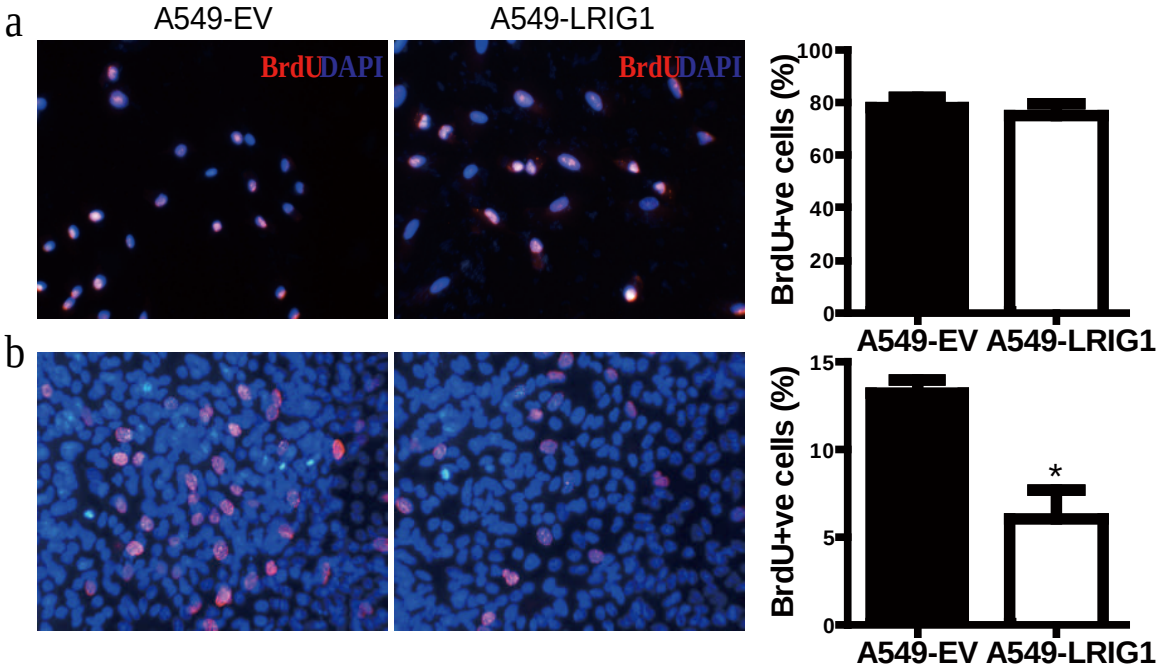

Figure 3.15 A549 immunostaining of BrdU in EV and LRIG1 transduced cells.

A549 immunostaining of BrdU in EV and LRIG1 transduced cells at pre (a) and post confluence (b), with corresponding histogram of BrdU positive cells. Original magnification x10. (Mann Whitney * $p<0.05$)

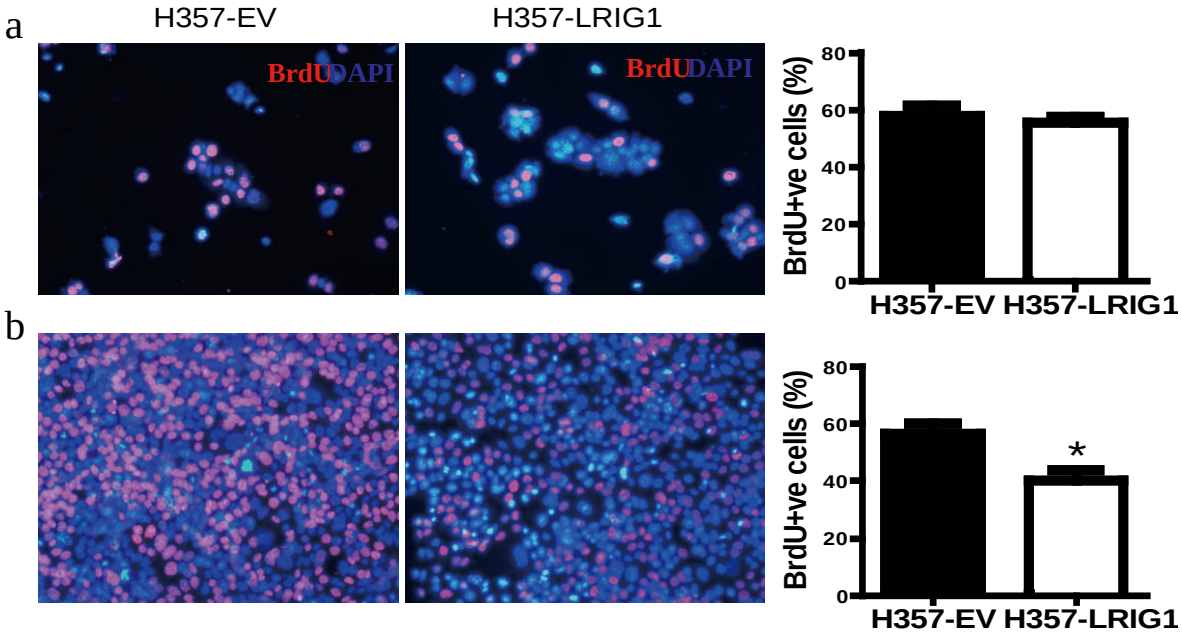

Figure 3.16 H357 immunostaining of BrdU in EV and LRIG1 transduced cells.

H357 immunostaining of BrdU in EV and LRIG1 transduced cells at pre (a) and post confluence (b), with corresponding histogram of BrdU positive cells. Original magnification x10. (Mann Whitney * $p<0.05$)

3.6.4 LRIG1 transduction of A549 and H357 cancer cells reduces colony formation efficiency (CFE)

LRIG1 transduced A549 and H357 cells also demonstrated a reduction in the number (A549-EV 28.7% ±3.4 vs A549-LRIG1 16.2 ±2.9, $p<0.05$; H357-EV 14.3 ±2.2 vs H357-LRIG1 7.5 ±1.2, $p<0.05$) and size of colonies (A549-EV 16.2% ±2.1 vs A549-LRIG1 4.8 ±1.0, $p<0.05$; H357-EV 2.6% ±0.5 vs H357-LRIG1 1.0 ±0.2, $p<0.05$) in colony forming assays (Figure 3.17 and 18).

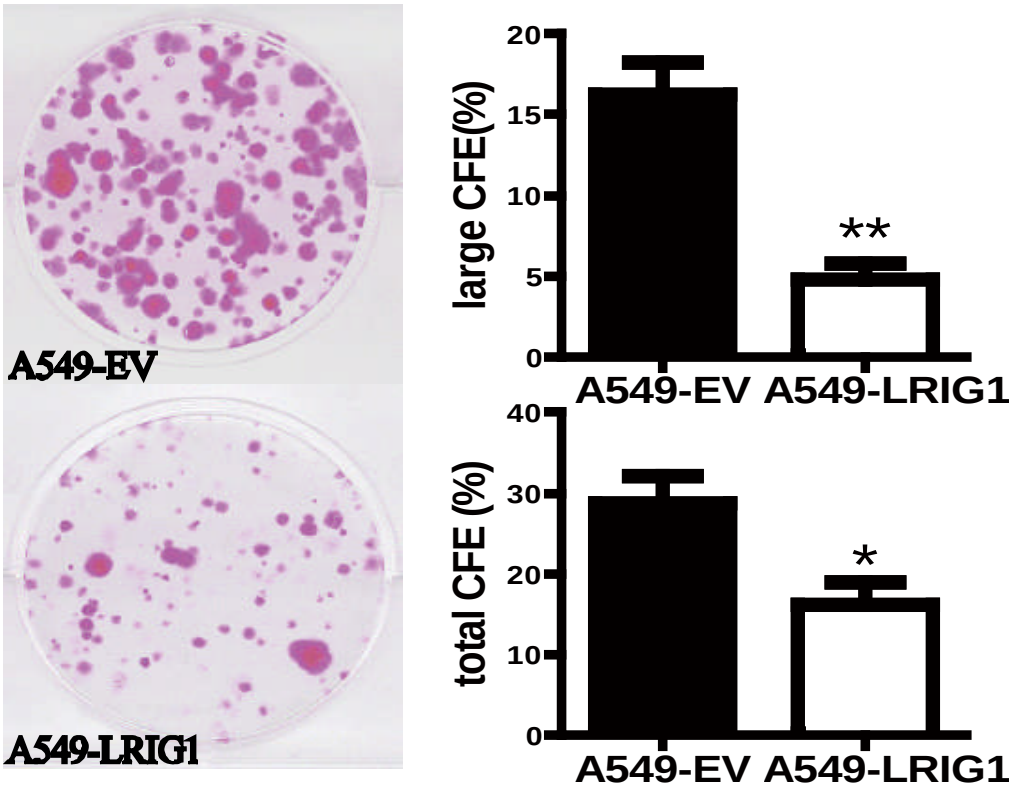

Figure 3.17 CFE of A549 transduced cells.

A549 cells showing LRIG1 transduction reduced size and number of colonies (Mann Whitney * $p<0.05$; ** $p<0.01$)

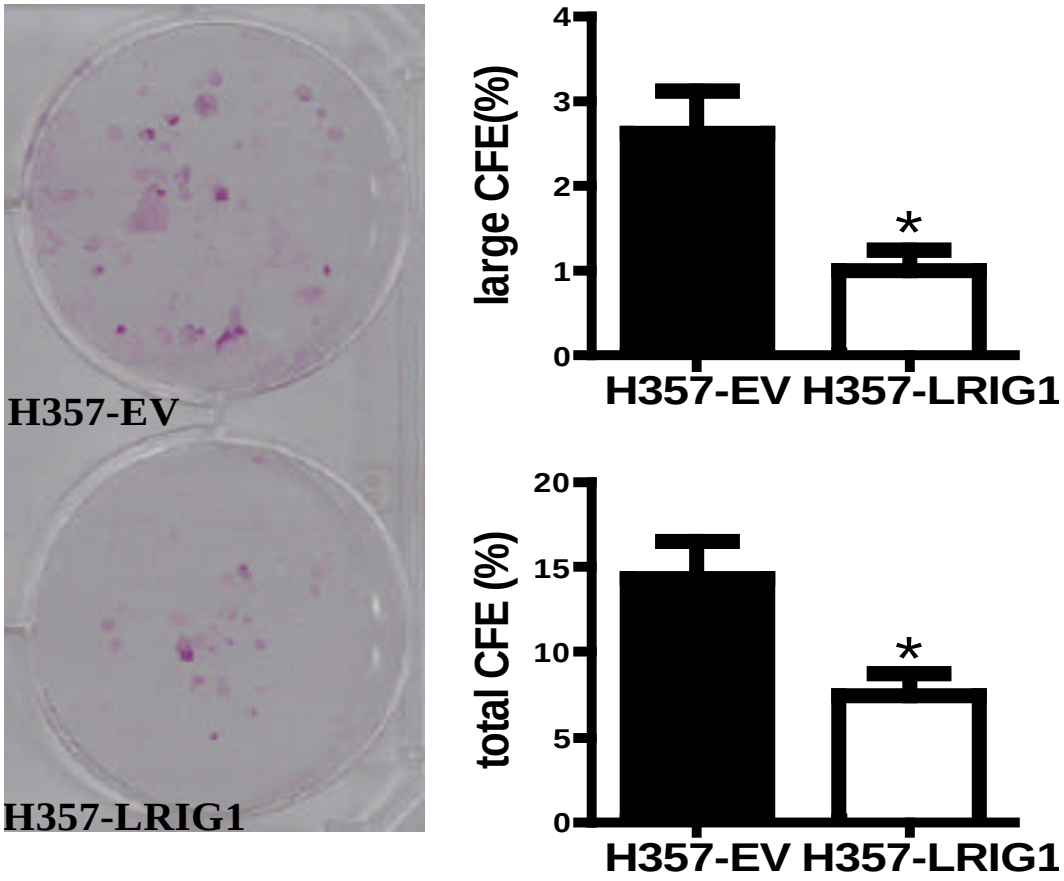

Figure 3.18 CFE of H357 transduced cells.

H357 cells showing LRIG1 transduction reduced size and number of colonies (Mann Whitney * $p<0.05$)

3.6.5 LRIG1 transduction of BEAS2b cells expressing endogenous LRIG1 does not affect proliferation or CFE

Of note normal bronchial epithelial cells (BEAS2b cells) that have endogenous expression (see Figure 3.12) of LRIG1 show no change in cell proliferation or colony forming efficiency with the introduction of additional synthetic LRIG1 (Figure 3.19-20).

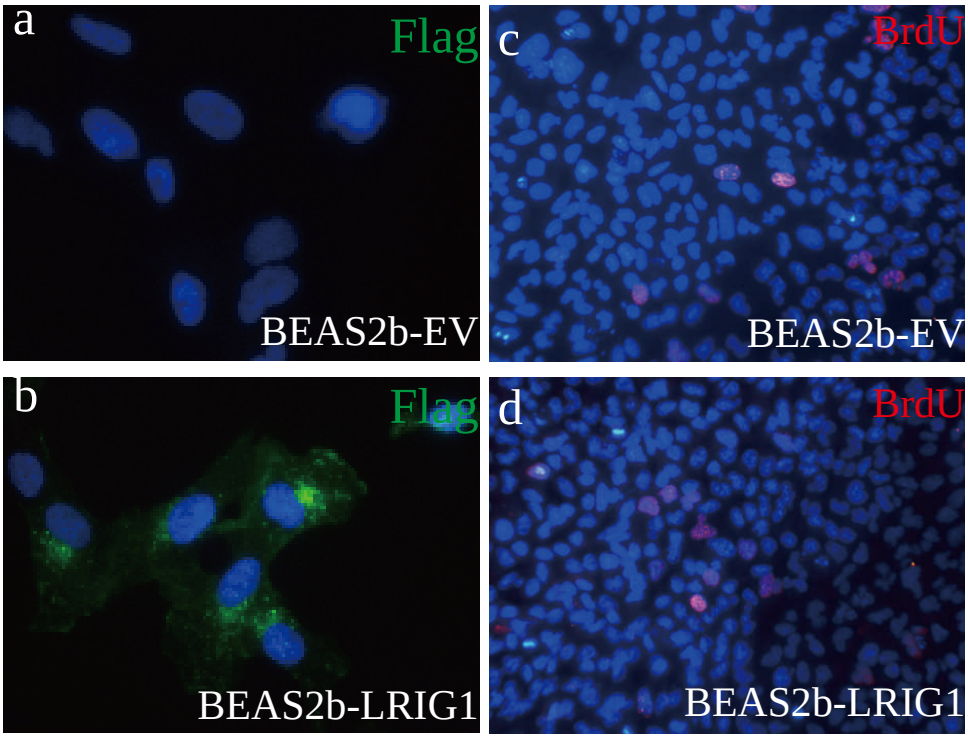

Figure 3.19 LRIG1 transduction causes no change in BEAS-2b proliferation.

Immunostaining of flag in BEAS2b-empty vector (EV) and BEAS2b-LRIG1flag transduced cells (a,b) ; and BrdU in EV and LRIG1 transduced cells at post confluence (c,d). Original magnification (a, b) x40; (c, d) x10

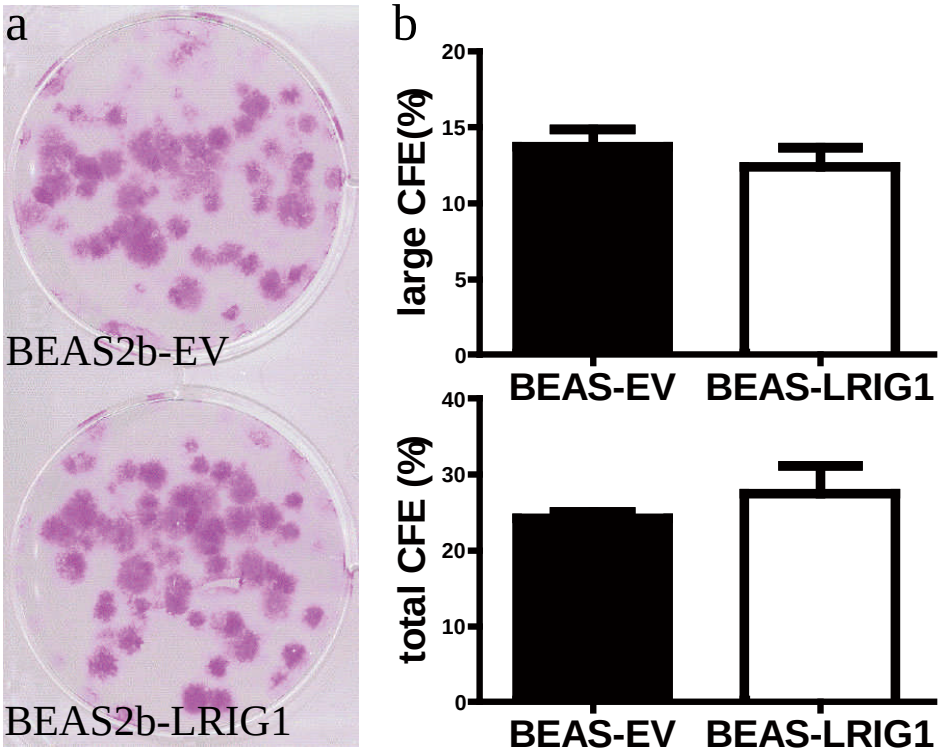

Figure 3.20 CFE of BEAS-2b EV and LRIG1-transduced cells.

CFE of BEAS-2b EV and LRIG1-transduced cells showing no difference in CFE (Total Number of colonies BEAS2b-EV 24.2% ±0.9vs BEAS2B-LRIG1 27.6 ±3.5, p=0.88; and large colonies BEAS2b-EV 13.7% ±1.1vs BEAS2B-LRIG1 12.4 ±1.2, p=0.70)

3.7 LRIG1 complexes with E-cadherin at the adherens junction.

3.7.1 Activity of EGFR signalling and E-cadherin expression in LRIG1 transduced A549

To understand how LRIG1 leads to reduced proliferation on cell-cell contact I first examined the activation of the EGFR signalling pathways in LRIG1 depleted cells compared to LRIG1 transduced cells. Using immunoblotting I found the introduction of LRIG1 to cancer cells reduced phospho-EGFR levels and the downstream effecter phospho-ERK1/2, while having no effect on the activation Akt measured by immunoblotting phospho-Akt (Figure 3.21a).

I hypothesised that LRIG1 was causing its effect at the adherens junction. Using immunoblotting and qPCR we found LRIG1 transduction did not significantly alter E-cadherin protein and mRNA levels (Figure 3.21b and 21c) within A549 cancer cells (Figure 3.21c).

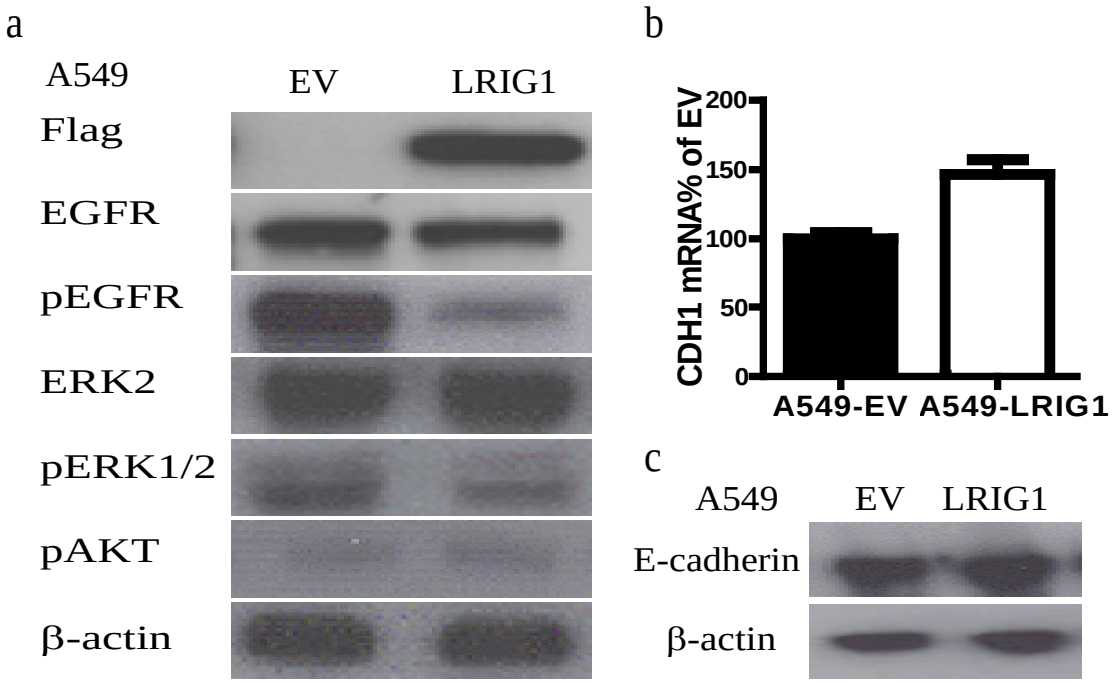

Figure 3.21 Immunoblots of A549-EV and A549-LRIG1 cells.

(a) immunoblots of A549-EV and A549-LRIG1 cells with the indicated antibodies. (b) qrt-PCR of E-cadherin (CHD1), in A549-EV and A549-LRIG1. (c) immunoblot of A549-EV and A549-LRIG1 cells for E-cadherin.

3.7.2 LRIG1 colocaiises at cell-cell junctions with EGFR and E-cadherin

EGFR and E-cadherin have been previously shown to co-localise at cell-cell contacts. I confirmed this in A549 cells using confocal microscopy and further showed co-localisation of Lrig1 with EGFR (Figure 3.22a and 22b). This association EGFR and LRIG1 at the cell membrane was blocked with the addition of EDTA for 2 hours (Tobey, Argote et al. 2004) to cultures to disrupt the adherens junction suggesting the complex is formed there with E-cadherin (Figure 3.22c).

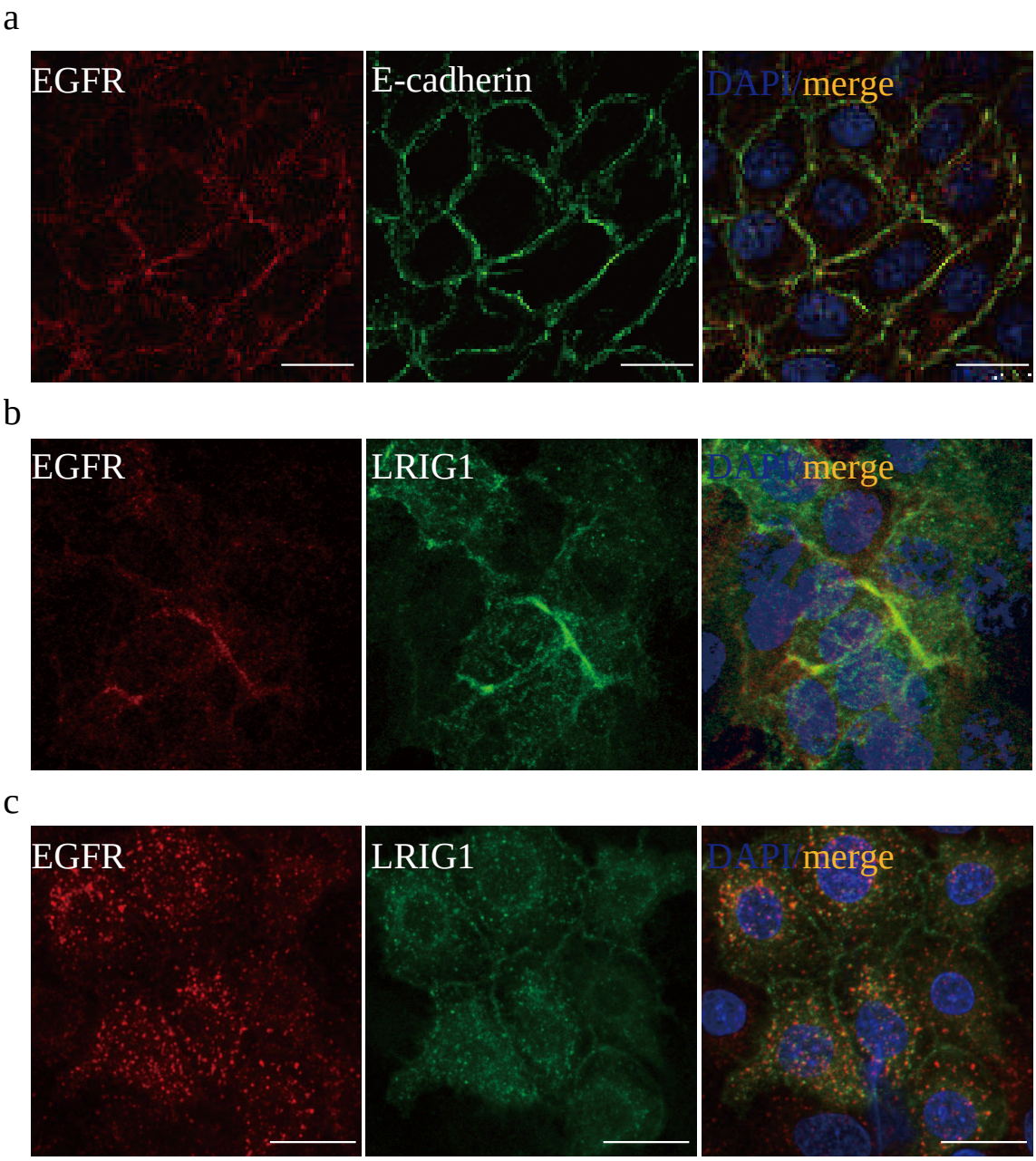

Figure 3.22 Confocal image of E-cadherin, LRIG1 and EGFR immunostaining in A549-LRIG1 cells.

3.7.3 LRIG1 co-immunoprecipitates with EGFR and E-cadherin

To confirm this association I next performed immunoprecipitation experiments showing that E-cadherin could be co-precipitated with EGFR at low levels in the absence of LRIG1, however after LRIG1 transduction this co-immunoprecipitation is greatly increased (Figure 3.23a and 23b). LRIG1 was also co-immunopreciptated with both EGFR and E-Cadherin suggesting the three molecules form a complex at cell confluence. This was shown using both EGFR and E-cadherin as the immunoprecipitation bait (Figure 3.23b). Further, EGFR and E-cadherin complex formation is reduced in the absence of LRIG1. Therefore in both tracheal epithelial cells and lung cancer cells it appears LRIG1 is required for effective density dependent growth inhibition through inhibition of the EGFR-ERK1/2 pathway and produces this effect after forming a complex at the cell membrane with E-cadherin and EGFR at cell-cell contact.

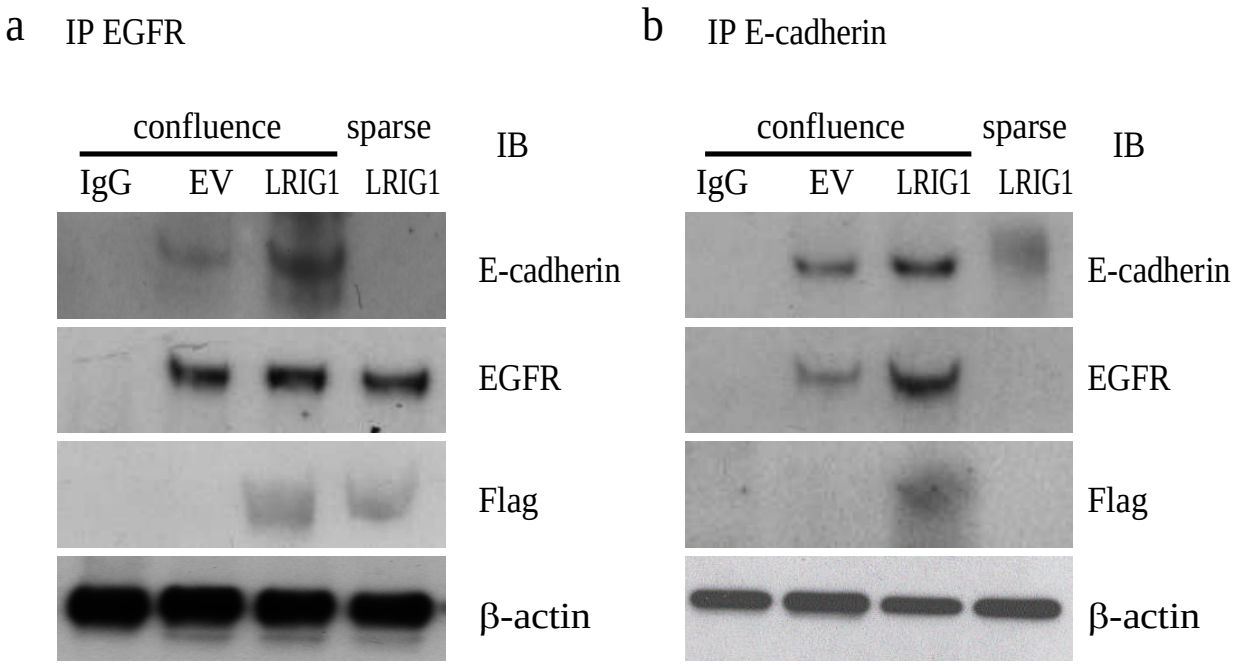

Figure 3.23 Immunoprecipitation of A549 transduced cells.

Immunoprecipitation experiments of cell lysates from A549-EV and A549-LRIG1 with an EGFR antibody (a) and an E-cadherin antibody (b) with subsequent immunoblots with the indicated antibodies.

3.8 Reduced LRIG1 expression occurs in pre-invasive lung cancer lesions

Several studies have shown loss of LRIG1 occurs in cancer and is associated with a poor prognosis (Tanemura, Nagasawa et al. 2005; Guo, Nilsson et al. 2006; Jensen, Jones et al. 2008; Lindstrom, Ekman et al. 2008). In the above experiments I show that loss of Lrig1 is associated with hyperproliferation in vivo and loss of density dependent growth inhibition in vitro. I therefore hypothesised that LRIG1 loss is an early initiation step for the development of cancers in the airways with the resultant high proliferative background allowing an increased accumulation of genetic abnormalities.

I therefore studied 10 pre-invasive lung cancer lesions and compared them to normal airway epithelial biopsies from the same patients.

Immunohistochemistry showed reduced immunoreactivity of LRIG1 in pre-invasive tissue compared to normal epithelium in all 10 patients, which was confirmed in 9 with a significant reduction in gene expression as measured by qPCR (one sample failed RNA extraction) (Figure 3.24a and b). This reduction in LRIG1 expression was mirrored by an increase in phospho-EGFR immunoreactivity and gene expression in the pre-invasive lesions compared to normal control epithelium (Figure 3.24c, d). This data confirms loss of LRIG1 expression is an early event in the pathogenesis of squamous cell lung cancer.

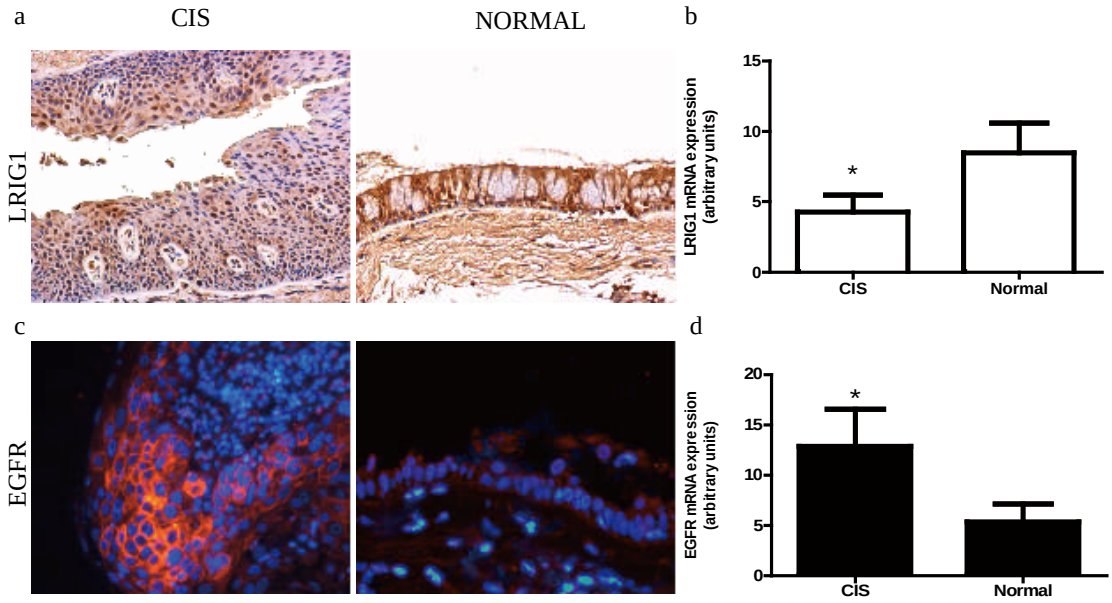

Figure 3.24 Early loss of LRIG1 in pre-invasive lung cancer lesions.

(a) representative LRIG1 immunostained section of human lung carcinoma-in-situ (CIS) and normal epithelium samples showing the downregulation of LRIG1 in CIS samples. (b) qrt-PCR analysis of relative mRNA expression of LRIG1 in CIS and normal lung epithelium samples. There was 2 fold change of LRIG1 mRNA level between CIS (n=10) and patient matched normal (n=10) samples. (c) Representative EGFR immunostaining human lung CIS and normal epithelial sample showing EGFR upregulation in CIS samples. (d) qPCR analysis of relative mRNA expression for EGFR in CIS and normal lung epithelium samples. There was 2.4 fold change difference between CIS (n=10) and normal (n=10) samples. Error bars represent the standard error of the mean; *p<0.05. Original magnification (a)x20, (c)x40

CHAPTER 4. RESULTSII- β-CATENIN

4.1 β–catenin expression in normal or repairing murine trachea

4.1.1 Basal stem cells activate β–catenin during wound repair

To assess whether β–catenin is active in normal or repairing airways I used TOPgal β–catenin reporter mice (Li, Li et al. 2009). Mice were untreated or given 2% polidocanol by oropharyngeal instillation to damage their tracheas. Normal and polidocanol damaged tracheas recovered for 7 days were stained with X-gal to detect β–galactosidase reporter gene activity (Li, Li et al. 2009). Only sporadic clusters of β-catenin signalling cells were present in two of four uninjured tracheas (blue stained cells, Figure 4.1A, B). After damage all tracheal samples exhibited robust reporter gene activity throughout their epithelium (Figure 4.1C, D). X-gal staining was never detected in transgene negative (wild type) controls (data not shown). These results demonstrate that tracheal β–catenin activation is predominantly associated with epithelial repair.

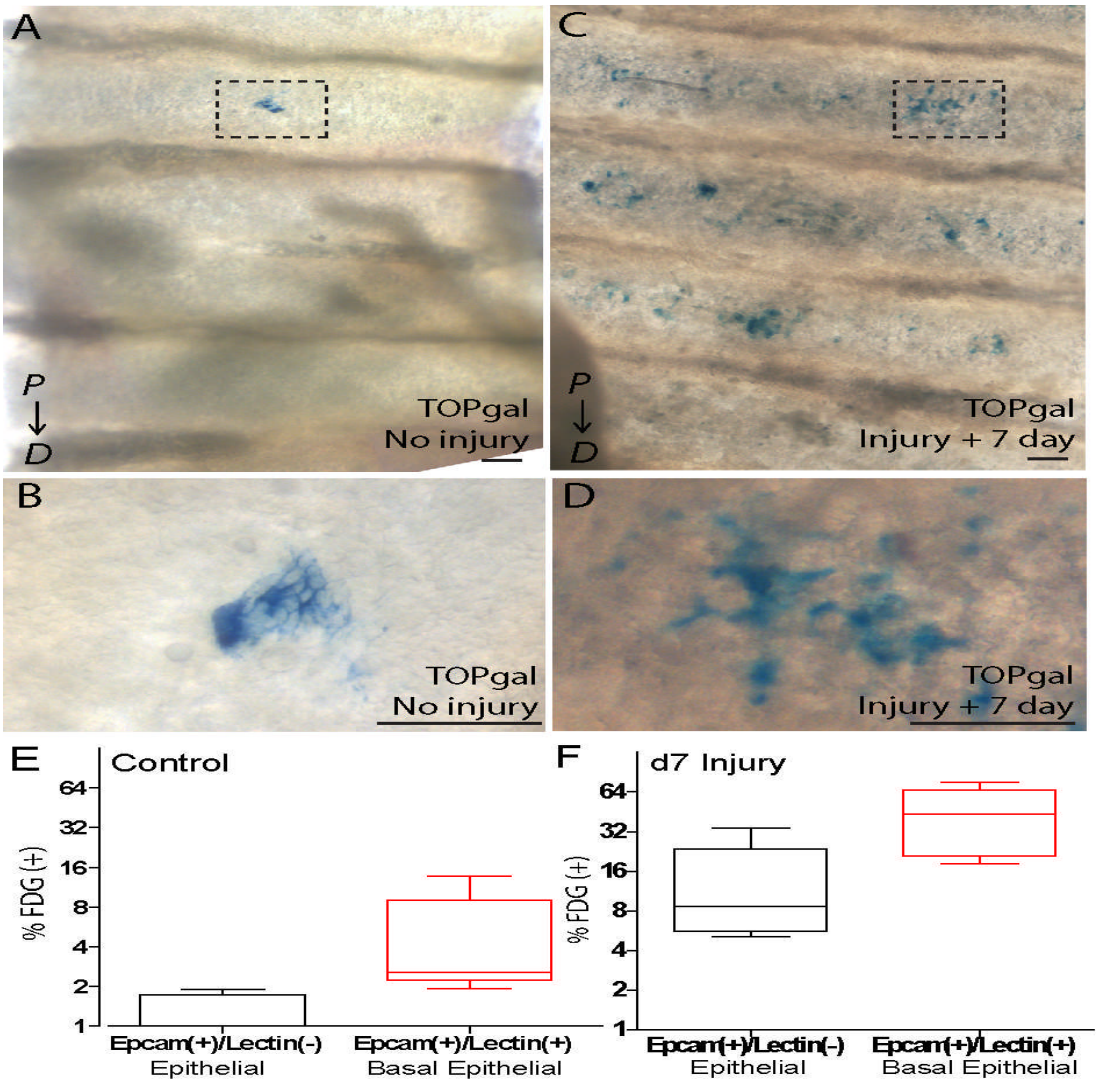

Figure 4.1 Tracheal repair is associated with stem cell β–catenin activation.

(A-D) Whole mounts of normal (A, B) and polidocanol damaged (C, D) TOPgal tracheas stained with X-gal to detect β-catenin (blue). Dashed boxes (A, C) indicate areas magnified in (B, D). The tracheal proximal-distal (P->D) axis is indicated (A, C) and scale bars represent 100μm (A-D). Cells isolated from tracheas were labelled using DAPI, CD45, EpCam, GSI-β4 lectin, and FDG (Figure 26), and FDG-reactive, nonhematopoietic EpCam (+)/lectin (-) nonbasal (black, E, F) and EpCam (+)/lectin (+) basal (red, E, F) epithelial stem cell abundance was determined for control and polidocanol damaged samples. The tracheal proximal-distal (P->D) axis is indicated (A, C) and scale bars represent 100μm (A-D).

4.1.2 β–catenin signalling occurs predominately within activated basal stem cells.

To determine the abundance and phenotype of β–catenin signalling cells I used FDG, EpCam and GSI-β4 lectin antibody staining and flow cytometry (to detect TOPgal signalling, epithelial, and basal stem cells, respectively (Figure 4.2). Nontransgenic mice and single stain controls were used to set all gates. In the absence of injury only rare EpCam (+)/GSI-β4 lectin (+) basal stem cells exhibited FDG staining resulting from TOPgal activity (red bar, Figure 4.1E**)**. In contrast, FDG staining was present in 20-60% of EpCam(+)/lectin(+) basal stem cells and 5-20% of non-basal EpCam(+)/lectin(-) cells 7 days after damage (Figure 4.1F). This indicates that β–catenin signalling occurs predominately within activated basal stem cells.

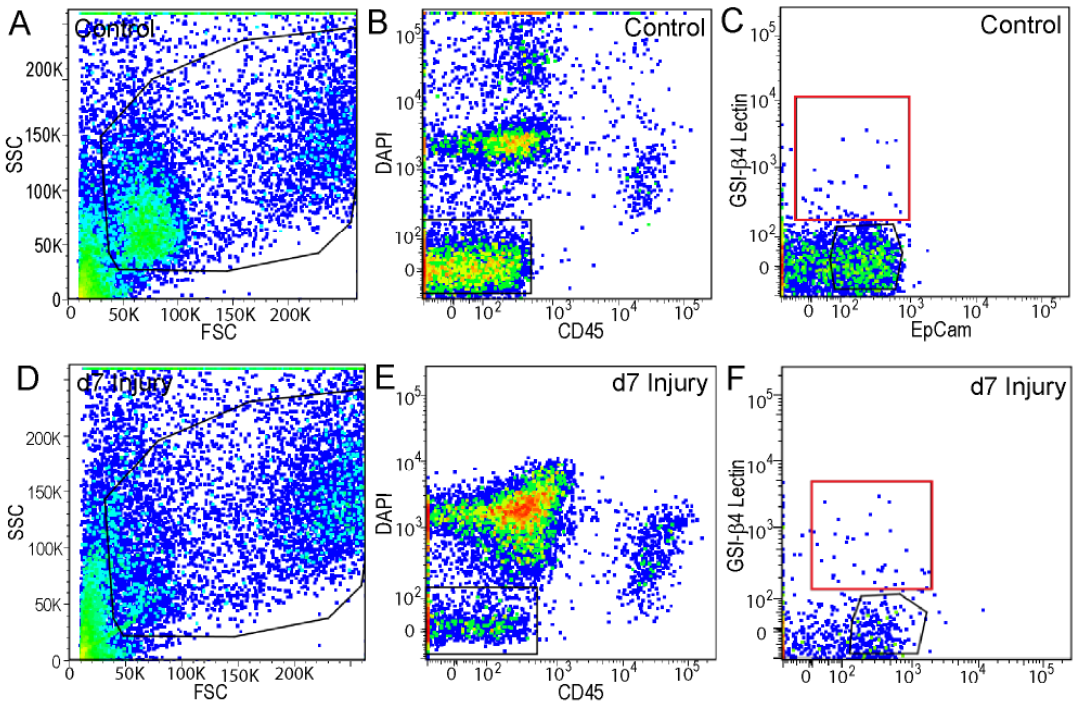

Figure 4.2 Flow cytometry plots of TOPgal tracheal epithelial cell preparations. Control (A-C) and polidocanol damaged, 7-day recovered (D-F) tracheal epithelial cells were selected on the basis of forward scatter (box, A, D), CD45 and DAPI negativity (box, B, E). (C, F) Basal and non-basal epithelial cells were further distinguished based on GSI-β4 lectin and EpCam reactivity (red and black boxes, respectively).

4.2 Basal stem cell β–catenin determines tracheal growth and differentiation

To assess the role of β–catenin in basal stem cell growth TOPgal reporter mice were crossed with a K14-dependent, oestrogen responsive and N-terminally truncated β-catenin transgenic line (ΔN-β-cateninER, termed D4) (Silva-Vargas, Lo Celso et al. 2005). These TOPgal x D4 (TOP-D4) bitransgenic mice activate β–catenin only in K14-expressing basal stem cells upon tamoxifen exposure. I treated TOP-D4 mice with 5 mg tamoxifen on days 0, 2, 4, 7, and 9 and culled mice on day 10.

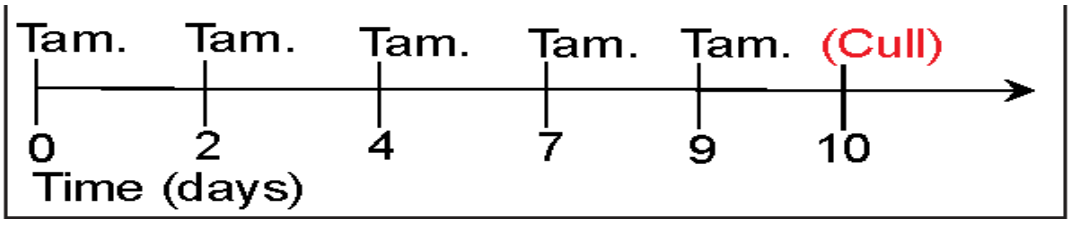

Figure 4.3 Tamoxifen dosimetry schedule.

FDG flow cytometry was used to compare the abundance, specificity and phenotype of β−catenin signalling cells (Figure 4.4A, B). I observed increased β−catenin signalling specifically within tracheal stem cells only after tamoxifen treatment.

H+E staining revealed that the tracheal height and cellular density of tamoxifen treated TOP-D4 mice was increased relative to controls (Figure 4.5A, B, G). Immunostaining revealed that TOP-D4 tracheas contained significantly more basal stem cells and increased CCSP-expressing cell differentiation (Figure 4.5C-F, H). There was additionally a trend toward reduced ciliated cell abundance after tamoxifen treatment (orange, Figure 4.5E, F, H) and significantly increased proliferation in tamoxifen treated TOP-D4 tracheas relative to controls (Figure 4.5I). Thus, adult tracheal stem cell β−catenin activity determines tracheal epithelial growth and differentiation.

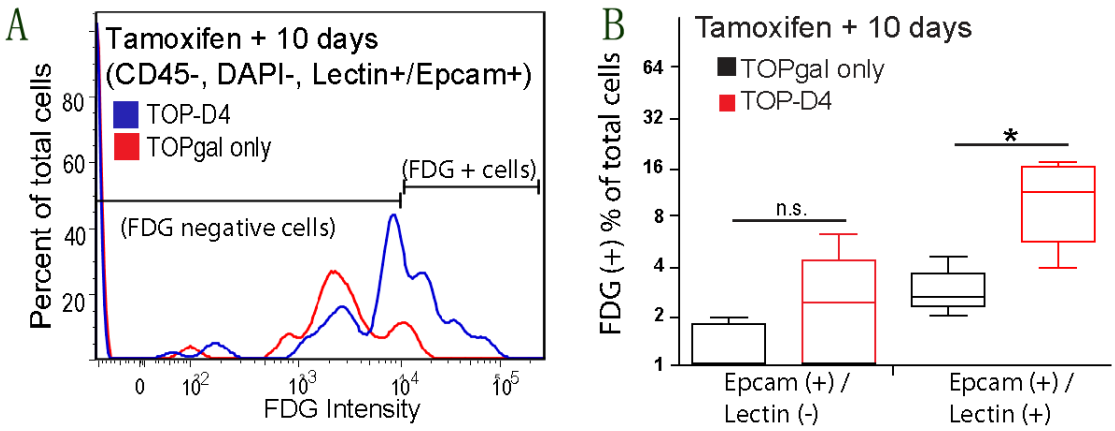

Figure 4.4 Basal stem cell β–catenin determines tracheal growth and lineage choice. (A, B) Representative flow cytometry plot (A) and quantitation of FDG reactive cell incidence (B) in TOP-D4 or TOPgal cells.

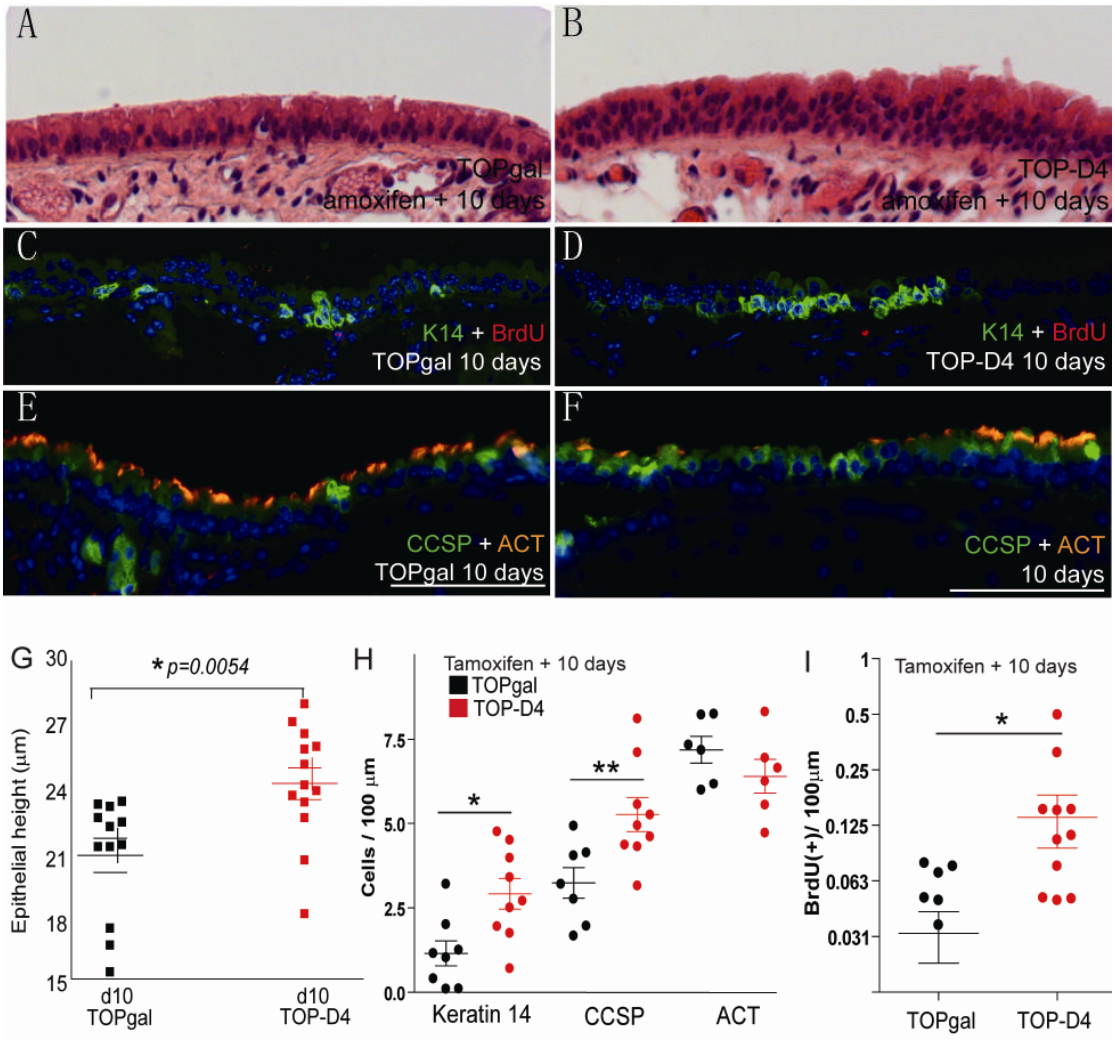

Figure 4.5 Phenotype of TOP-D4 mice. (A, B) Representative H+E stained, tamoxifen treated TOPgal (A) and TOP-D4 (B) trachea sections. (C-F) Representative tamoxifen treated TOPgal (C, E) and TOP-D4 (D, F) sections stained with antibodies directed against K14 (green, C, D), BrdU (red, C, D), CCSP (green, E, F) and acetylated tubulin (orange, E, F). (J-L) Quantitation of epithelial height (J), cellular phenotype (K), and BrdU incidence (L) in TOPgal (black) and TOP-D4 (red) tracheas. Scale bars (D-I) are 100μm; asterisks (C, J-L) represent statistical significance at $p<0.05$ (*) or $p<0.005$ (**) as indicated.

4.2 β–catenin signalling is dispensable for airway homeostasis

Separately I investigated whether stem cell β–catenin signalling was necessary for tracheal homeostasis or repair using a K14-dominant negative (N-terminally truncated) Lef1 transgenic mouse model (K14-dnLef1, (Niemann, Owens et al. 2002)). H+E staining and indirect antibody immunofluorescence revealed no differences between uninjured wildtype and K14-dnLef1 tracheal morphology, stem cell abundance, and epithelial proliferation (Figure 4.6A-D, quantitation in Figure 4.6M, N). Additionally, although it has been previously reported that Lef1 was required for tracheal submucosal gland development (Duan, Sehgal et al. 1998; Duan, Yue et al. 1999), both K14-dnLef1 and wildtype tracheas exhibited comparable submucosal gland abundance, distribution, and cellular phenotypes (Figure 4.7). This agreed with previous reports that β–catenin signalling is dispensable for airway homeostasis (Zemke, Teisanu et al. 2009).

To assess whether tracheal repair was perturbed in the absence of β–catenin signalling I compared polidocanol damaged wildtype and K14-dnLef1 transgenic tracheas. Three days after damage the epithelial height and cell density of K14-dnLef1 transgenic tracheas was reduced compared with wildtype (Figure 4.6E, F; quantitated in Figure 4.6M). Although this difference was not dependent on reduced K14-dnLef1 basal cell abundance I did observe significantly reduced cell proliferation in transgenic mice recovered for three days (Figure 4.6G, H, N). Seven days after damage cell proliferation, epithelial height, and cellular phenotype were all similar between wildtype and transgenic mice. Thus, stem cell β–catenin signalling was necessary for tracheal repair but not required in normal tracheal development or homeostasis (Niemann, Owens et al. 2002).

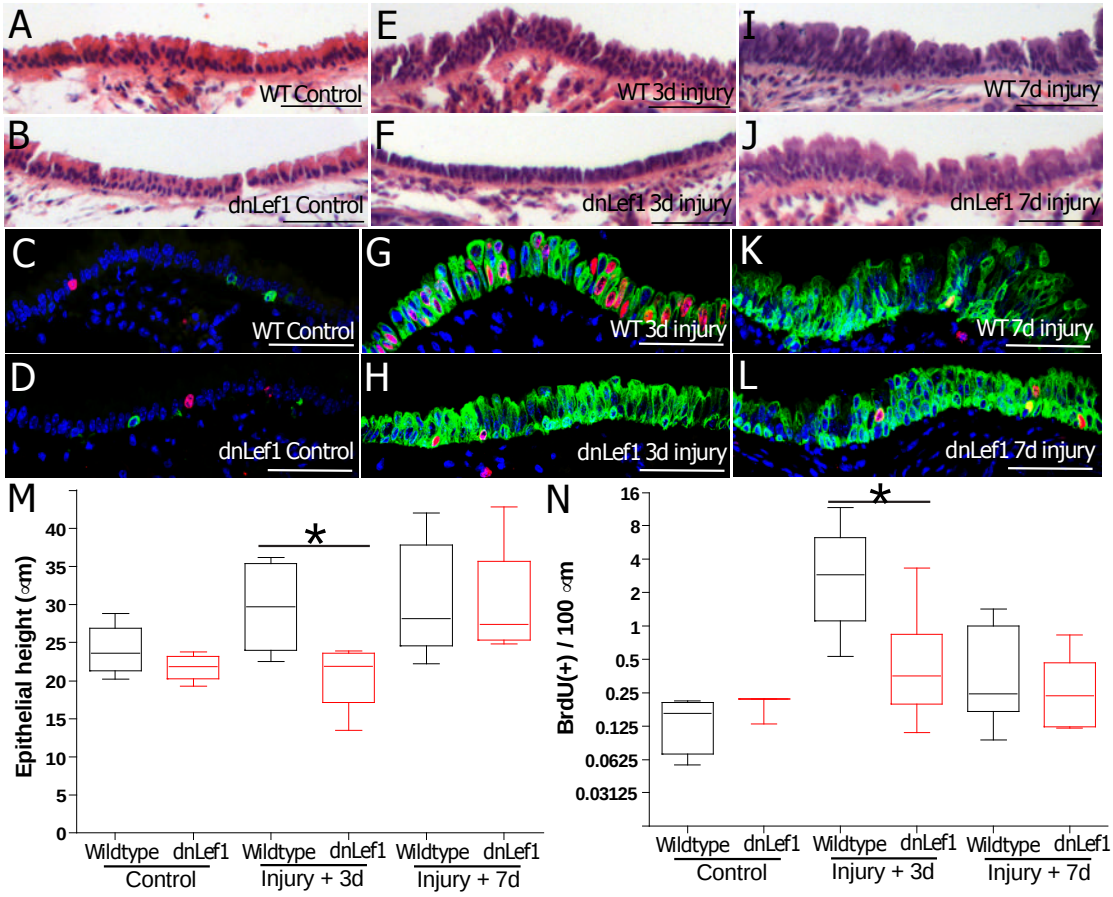

Figure 4.6 Stem cell β–catenin inhibition delays normal epithelial repair.

(A-L) H+E staining (A, B, E, F, I, J) and indirect immunofluorescence (C, D, G, H, K, L) using keratin 14 (green) plus BrdU (red) antibodies in uninjured (A-D) or polidocanol injured, 3 (E-H) and 7 day (I-L) recovered wildtype (A, E, I, C, G, K) and K14-dnLef1 transgenic tracheas (B, F, J, D, H, L). (M) Quantitation of average epithelial height in uninjured control and polidocanol damaged wildtype and K14-dnLef1 tracheas (black and red bars, respectively). (N) Quantitation of BrdU-reactive cell incidence per 100μm basement membrane length in control, 3-day and 7-day recovered wildtype and transgenic tracheas (black and red bars). Scale bars (A-L) are 100μm; asterisks (M, N) denote significance at $p<0.05$.

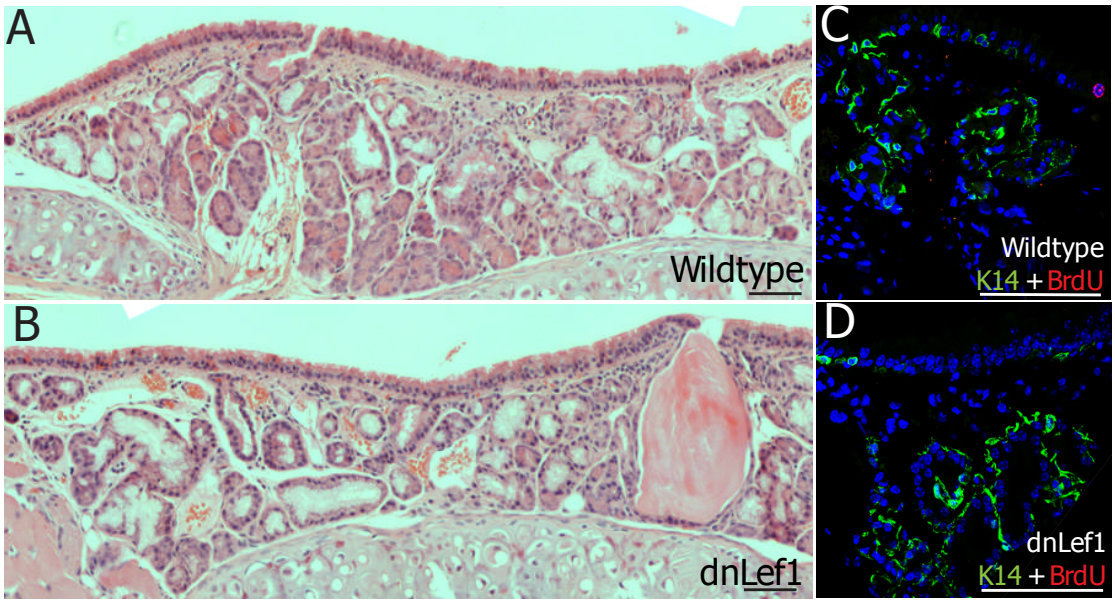

Figure 4.7 Submucosal gland development and homeostasis are unaffected by β–catenin inhibition. (A, B) Representative H+E stained tissue sections of wildtype (A) and K14-dnLef1 (B) tracheal submucosal glands. (C, D) Wildtype (C) and dnLef1 (D) submucosal glands stained using antibodies directed against K14 (green) plus BrdU (red). Scale bars are 100μm.

4.4 Basal stem cell β–catenin activity promotes an EMT phenotype

Previous studies have established that β–catenin may regulate epithelial fate via modulation of EMT phenotypes (Heuberger and Birchmeier 2010). To determine whether stem cell β–catenin activity induced an EMT within the trachea I examined E-cadherin abundance and target gene expression. Tamoxifen treated TOP-D4 tracheas exhibited significantly reduced E-cadherin levels throughout their epithelium relative to controls (Figure 4.8A, B; control average pixel intensity 141.7±11.1 out of 256 versus 97.3±8.2 in TOP-D4). I isolated RNA from 5 control and 5 TOP-D4 tamoxifen-treated tracheas and examined the expression of EMT-associated target genes Twist, Snail, Slug and Cyclin D1. TOP-D4 samples exhibited increased expression of Cyclin D1, Twist, and Snail (but not Slug) relative to controls (Figure 4.9C-F). Dual fluorescent immunostaining confirmed that β–catenin increased Snail expression throughout the trachea (red, Figure 4.9A, B). I also assessed epithelial smooth muscle actin (SMA) and Muc5AC cell abundance to determine whether β–catenin induced a complete or partial EMT and or metaplasia (Figure 4.10). I found that β–catenin activation increased Muc5AC(+) goblet cell abundance but did not promote tracheal epithelial SMA expression.

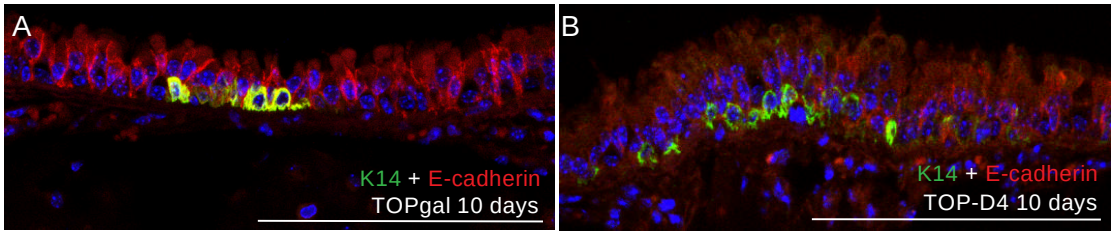

Figure 4.8 Tracheal stem cell β-catenin signalling reduces E-cadherin levels.

(A, B) Representative tamoxifen treated TOPgal (A) and TOP-D4 (B) sections stained with K14 (green) and E-cadherin (red). Scale bars (A, B) are 100μm

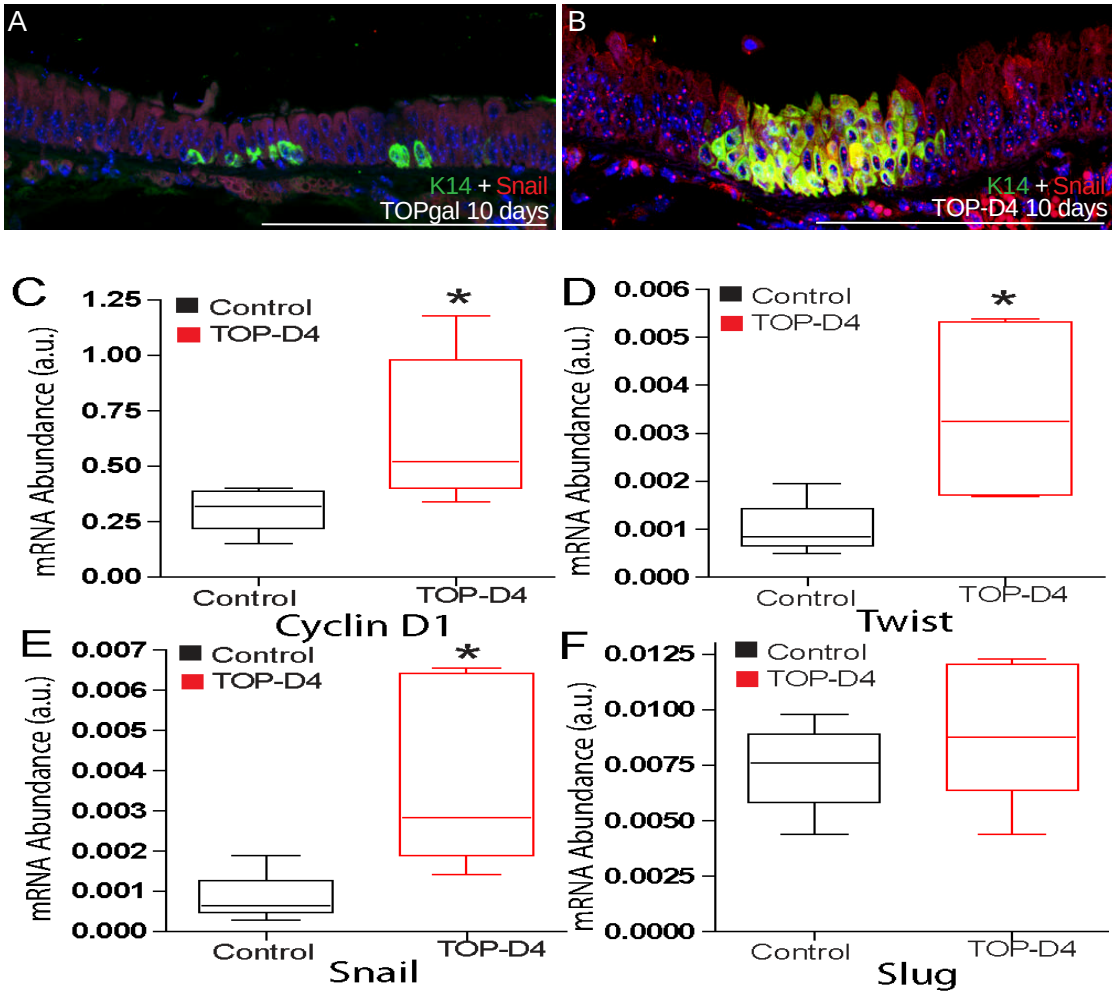

Figure 4.9 Tracheal stem cell β-catenin signalling increases the expression of EMT-associated target genes (A, B) Representative tamoxifen treated TOPgal (A) and TOP-D4 (B) sections stained with K14 (green) and Snail (red). (C-F) Quantitative PCR analysis of total RNA from TOPgal (control, black) and TOP-D4 (red) tracheal epithelial cells following tamoxifen treatment. Cyclin D1 (C), Twist (D), Snail (E), and Slug (F) abundance was assessed and normalised to β2-microglobulin using ΔCT calculations. Scale bars (A, B) are 100μm; asterisks (C-E) represent statistical significance at $p<0.05$ (*).

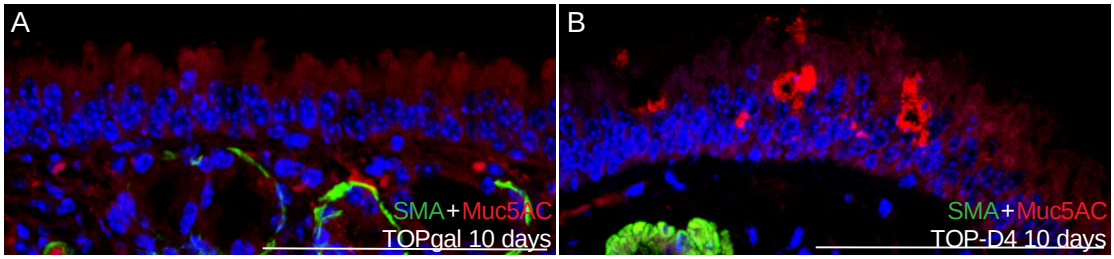

Figure 4.10 Tracheal stem cell β-catenin activation promotes a partial EMT

(A, B) Tamoxifen-treated TOPgal (G, I) and TOP-D4 tracheal sections were stained with antibodies directed against smooth muscle actin (SMA, green), and Muc5AC (red). Scale bars (A, B) are 100μm.

4.5 E-cadherin inhibition phenocopies β-catenin activation

To assess whether β–catenin regulated tracheal differentiation by modulating intercellular adhesiveness I used an air-liquid interface (ALI) model (Figure 4.11) (You, Richer et al. 2002).

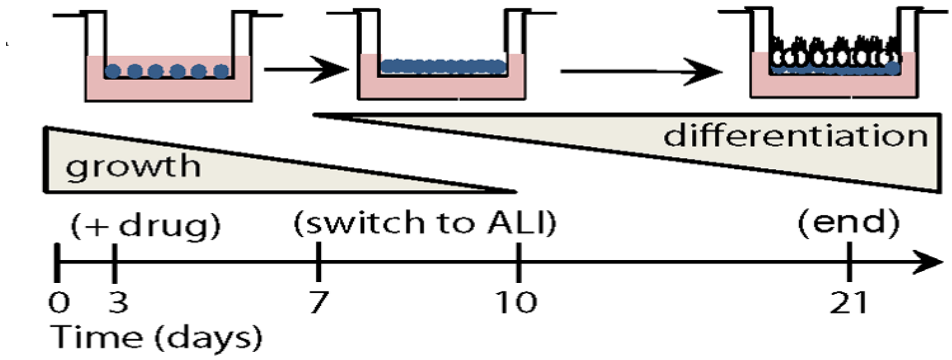

Figure 4.11 Diagram of ALI model and inhibitory drug dosimetry schedule

Murine ALI cultures were grown in the presence of the GSK3β inhibitory (β–catenin activating) drug SB415286 or the E-cadherin inhibitory monoclonal antibody DECMA-1; DMSO was used as a control (Coghlan, Culbert et al. 2000; Kobayashi, Ikesue et al. 2006). Protein analysis of cell lysates harvested at day 21 revealed that treatment with either 10 or 30μM SB415286 increased GSK3β Serine 9 protein phosphorylation (Figure 4.12A). I also observed increased expression of the β–catenin target protein Cyclin D1 upon treatment with 30μM SB415286 (Figure 4.12B, C).

Interestingly, although SB415286, DECMA-1, and DMSO treated cells appeared similar

while in submersion culture, only DMSO treated cells exhibited abundant acetylated tubulin differentiation following the switch to ALI (red, Figure 4.13A-C). Western blots of protein isolated from these cultures confirmed this result (Figure 4.12). Treatment with SB415286 and DECMA-1 also moderately increased K14-expressing cell abundance (green, Figure 4.13A-C). Separately, I assessed cell proliferation following treatment with SB415286 or DECMA-1 by examining BrdU nucleoside incorporation. I found that both β–catenin activation and E-cadherin inhibition increased epithelial cell proliferation relative to controls (Figure 4.13D-F). I also examined cell surface E-cadherin (green, Figure 4.13G-I) and ZO-1 protein abundance (red, Figure 4.13G-I) in ALI cultures treated with SB415286, DECMA-1, and DMSO. E-cadherin staining was reduced while ZO-1 levels were maintained in confluent ALI cultures treated with SB415286 or DECMA-1.

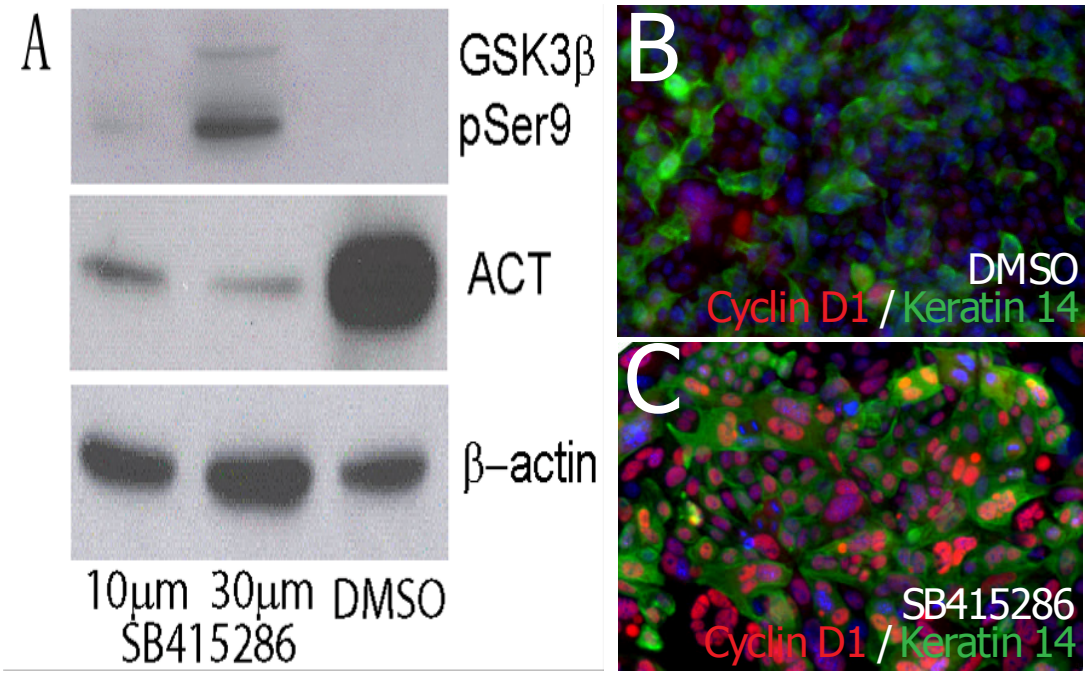

Figure 4.12 GSK3β inhibitor activates β–catenin pathway.

(A) Protein blot of DMSO, 10- and 30-μM SB415286-treated ALI cultures using indicated antibodies. (B, C) Wholemount cyclin D1 (red) and keratin 14 (green) staining of DMSO (B), 30μM SB415286 (C) differentiated ALI cultures.

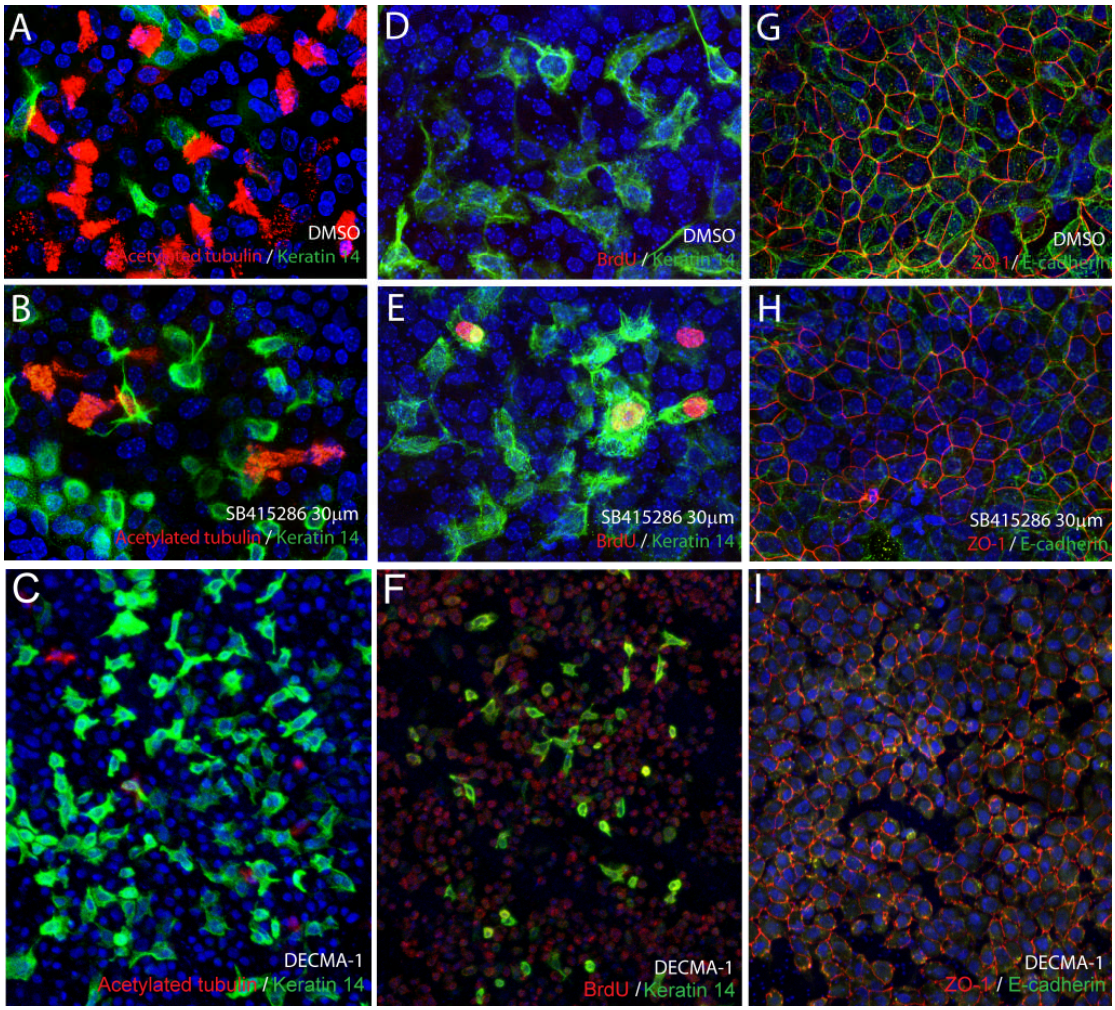

Figure 4.13 E-cadherin inhibition phenocopies β–catenin activation.

Wholemount antibody staining of DMSO (A, D, G), 30μM SB415286 (B, E, H), and DECMA-1 treated (C, F, I) differentiated ALI cultures. Antibodies included Keratin 14 (green, A-F), ACT (red, A-C), BrdU (red, D-F), ZO-1 (red, G-I) and E-cadherin (green, G-I). DAPI (blue) was used as a nuclear counterstain (A-I).

4.6 β–catenin signalling promotes a preinvasive SCC cellular phenotype

Finally to confirm if β–catenin activation could promote cellular phenotypes in human airway cells in vitro consistent with those seen in preinvasive human SCCs I treated immortalised human bronchial epithelial cells (iHBECs) with SB415286. iHBECs express keratins 5 and 14, form tight intercellular adhesions, and exhibit multipotent differentiation when cultured at an air-liquid interface (Borthwick, Shahbazian et al. 2001). Flow cytometric analysis of SB415286-treated iHBECs revealed significantly reduced G0/1 and increased G2/M phase cells relative to DMSO-treated controls (Figure 4.14). This was accompanied by reduced cell-surface E-cadherin protein abundance (Figure 4.15A, B) and an increase in EMT-associated β–catenin target gene expression (Figure 4.14B, Figure 4.15C).

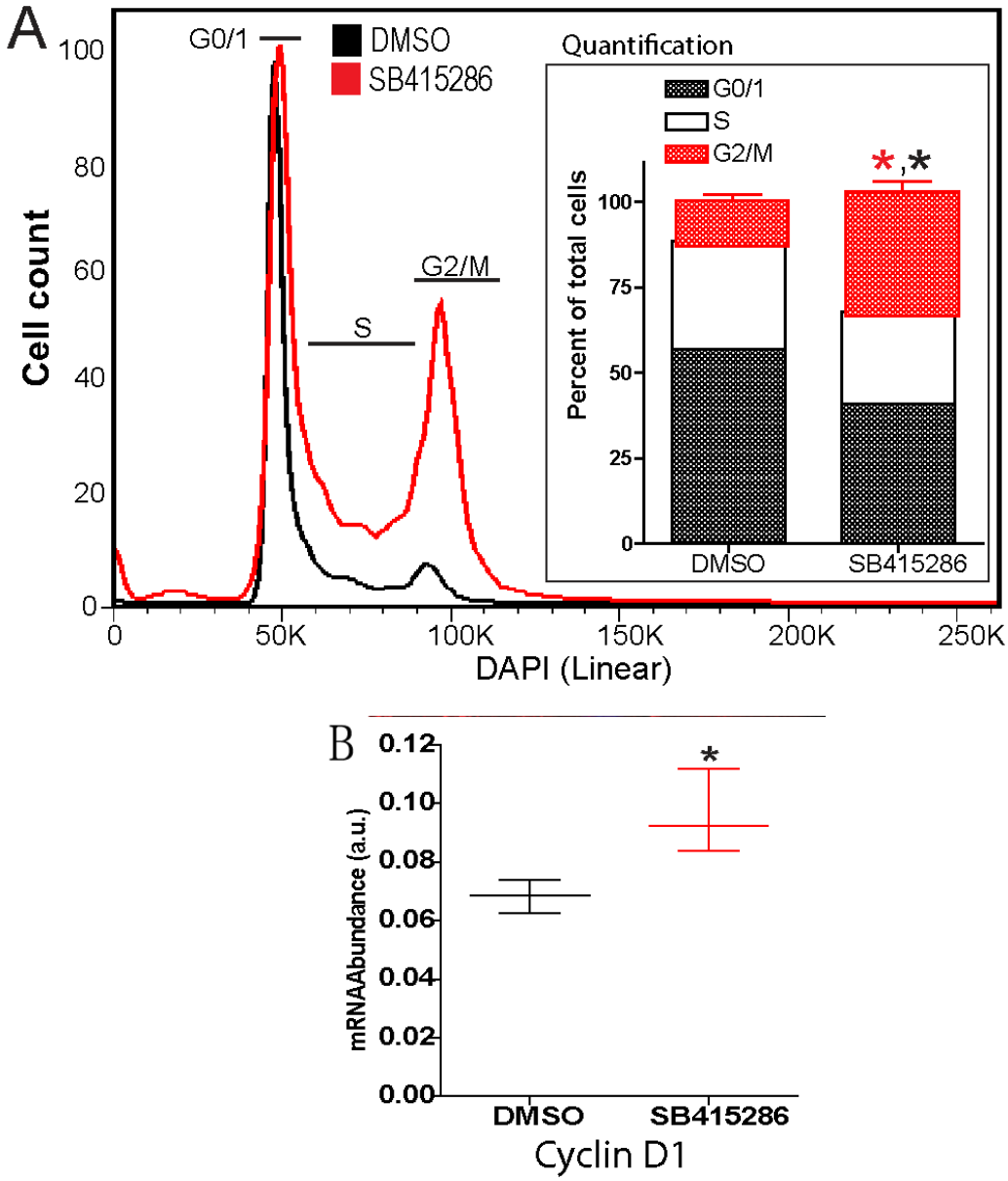

Figure 4.14 β-catenin determines human airway proliferation

(A) Representative flow cytometry plot and quantitation of human bronchial epithelial cell (iHBEC) cell cycle following DMSO (black line) or 30μM SB415286 treatment (red line). (B) Cyclin D1 quantitative PCR analysis of total RNA isolated from iHBECs treated for 24 hours with DMSO (black) or 30μM SB415286 (red). Transcript abundance was normalised to 18S and quantitated using ΔCT calculations. Asterisks (A, B) represent significance of $p<0.05$ (*) or $p<0.005$ (**).

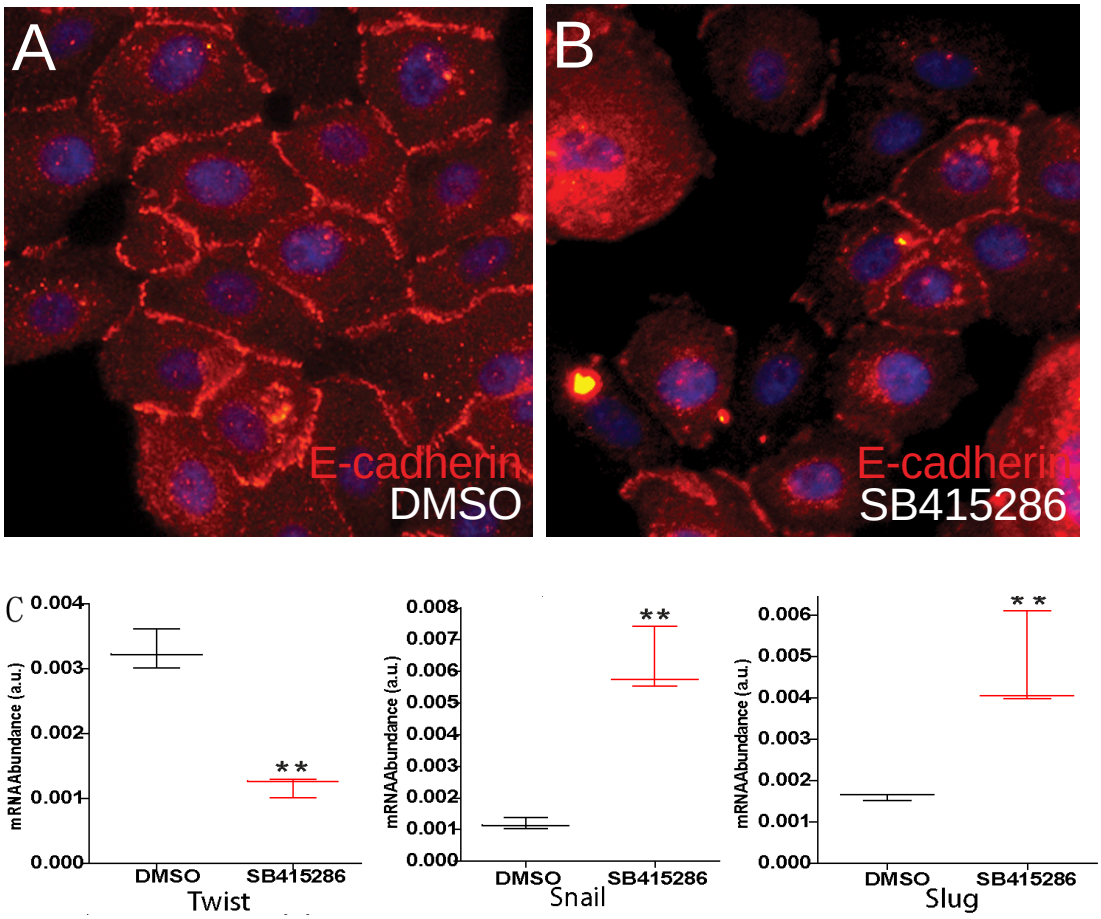

Figure 4.15 β-catenin determines human airway EMT phenotype

(A, B) E-cadherin antibody staining of iHBECs treated for 24 hours with DMSO (A) or 30μM SB415286 (B). (C) Quantitative PCR analysis of total RNA isolated from iHBECs treated for 24 hours with DMSO (black) or 30μM SB415286 (red). Twist, Snail, and Slug transcript abundance was normalised to 18S and quantitated□using ΔCT calculations. Asterisks (C) represent significance of $p<0.05$ (*) or $p<0.005$ (**).

4.7 β–catenin is associated with increased SCC severity

To first ascertain whether β–catenin was associated with SCC severity I examined β–catenin localisation in 45 biopsy samples from patients with various stages of preinvasive SCC (normal, metaplasia, mild, moderate, and severe dysplasia, carcinoma in situ). Hematoxylin and eosin (H+E) staining revealed dramatic differences in tissue morphology between each stage (compare metaplasia and severe dysplasia, Figure 4.16A, B). All normal and metaplastic lung tissue sections stained for β–catenin exhibited robust membrane associated β–catenin and no nuclear or cytoplasmic protein localisation (Figure 4.16C). In contrast samples with mild to severe dysplasia and carcinoma in situ exhibited extensive nuclear and cytoplasmic β–catenin abundance (Figure 4.16D, data quantitated in Figure 4.16E).

Using Ki67 and E-cadherin immunostaining I determined cell proliferation was increased in samples exhibiting nuclear or cytoplasmic β–catenin localisation relative to those with membrane-associated β-catenin (Figure 4.17A, B). Further, in severely dysplastic and carcinoma in situ samples with nuclear or cytoplasmic β–catenin expression cell proliferation was not restricted to the basal layer (arrow, Figure 4.17B). E-cadherin was also reduced in basal cells with nuclear or cytoplasmic β-catenin localisation (Figure 4.17C, D). Thus, increased airway β–catenin signalling is positively associated with elevated proliferation and reduced E-cadherin abundance (Figure 4.17E, F).

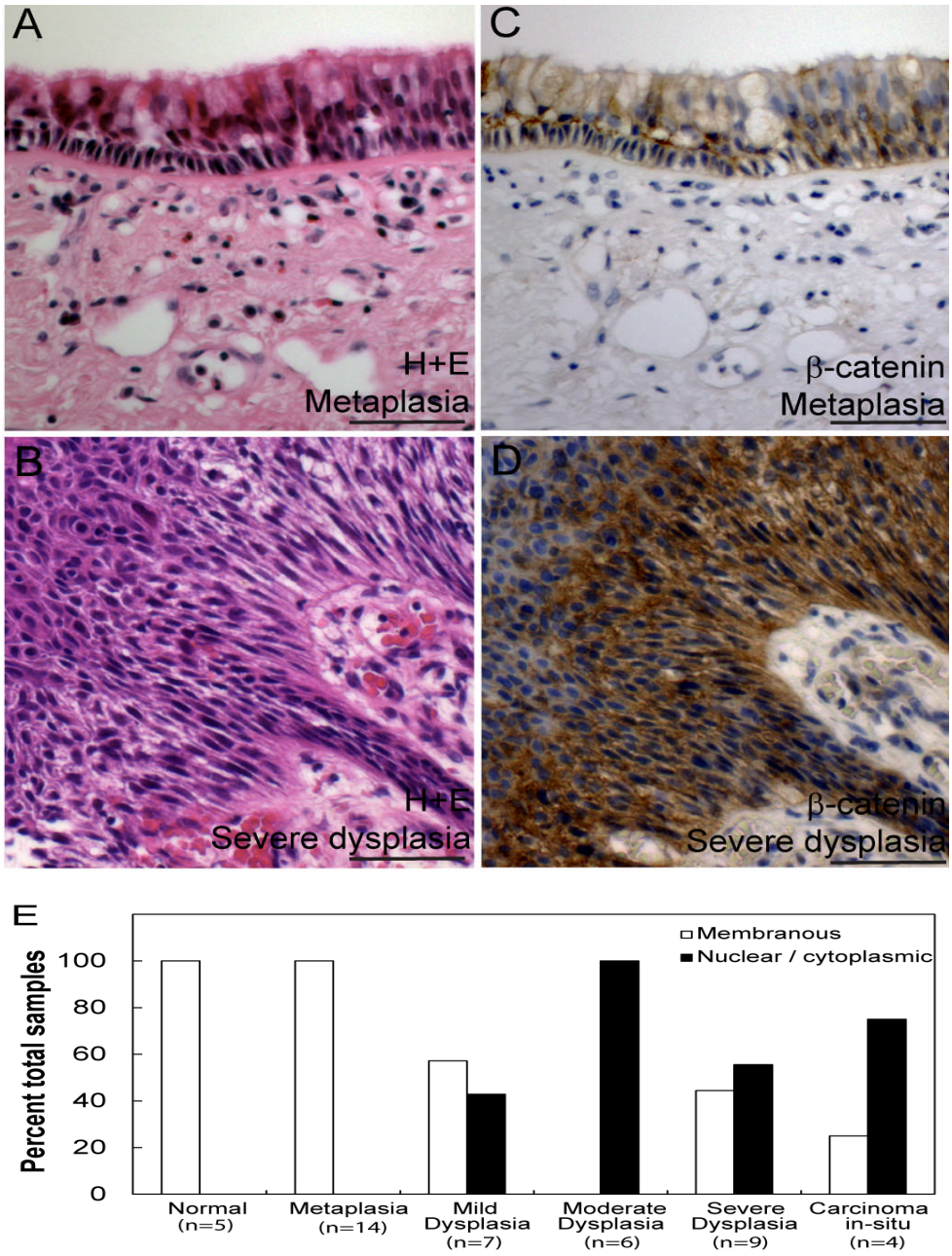

Figure 4.16 β–catenin activation is associated with increased preinvasive SCC severity. (A-D) Representative images of metaplastic (A, C) and severely dysplastic (B, D) SCC biopsies stained with H+E (A, B) or antibodies directed against β-catenin (C, D). (E) Quantitation of the percent of biopsy samples exhibiting membranous (white bars) or nuclear / cytoplasmic β-catenin (black bars). Scale bars (A-D) are 100μm.

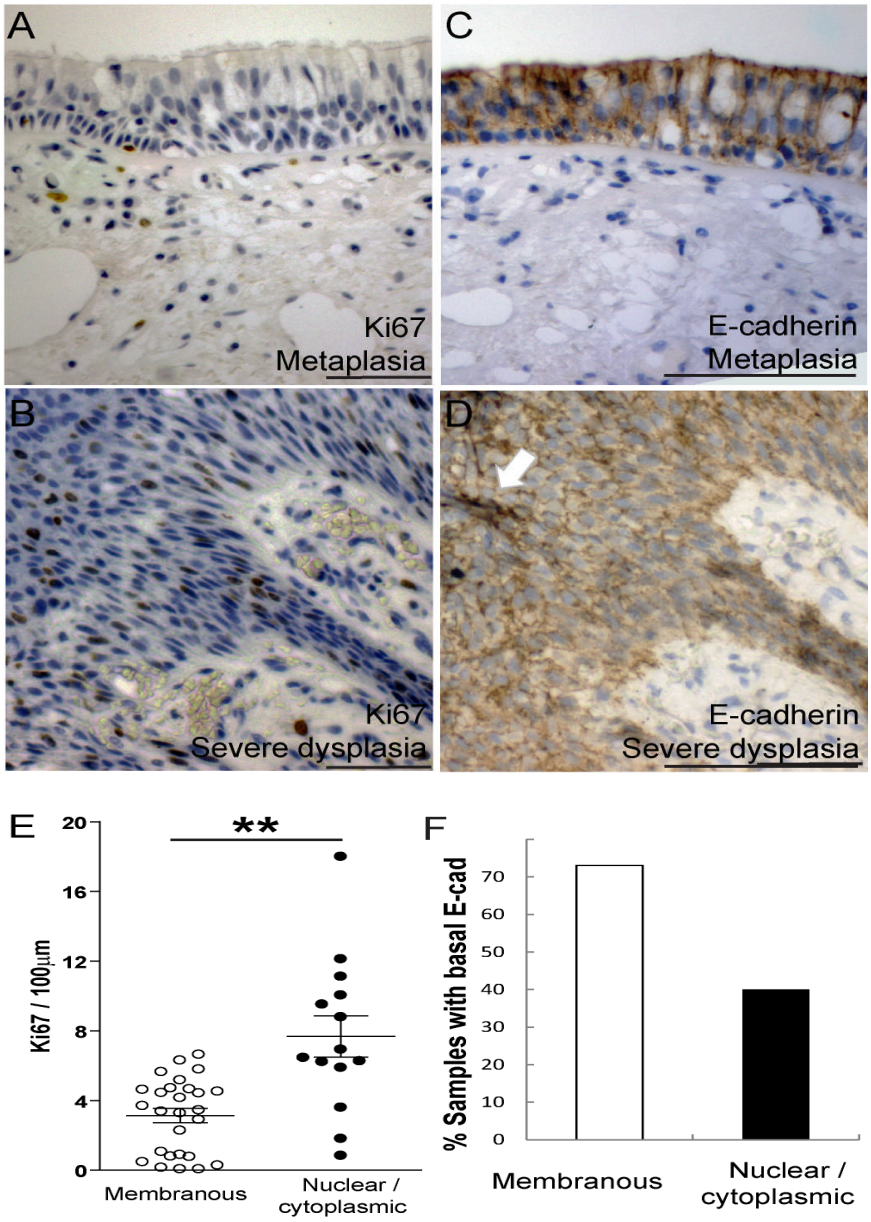

Figure 4.17 β–catenin activation is associated with increased proliferation and loss of E-cadherin in preinvasive SCC lesion (A-E) Representative images of metaplastic (A, C) and severely dysplastic (B, D) SCC biopsies stained with antibodies directed against Ki67 (A, B), and E-cadherin (C, D). (E, F) Overall Ki67 incidence and basal E-cadherin abundance in samples with membranous or nuclear/cytoplasmic β-catenin (white and black bars). Scale bars (A-D) are 100μm; asterisks (E) denote significance at $p<0.005$.

CHAPTER 5. DISCUSSION

I have examined two key signalling systems and their regulation of normal airway homeostasis and importantly their role in the formation of early lung cancer lesions. Understanding the mechanism of lung cancer development may lead to chemopreventative strategies in the fight against this disease that currently presents late in its course and has a very low cure rate.

The EGFR pathway

From my data in chapter 3 I identify LRIG1 as an important regulator of tissue homeostasis in the major airways. I demonstrate that LRIG1 acts as a tumour suppressor by forming a ternary complex at adhering junctions with E-cadherin and EGFR. This complex controls EGFR/ERK1/2 activation upon cell-cell contact.

Pre-invasive lung cancer lesions are characterised by loss of contact inhibition, increased epithelial proliferation and elevated EGFR activation and my findings identify loss of LRIG1 as an early event in the pathogenesis of squamous cell lung carcinomas and provide insight into elevated EGFR activation.

As loss of LRIG1 has been identified as one of four key events that predict patient outcome across 5 tumour types including 129 lung squamous cell carcinoma patients

(Rouam, Moreau et al. 2010) I propose that this as a general mechanism for controlling homeostasis in other epithelial tissues. This has widespread implications for the role of cell-cell contact inhibition and regulation of EGFR signalling in development, tissue homeostasis and disease.

EGFR and E-cadherin are known to co-localise on cell-cell contact as I have also demonstrated. Others have shown that while E-cadherin protein levels increase five times at cell confluence, EGFR mRNA and protein levels remain constant but tyrosine kinase activity is reduced (Takahashi and Suzuki 1996). The mechanism by which EGFR activation is reduced at cell confluence was not previously understood. A postulated way of producing this fall in EGFR phosphorylation is a direct inhibitory interaction between E-cadherin and EGFR but there is no data to my knowledge to support this. My data however shows that the endogenous EGFR inhibitory molecule LRIG1 is also recruited to the complex at cell confluency and is required for density dependent growth inhibition.

LRIG1 is expressed in all tissues (Nilsson, Vallbo et al. 2001) and endogenous and synthetic LRIG1 has been confirmed to be plasma membrane bound by cell surface biotinylation/precipitation and confocal immunofluorescence and laser microscopy (Nilsson, Starefeldt et al. 2003). Previous data suggest LRIG1 blocks EGFR activation through two possible mechanisms. First, LRIG1 transcript and protein are known to be upregulated after EGF stimulation which is thought to be a negative feedback mechanism whereby it associates with all four EGFR analogues and both proteins are subsequently ubiquitinated by ubiquitin ligases (Gur, Rubin et al. 2004). Alternatively LRIG1 has been postulated to bind EGFR in a monomeric ‘attenuated’ state. This is because LRIG1 with the intracellular domain, including c-Cbl E3 ubiquitin ligase binding domain deleted, still attenuates EGFR activity without physical down regulation of the protein and without

competing for EGF binding (Goldoni, Iozzo et al. 2007). My data suggest the latter maybe the case in density dependent growth inhibition as I see no down regulation of the EGFR protein itself but a dramatic fall in EGFR activity at cell-cell contact with LRIG1 expression.

I have therefore established LRIG1 as an important tumour suppressor gene in lung cancer with its loss occurring in the pre-invasive stages of cancer development. LRIG1 loss appears to be among the earliest abnormalities occurring in pre-cancerous airway epithelium possibly leading to abnormal areas of proliferative epithelium that attract subsequent genetic mutations. Examination of data from expression profiling of CIS lesions confirms LRIG1 loss in CIS with a six fold fall compared to normal epithelium (Lonergan, Chari et al. 2010). Understanding the mechanism of LRIG1 loss in the airways of smokers and whether this phenotype can be reversed may have important impacts on future chemopreventative strategies.

For future work I would like to examine the mechanism of LRIG1 downregulation in human tissues. First I would examine for LOH at its chromosomal location of 3p14 and second I would like to look at the methylation profile of the gene and its promotor.

The Wnt Pathway

In chapter 4, I examine the canonical Wnt pathway. I find that β-catenin regulates tracheal epithelial stem cell growth and lineage choice through modulation of E-cadherin and intercellular adhesiveness. I demonstrate that β-catenin becomes activated within basal stem cells subsequent to tracheal damage and that inhibition of β-catenin signalling

decreases cell proliferation and inhibits normal epithelial repair. Separately, K14 positive basal cell-specific β-catenin activation restricts ciliated cell differentiation, promotes increased proliferation, and reduces cell adhesiveness both in vitro and in vivo. In humans with basal cell-derived pre-invasive squamous lung cancer lesions there are positive correlations between elevated β-catenin signalling, disease severity, epithelial proliferation, and an EMT phenotype. All of these effects are recapitulated following direct inhibition of E-cadherin, supporting a mechanism in which stem cell β-catenin signalling directs airway epithelial growth and lineage choice via modulation of intercellular adhesions.

My discovery of a role for β-catenin in upper airway repair is consistent with earlier works investigating the role of β-catenin in distal lung development, homeostasis and repair. In particular, genetically modified mouse models in which β-catenin is activated throughout developing airways exhibit reduced ciliated cell differentiation, expansion of bronchio-alveolar duct junction stem cells (BASCs), and increased epithelial proliferation (Okubo and Hogan 2004; Mucenski, Nation et al. 2005; Reynolds, Zemke et al. 2008; Zhang, Goss et al. 2008; Li, Li et al. 2009; Voronina, Takemaru et al. 2009). Some of these models also exhibit tumour development and hyperplasic epithelial polyp formation that are reminiscent of human lung cancers (Mucenski, Nation et al. 2005; Li, Li et al. 2009). However, my studies are the first to demonstrate a direct relationship between stem cell β-catenin signalling, intercellular adhesions, epithelial growth and lineage choice in human preinvasive lung cancers.

In addition to the aforementioned similarities there are several distinctions between my results and those of earlier studies. These differences include my observation that

β-catenin signalling within tracheal stem cells is by itself sufficient to promote epithelial proliferation, enhanced basal and secretory cell differentiation, and hyperplasia. I also found that β-catenin signalling within tracheal stem cells was necessary for normal epithelial repair. I feel these differences are best explained by the choice of transgenic mouse model. Importantly, the present work represents an investigation of the role of β-catenin signalling specifically within K14-expressing stem cells of adult mice upon exposure to exogenously administered tamoxifen. These mouse models therefore avoid any potentially confounding developmental, compensatory, and / or off-target transgene effects that are a component of earlier studies (Okubo and Hogan 2004; Mucenski, Nation et al. 2005; Reynolds, Zemke et al. 2008; Li, Li et al. 2009).

A key finding was my observation in work done with Dr Adam Giangreco that β-catenin directly modulates cellular EMT phenotypes including E-cadherin abundance and transcription of Twist, Snail, Slug, and Cyclin D1. I found that E-cadherin inhibition and subsequent loss of adherens junctions, functions as a molecular switch to regulate tracheal epithelial cell growth and differentiation.These results are consistent with identified roles for both β-catenin and E-cadherin in directing epithelial stem cell phenotypes in other tissues (Heuberger and Birchmeier 2010). Notably, skin development and tumour initiation are both known to be regulated by basal stem cell β-catenin signalling influencing intercellular adhesions (Jamora and Fuchs 2002; Jamora, DasGupta et al. 2003).

Although associations between pre-invasive cancer severity and cellular epithelial-to-mesenchymal transition (EMT) phenotypes already exist, the mechanisms responsible for regulating EMT phenotypes during lung tumour initiation and progression

have largely remained elusive (Foster, Banerjee et al. 2005). It is now appreciated that dysregulated β-catenin signalling is of central importance in driving an EMT phenotype associated with epithelial diseases (Heuberger and Birchmeier 2010). My data provides the first evidence that increased β-catenin signalling directly influences lung EMT phenotypes via modulation of cellular adhesions. My results also provide a simple mechanism to explain the recent observation that several β-catenin signalling pathway components are associated with poor human lung cancer outcomes (Nguyen, Chiang et al. 2009).

My demonstration of functional links between β-catenin signalling, E-cadherin inhibition via Twist, Slug and Snail, and airway stem cell growth and differentiation may explain how β-catenin signalling pathway components can become overexpressed in squamous cell carcinomas despite a paucity of identified β-catenin mutations associated with this disease (Konigshoff and Eickelberg 2010). My study identifies novel roles for β-catenin in normal and disease-associated tracheal stem cell growth and lineage choice advances our understanding both of fundamental airway stem cell biology as well as identifies an important regulatory mechanism for human lung cancer differentiation.

Future work could pursue the known regulators of EMT that are activated in my murine models. I have demonstrated that the canonical β-catenin pathway is important but there are currently no therapeutic options involving this pathway due to its global influence in tissue homeostasis. If a particular downstream pathway (Snail, Slug, Twist) is responsible for the majority of the phenotype demonstrated I could pursue this in cancer models and determine its role in the early stages of lung cancer development, again possibly discovering a new therapeutic for this miserable disease.

CHAPTER 6. REFERENCES

Alao, J. P., S. C. Gamble, et al. (2006). "The cyclin D1 proto-oncogene is sequestered in the cytoplasm of mammalian cancer cell lines." Mol Cancer **5**: 7.

Anastasi, S., M. F. Baietti, et al. (2007). "The evolutionarily conserved EBR module of RALT/MIG6 mediates suppression of the EGFR catalytic activity." Oncogene **26**(57): 7833-46.

Andl, C. D. and A. K. Rustgi (2005). "No one-way street: cross-talk between e-cadherin and receptor tyrosine kinase (RTK) signaling: a mechanism to regulate RTK activity." Cancer Biol Ther **4**(1): 28-31.

Arce, L., N. N. Yokoyama, et al. (2006). "Diversity of LEF/TCF action in development and disease." Oncogene **25**(57): 7492-504.

Baselga, J. "Targeting the phosphoinositide-3 (PI3) kinase pathway in breast cancer." Oncologist **16 Suppl 1**: 12-9.

Behrens, J. (2000). "Control of beta-catenin signaling in tumor development." Ann N Y Acad Sci **910**: 21-33; discussion 33-5.

Boelens, M. C., A. van den Berg, et al. (2009). "Current smoking-specific gene expression signature in normal bronchial epithelium is enhanced in squamous cell lung cancer." J Pathol **218**(2): 182-91.

Borthwick, D. W., M. Shahbazian, et al. (2001). "Evidence for stem-cell niches in the tracheal epithelium." Am J Respir Cell Mol Biol **24**(6): 662-70.

Burgel, P. R. and J. A. Nadel (2004). "Roles of epidermal growth factor receptor activation in epithelial cell repair and mucin production in airway epithelium."

Thorax **59**(11): 992-6.

Case, N. and J. Rubin (2010). "Beta-catenin--a supporting role in the skeleton." J Cell Biochem **110**(3): 545-53.

Citri, A. and Y. Yarden (2006). "EGF-ERBB signalling: towards the systems level." Nat Rev Mol Cell Biol **7**(7): 505-16.

Coghlan, M. P., A. A. Culbert, et al. (2000). "Selective small molecule inhibitors of glycogen synthase kinase-3 modulate glycogen metabolism and gene transcription." Chem Biol **7**(10): 793-803.

Cordero, J. B., M. Cozzolino, et al. (2002). "1,25-Dihydroxyvitamin D down-regulates cell membrane growth- and nuclear growth-promoting signals by the epidermal growth factor receptor." J Biol Chem **277**(41): 38965-71.

Cross, D. A., A. A. Culbert, et al. (2001). "Selective small-molecule inhibitors of glycogen synthase kinase-3 activity protect primary neurones from death." J Neurochem **77**(1): 94-102.

Dale, T. C. (1998). "Signal transduction by the Wnt family of ligands." Biochem J **329 (Pt 2)**: 209-23.

DasGupta, R. and E. Fuchs (1999). "Multiple roles for activated LEF/TCF transcription complexes during hair follicle development and differentiation." Development **126**(20): 4557-68.

Dittmann, K., C. Mayer, et al. (2005). "Radiation-induced epidermal growth factor receptor nuclear import is linked to activation of DNA-dependent protein kinase." J Biol Chem **280**(35): 31182-9.

Dor, Y., J. Brown, et al. (2004). "Adult pancreatic beta-cells are formed by self-duplication rather than stem-cell differentiation." Nature **429**(6987): 41-6.

Dor, Y. and D. A. Melton (2004). "How important are adult stem cells for tissue

maintenance?" Cell Cycle **3**(9): 1104-6.

Duan, D., A. Sehgal, et al. (1998). "Lef1 transcription factor expression defines airway progenitor cell targets for in utero gene therapy of submucosal gland in cystic fibrosis." Am J Respir Cell Mol Biol **18**(6): 750-8.

Duan, D., Y. Yue, et al. (1999). "Submucosal gland development in the airway is controlled by lymphoid enhancer binding factor 1 (LEF1)." Development **126**(20): 4441-53.

El-Bahrawy, M. A., I. C. Talbot, et al. (2002). "The expression of E-cadherin and catenins in colorectal tumours from familial adenomatous polyposis patients." J Pathol **198**(1): 69-76.

Felip, E., S. Cedres, et al. (2010). "How to integrate current knowledge in selecting patients for first line in NSCLC?" Ann Oncol **21 Suppl 7**: vii230-vii233.

Ferby, I., M. Reschke, et al. (2006). "Mig6 is a negative regulator of EGF receptor-mediated skin morphogenesis and tumor formation." Nat Med **12**(5): 568-73.

Foster, N. A., A. K. Banerjee, et al. (2005). "Somatic genetic changes accompanying lung tumor development." Genes Chromosomes Cancer **44**(1): 65-75.

Fujita, Y., G. Krause, et al. (2002). "Hakai, a c-Cbl-like protein, ubiquitinates and induces endocytosis of the E-cadherin complex." Nat Cell Biol **4**(3): 222-31.

Giangreco, A., E. N. Arwert, et al. (2009). "Stem cells are dispensable for lung homeostasis but restore airways after injury." Proc Natl Acad Sci U S A **106**(23): 9286-91.

Giangreco, A., K. R. Groot, et al. (2007). "Lung cancer and lung stem cells: strange bedfellows?" Am J Respir Crit Care Med **175**(6): 547-53.

Giangreco, A., K. B. Jensen, et al. (2009). "Necl2 regulates epidermal adhesion and

wound repair." Development **136**(20): 3505-14.

Goldoni, S., R. A. Iozzo, et al. (2007). "A soluble ectodomain of LRIG1 inhibits cancer cell growth by attenuating basal and ligand-dependent EGFR activity." Oncogene **26**(3): 368-81.

Guo, D., J. Nilsson, et al. (2006). "Perinuclear leucine-rich repeats and immunoglobulin-like domain proteins (LRIG1-3) as prognostic indicators in astrocytic tumors." Acta Neuropathol **111**(3): 238-46.

Gur, G., C. Rubin, et al. (2004). "LRIG1 restricts growth factor signaling by enhancing receptor ubiquitylation and degradation." Embo J **23**(16): 3270-81.

Hanada, N., H. W. Lo, et al. (2006). "Co-regulation of B-Myb expression by E2F1 and EGF receptor." Mol Carcinog **45**(1): 10-7.

He, B., L. You, et al. (2004). "A monoclonal antibody against Wnt-1 induces apoptosis in human cancer cells." Neoplasia **6**(1): 7-14.

Hedman, H. and R. Henriksson (2007). "LRIG inhibitors of growth factor signalling - double-edged swords in human cancer?" Eur J Cancer **43**(4): 676-82.

Heuberger, J. and W. Birchmeier (2010). "Interplay of cadherin-mediated cell adhesion and canonical Wnt signaling." Cold Spring Harb Perspect Biol **2**(2): a002915.

Hong, K. U., S. D. Reynolds, et al. (2004). "In vivo differentiation potential of tracheal basal cells: evidence for multipotent and unipotent subpopulations." Am J Physiol Lung Cell Mol Physiol **286**(4): L643-9.

Hordijk, P. L., J. P. ten Klooster, et al. (1997). "Inhibition of invasion of epithelial cells by Tiam1-Rac signaling." Science **278**(5342): 1464-6.

Huber, A. H., W. J. Nelson, et al. (1997). "Three-dimensional structure of the armadillo repeat region of beta-catenin." Cell **90**(5): 871-82.

Jamora, C., R. DasGupta, et al. (2003). "Links between signal transduction, transcription

and adhesion in epithelial bud development." Nature **422**(6929): 317-22.

Jamora, C. and E. Fuchs (2002). "Intercellular adhesion, signalling and the cytoskeleton." Nat Cell Biol **4**(4): E101-8.

Jensen, K. B., C. A. Collins, et al. (2009). "Lrig1 expression defines a distinct multipotent stem cell population in mammalian epidermis." Cell Stem Cell **4**(5): 427-39.

Jensen, K. B., J. Jones, et al. (2008). "A stem cell gene expression profile of human squamous cell carcinomas." Cancer Lett **272**(1): 23-31.

Jensen, K. B. and F. M. Watt (2006). "Single-cell expression profiling of human epidermal stem and transit-amplifying cells: Lrig1 is a regulator of stem cell quiescence." Proc Natl Acad Sci U S A **103**(32): 11958-63.

Kobayashi, N., A. Ikesue, et al. (2006). "Inhibition of e-cadherin-mediated homotypic adhesion of Caco-2 cells: a novel evaluation assay for peptide activities in modulating cell-cell adhesion." J Pharmacol Exp Ther **317**(1): 309-16.

Konigshoff, M. and O. Eickelberg (2010). "WNT signaling in lung disease: a failure or a regeneration signal?" Am J Respir Cell Mol Biol **42**(1): 21-31.

Laederich, M. B., M. Funes-Duran, et al. (2004). "The leucine-rich repeat protein LRIG1 is a negative regulator of ErbB family receptor tyrosine kinases." J Biol Chem **279**(45): 47050-6.

Lee, H. M., K. Takeyama, et al. (2000). "Agarose plug instillation causes goblet cell metaplasia by activating EGF receptors in rat airways." Am J Physiol Lung Cell Mol Physiol **278**(1): L185-92.

Li, C., A. Li, et al. (2009). "Stabilized beta-catenin in lung epithelial cells changes cell fate and leads to tracheal and bronchial polyposis." Dev Biol **334**(1): 97-108.

Lin, S. Y., K. Makino, et al. (2001). "Nuclear localization of EGF receptor and its potential new role as a transcription factor." Nat Cell Biol **3**(9): 802-8.

Lindstrom, A. K., K. Ekman, et al. (2008). "LRIG1 and squamous epithelial uterine cervical cancer: correlation to prognosis, other tumor markers, sex steroid hormones, and smoking." Int J Gynecol Cancer **18**(2): 312-7.

Linggi, B. and G. Carpenter (2006). "ErbB receptors: new insights on mechanisms and biology." Trends Cell Biol **16**(12): 649-56.

Lo Celso, C., D. M. Prowse, et al. (2004). "Transient activation of beta-catenin signalling in adult mouse epidermis is sufficient to induce new hair follicles but continuous activation is required to maintain hair follicle tumours." Development **131**(8): 1787-99.

Lo, H. W., S. C. Hsu, et al. (2005). "Nuclear interaction of EGFR and STAT3 in the activation of the iNOS/NO pathway." Cancer Cell **7**(6): 575-89.

Lonergan, K. M., R. Chari, et al. (2010). "Transcriptome profiles of carcinoma-in-situ and invasive non-small cell lung cancer as revealed by SAGE." PLoS One **5**(2): e9162.

MacDonald, B. T., K. Tamai, et al. (2009). "Wnt/beta-catenin signaling: components, mechanisms, and diseases." Dev Cell **17**(1): 9-26.

Madtes, D. K., H. K. Busby, et al. (1994). "Expression of transforming growth factor-alpha and epidermal growth factor receptor is increased following bleomycin-induced lung injury in rats." Am J Respir Cell Mol Biol **11**(5): 540-51.

Majo, F., A. Rochat, et al. (2008). "Oligopotent stem cells are distributed throughout the mammalian ocular surface." Nature **456**(7219): 250-4.

Malumbres, M. and M. Barbacid (2003). "RAS oncogenes: the first 30 years." Nat Rev Cancer **3**(6): 459-65.

McQualter, J. L., K. Yuen, et al. (2010). "Evidence of an epithelial stem/progenitor cell hierarchy in the adult mouse lung." Proc Natl Acad Sci U S A **107**(4): 1414-9.

Mercer, R. R., M. L. Russell, et al. (1994). "Cell number and distribution in human and rat

airways." Am J Respir Cell Mol Biol **10**(6): 613-24.

Montagut, C. and J. Settleman (2009). "Targeting the RAF-MEK-ERK pathway in cancer therapy." Cancer Lett **283**(2): 125-34.

Mucenski, M. L., J. M. Nation, et al. (2005). "Beta-catenin regulates differentiation of respiratory epithelial cells in vivo." Am J Physiol Lung Cell Mol Physiol **289**(6): L971-9.

Mucenski, M. L., S. E. Wert, et al. (2003). "beta-Catenin is required for specification of proximal/distal cell fate during lung morphogenesis." J Biol Chem **278**(41): 40231-8.

Nakajima, M., M. Fukuchi, et al. (2003). "Reduced expression of Axin correlates with tumour progression of oesophageal squamous cell carcinoma." Br J Cancer **88**(11): 1734-9.

Nguyen, D. X., A. C. Chiang, et al. (2009). "WNT/TCF signaling through LEF1 and HOXB9 mediates lung adenocarcinoma metastasis." Cell **138**(1): 51-62.

Niemann, C., D. M. Owens, et al. (2002). "Expression of DeltaNLef1 in mouse epidermis results in differentiation of hair follicles into squamous epidermal cysts and formation of skin tumours." Development **129**(1): 95-109.

Nilsson, J., A. Starefeldt, et al. (2003). "LRIG1 protein in human cells and tissues." Cell Tissue Res **312**(1): 65-71.

Nilsson, J., C. Vallbo, et al. (2001). "Cloning, characterization, and expression of human LIG1." Biochem Biophys Res Commun **284**(5): 1155-61.

Okubo, T. and B. L. Hogan (2004). "Hyperactive Wnt signaling changes the developmental potential of embryonic lung endoderm." J Biol **3**(3): 11.

Paul, S. and A. Dey (2008). "Wnt signaling and cancer development: therapeutic implication." Neoplasma **55**(3): 165-76.

Qian, X., T. Karpova, et al. (2004). "E-cadherin-mediated adhesion inhibits ligand-dependent activation of diverse receptor tyrosine kinases." Embo J **23**(8): 1739-48.

Rakhmanova, V. A. and R. C. MacDonald (1998). "A microplate fluorimetric assay for transfection of the beta-galactosidase reporter gene." Anal Biochem **257**(2): 234-7.

Rawlins, E. L. and B. L. Hogan (2008). "Ciliated epithelial cell lifespan in the mouse trachea and lung." Am J Physiol Lung Cell Mol Physiol **295**(1): L231-4.

Rawlins, E. L., T. Okubo, et al. (2009). "The role of Scgb1a1+ Clara cells in the long-term maintenance and repair of lung airway, but not alveolar, epithelium." Cell Stem Cell **4**(6): 525-34.

Reynolds, S. D., A. C. Zemke, et al. (2008). "Conditional stabilization of beta-catenin expands the pool of lung stem cells." Stem Cells **26**(5): 1337-46.

Riese, D. J., 2nd and D. F. Stern (1998). "Specificity within the EGF family/ErbB receptor family signaling network." Bioessays **20**(1): 41-8.

Rock, J. R., M. W. Onaitis, et al. (2009). "Basal cells as stem cells of the mouse trachea and human airway epithelium." Proc Natl Acad Sci U S A **106**(31): 12771-5.

Rock, J. R., S. H. Randell, et al. (2010). "Airway basal stem cells: a perspective on their roles in epithelial homeostasis and remodeling." Dis Model Mech **3**(9-10): 545-56.

Rouam, S., T. Moreau, et al. (2010). "Identifying common prognostic factors in genomic cancer studies: a novel index for censored outcomes." BMC Bioinformatics **11**: 150.

Rubin, C., G. Gur, et al. (2005). "Negative regulation of receptor tyrosine kinases: unexpected links to c-Cbl and receptor ubiquitylation." Cell Res **15**(1): 66-71.

Rubinfeld, B., I. Albert, et al. (1996). "Binding of GSK3beta to the APC-beta-catenin complex and regulation of complex assembly." Science **272**(5264): 1023-6.

Silva-Vargas, V., C. Lo Celso, et al. (2005). "Beta-catenin and Hedgehog signal strength can specify number and location of hair follicles in adult epidermis without recruitment of bulge stem cells." Dev Cell **9**(1): 121-31.

Snyder, J. C., R. M. Teisanu, et al. (2009). "Endogenous lung stem cells and contribution to disease." J Pathol **217**(2): 254-64.

Stutz, M. A., D. L. Shattuck, et al. (2008). "LRIG1 negatively regulates the oncogenic EGF receptor mutant EGFRvIII." Oncogene **27**(43): 5741-52.

Suzuki, Y., H. Miura, et al. (2002). "Targeted disruption of LIG-1 gene results in psoriasiform epidermal hyperplasia." FEBS Lett **521**(1-3): 67-71.

Takahashi, K. and K. Suzuki (1996). "Density-dependent inhibition of growth involves prevention of EGF receptor activation by E-cadherin-mediated cell-cell adhesion." Exp Cell Res **226**(1): 214-22.

Takeyama, K., K. Dabbagh, et al. (1999). "Epidermal growth factor system regulates mucin production in airways." Proc Natl Acad Sci U S A **96**(6): 3081-6.

Takeyama, K., B. Jung, et al. (2001). "Activation of epidermal growth factor receptors is responsible for mucin synthesis induced by cigarette smoke." Am J Physiol Lung Cell Mol Physiol **280**(1): L165-72.

Tanemura, A., T. Nagasawa, et al. (2005). "LRIG-1 provides a novel prognostic predictor in squamous cell carcinoma of the skin: immunohistochemical analysis for 38 cases." Dermatol Surg **31**(4): 423-30.

Teisanu, R. M., E. Lagasse, et al. (2009). "Prospective isolation of bronchiolar stem cells based upon immunophenotypic and autofluorescence characteristics." Stem Cells **27**(3): 612-22.

Teta, M., M. M. Rankin, et al. (2007). "Growth and regeneration of adult beta cells does not involve specialized progenitors." Dev Cell **12**(5): 817-26.

Thiery, J. P. (2002). "Epithelial-mesenchymal transitions in tumour progression." Nat Rev Cancer **2**(6): 442-54.

Thomasson, M., H. Hedman, et al. (2003). "LRIG1 and epidermal growth factor receptor in renal cell carcinoma: a quantitative RT--PCR and immunohistochemical analysis." Br J Cancer **89**(7): 1285-9.

Tobey, N. A., C. M. Argote, et al. (2004). "Calcium-switch technique and junctional permeability in native rabbit esophageal epithelium." Am J Physiol Gastrointest Liver Physiol **286**(6): G1042-9.

Uematsu, K., B. He, et al. (2003). "Activation of the Wnt pathway in non small cell lung cancer: evidence of dishevelled overexpression." Oncogene **22**(46): 7218-21.

Van Winkle, L. S., J. M. Isaac, et al. (1997). "Distribution of epidermal growth factor receptor and ligands during bronchiolar epithelial repair from naphthalene-induced Clara cell injury in the mouse." Am J Pathol **151**(2): 443-59.

Vaughan, M. B., R. D. Ramirez, et al. (2006). "A three-dimensional model of differentiation of immortalized human bronchial epithelial cells." Differentiation **74**(4): 141-8.

Voronina, V. A., K. Takemaru, et al. (2009). "Inactivation of Chibby affects function of motile airway cilia." J Cell Biol **185**(2): 225-33.

Waterman, H., M. Katz, et al. (2002). "A mutant EGF-receptor defective in ubiquitylation and endocytosis unveils a role for Grb2 in negative signaling." Embo J **21**(3): 303-13.

Xu, D., A. Makkinje, et al. (2005). "Gene 33 is an endogenous inhibitor of epidermal growth factor (EGF) receptor signaling and mediates dexamethasone-induced suppression of EGF function." J Biol Chem **280**(4): 2924-33.

Yang, W. M., Z. J. Yan, et al. (2006). "LRIG1, a candidate tumour-suppressor gene in

human bladder cancer cell line BIU87." BJU Int **98**(4): 898-902.

Yarden, Y. and M. X. Sliwkowski (2001). "Untangling the ErbB signalling network." Nat Rev Mol Cell Biol **2**(2): 127-37.

Yi, W., C. Holmlund, et al. (2011). "Paracrine regulation of growth factor signaling by shed leucine-rich repeats and immunoglobulin-like domains 1." Exp Cell Res **317**(4): 504-12.

Yoon, S. and R. Seger (2006). "The extracellular signal-regulated kinase: multiple substrates regulate diverse cellular functions." Growth Factors **24**(1): 21-44.

You, Y., E. J. Richer, et al. (2002). "Growth and differentiation of mouse tracheal epithelial cells: selection of a proliferative population." Am J Physiol Lung Cell Mol Physiol **283**(6): L1315-21.

Zemke, A. C., R. M. Teisanu, et al. (2009). "beta-Catenin is not necessary for maintenance or repair of the bronchiolar epithelium." Am J Respir Cell Mol Biol **41**(5): 535-43.

Zhang, Y., A. M. Goss, et al. (2008). "A Gata6-Wnt pathway required for epithelial stem cell development and airway regeneration." Nat Genet **40**(7): 862-70.

Zhu, A. J. and F. M. Watt (1999). "beta-catenin signalling modulates proliferative potential of human epidermal keratinocytes independently of intercellular adhesion." Development **126**(10): 2285-98.